EVALUATION OF THE HARDNESS OF ALKALINE EARTH ALUMINOSILICATE GLASSES

BY

HYOJIN LEE

A THESIS

SUBMITTED TO THE FACULTY OF

ALFRED UNIVERSITY

IN PARTIAL FULFILLMENT OF THE REQUIREMENTS
FOR THE DEGREE OF

DOCTOR OF PHILOSOPHY

IN

CERAMICS

ALFRED, NEW YORK

DECEMBER, 2021

EVALUATION OF THE HARDNESS OF ALKALINE EARTH ALUMINOSILICATE GLASSES

BY

HYOJIN LEE

M.S. GYONGGI UNIVERSITY, KOREA (1995)

M.S. ALFRED UNIVERSITY, NY (1997)

SIGNATURE OF AUTHOR _____

APPROVED BY _____
WILLIAM M. CARTY, ADVISOR

_____
WILLIAM LACOURSE, ADVISORY COMMITTEE

_____
DORIS MÖNCKE, ADVISORY COMMITTEE

_____
TIM KEENAN, ADVISORY COMMITTEE

_____
JUNJUN DING, CHAIR, ORAL THESIS DEFENSE

ACCEPTED BY _____
GABRIELLE GAUSTAD, DEAN
KAZUO INAMORI SCHOOL OF ENGINEERING

ACCEPTED BY _____
BETH ANN DOBIE
PROVOST AND VP FOR ACADEMIC AFFAIRS
ALFRED UNIVERSITY

Acknowledgments

If I must pick only one person to thank, that would be Dr. Carty. I came to Alfred 25 years ago and I started my first day with him. I did not start writing my thesis 25 then. However, I wanted to thank him for all that he has done for me over the last 25 years as a great boss, supporter, brother, counselor, friend, and thesis advisor. I would like to thank him for his support to complete my thesis. More importantly, he made (and still makes) my life more exciting and valuable in Alfred. I'm still excited to have a discussion with him about new projects tomorrow morning.

I would like to thank my committee members, Dr. William LaCourse, Dr. Möncke, and Dr. Keenan. I always enjoyed discussions with Bill in the McMahon hallway. Doris gave me detailed advice on my papers. I appreciate Tim's great support for the last a couple of years.

I'd like to thank all the undergraduate and graduate students who have been involved in lab work with me. I couldn't have finished this thesis without their help and I deeply appreciate all that they have done. Particularly, I want to express my thanks to Dan Delia who was (and is) always a "go-to-guy" when I have any troubles. I have really enjoyed all the discussions we have had as well. I'd also like to thank Krishna Amin. She liked to scare me in hallway.

In addition, I'd like to thank my parents for their support and patience. Although it took me a while to write this, they still will be very happy to read it.

And finally,

I love you, Seonyoung and Jaesuk.

Hyojin Lee

December 2021

Table of Contents

List of Tables

List of Figures

ABSTRACT

The hardness of alkaline earth aluminosilicate glasses was evaluated focusing on the alumina level and atomic packing density of the systems. To identify the compositional matrices, a comprehensive investigation was conducted to determine the glass formation region in ternary aluminosilicates ($R_2O{\cdot}RO{\cdot}Al_2O_3{\cdot}SiO_2$). Vickers hardness of the glasses were evaluated in steps: the calcium aluminosilicate system; a range of RO or R_2O modifiers, including blended flux systems; and finally, the introduction of a high valency cation into the high hardness glasses to locally increase the density of the glass structure. The alumina edge of the glass formation boundary was similarly defined by a fixed molar ratio of 1.2 (±0.1) Al_2O_3 to R_2O (Na_2O or K_2O), RO (MgO, CaO, etc.), or a mixture of fluxes (R_2O+RO) over a broad range of silica levels and was shown to be independent of cooling rate. The alumina saturation level determined the experimental matrix to prepare samples for hardness measurement. The hardness results for $CaO\text{-}Al_2O_3\text{-}SiO_2$ glasses demonstrated that hardness is strongly related to the alumina level and that the hardness of CAS glasses correlates with the melting behavior as predicted by the phase diagram. The hardness of CAS and MAS glasses were similar, ranging from 6.7 GPa to 7.2 GPa, and the replacement of CaO with MgO produced only a marginal increase in hardness. Conversely, the blending of CaO with SrO and BaO generally resulted in a decrease in hardness. The sensitivity to alumina and silica levels, however, was much greater ranging from ~4.5 to a maximum of ~8.2 GPa. Finally, high valency cations (Mo^{6+}) were added to high hardness CAS glasses. High valency cations should have locally increased the compactness of the glass structure and thus enhanced the indentation hardness, but there was no increase in hardness. Mo serves as a heterogeneous nucleation site for crystallization resulting in anorthite precipitation. While there was a clear trend of increasing hardness with increasing Cation Field Strength (CFS), this trend did not extend to the introduction of high valency cations did not show further improvement in hardness. Overall, it was concluded that, in general, the hardness of aluminosilicate glasses correlates to melting behavior, and that within specific compositions, with the composite CFS of the modifier cations.

I INTRODUCTION

This study was rooted in a project to develop high hardness oxynitride glasses. The hardness of glass is defined as the ability to resist deformation and localized densification when the glass is exposed to an external force during indentation. Historically it was known that the incorporation of nitrogen into the glass structure improves the glass hardness by increasing the bonding density of the network. However, the color control in the oxynitride glass is difficult and limits application. Another major obstacle to the creation of oxynitride glasses is the processing: to prevent nitrogen loss, the melting environment must be maintained at a high nitrogen pressure. This requirement makes the processing difficult.

Historical research has indicated that manipulation of the glass structure offers the potential to obtain high hardness glasses. The main approaches focused on deformation mechanisms as controlled by network connectivity and polymerization. Improvements in hardness were obtained by controlling intermediate concentration related to non-bridging oxygen reduction and by the introduction of higher cation field strength modifiers (and charge compensators) to enhance the modifier-oxygen bonding numbers and atomic packing density. Glass hardness is also determined by the elastic properties of the material, i.e., atom self-adaptivity, defined as the degree of atom coordination and the ability to resist density changes under pressure. For aluminosilicate glasses, a large amount of work focused on Al^{3+} coordination and the molar ratio of alumina to alkaline earth.

The first steps, however, to the evaluation of the hardness in aluminosilicate glasses was to define the glass formation regions for a range of fluxes (Chapter III). To this end, the study was initiated with the determination of glass phase formation in aluminosilicate ceramic systems. The results demonstrated that the alumina limit for glass formation was independent of the flux chosen, consistently showing a glass formation boundary of 1.2 moles of alumina per mole of flux (R_2O+RO). In general, the glass formation region is similarly broad for CAS, NAS, and KAS glasses but is truncated to a narrower range of silica levels when MgO is the primary flux.

After mapping hardness in CAS glasses, the contribution of CFS was evaluated through the substitution of Mg, Sr, or Ba for Ca. And finally, the potential to improve glass hardness, by the incorporation of a high valency cation, Mo^{6+} was investigated. High valency cation reduces the cation bonding length to neighbor anions, typically for 6-fold oxygen coordination, possibly including NBO. The local area distortion could potentially shrink the glass network and thereby limiting compressibility and increasing hardness. Mo^{6+} was introduced in an ionic form to avoid the crystallization of MoO_3, but regardless, no improvement in hardness was observed.

II LITERATURE REVIEW

II.1 Glass structure

All glass compositions in this study are presented in the format of a Seger formula or Unity Molecular Formula (UMF) – a molar ratio approach for describing the chemistry of glass in which the chemistry is normalized to the moles of flux.[1, 2] Seger grouped oxides by the cation to oxygen ratio, postulating that the structure of the oxides predicted their role in glass formation. For simple aluminosilicate glasses, this approach is reasonable, with fluxes being defined as R_2O (Li_2O, Na_2O, K_2O, etc.) and RO (MgO, CaO, SrO, and BaO, as well as FeO, CuO, ZnO, etc.) and fluxes are additive. Intermediates are represented as R_2O_3 and include Al_2O_3 and Fe_2O_3. RO_2 represents the glass formers, specifically SiO_2. This approach breaks down for B_2O_3, which is a glass former, and for TiO_2 and ZrO_2 which are not good glass formers. Overall, Seger formulas offer an excellent format to describe aluminosilicate glass chemistry. Alumina and silica levels are then represented by the molar ratio to flux, so a glass obtained directly from orthoclase (potassium feldspar) would have the chemistry $K_2O \cdot Al_2O_3 \cdot 6SiO_2$, or 1.0:1.0:6.0 with one mole of flux, one mole of alumina and six moles of silica.

Silicate glass networks are constructed of $[SiO_4]^-$ silica tetrahedral building blocks. Monovalent (R^+ or R_2O) and divalent (R^{2+} or RO) cations, typical fluxes (modifiers), create a non-bridging oxygen (NBO) weakening the glass network connectivity. NBOs are widely blamed for the decline in mechanical properties of glasses.

When alumina is added to a silicate glass, some Al^{3+} ions substitute for Si^{4+} ions in tetrahedrally coordinated positions (Al_T).[3-5] Each Al_T replacement generates one negative charge. Alkali and alkaline earth ions satisfy this charge and are thus charge-coupled to the Al_T. At an Al_2O_3 level of 1.0, it can be assumed that all Al^{3+} ions occupy tetrahedral sites. At this level all R^+ and R^{2+} ions function as charger compensators for $[AlO_4]^-$. When the Al_2O_3 level is greater than 1, aluminum ions are either in 5-fold or 6-fold coordination.

II.1.1 Aluminum Coordinations

Nuclear Magnetic Resonance (NMR) studies have provided details regarding Al^{3+} coordination in the context of the Al_2O_3:(R_2O+RO) ratio.[6-26] It is sensitive to the local atomic environment both in terms of chemical and structural features. NMR uses a magnetic moment characteristic of nuclei which can provide details of their local environments including near neighbor elements, element coordination, and bonding angles. It operates by applying a magnetic field to nuclei and measuring the energy necessary to place those nuclei into resonance. Nuclei in different electronic environments require different energy levels to resonate. NMR spectrum provides signal representing the energy level.[27] Typical glass formers and intermediates including silicon, aluminum, and boron are favorable while many of the modifiers such as magnesium and calcium are difficult because of the poor signal quality. For example, ^{43}Ca has very low NMR sensitivity because it is a quadrupolar nucleus with a very low natural abundance and low resonance frequency.[28]

History of the application of the NMR to glass characterization is relatively short but the developmental progress was rapid. In 1970's this technique was significantly advanced by developing the magic angle spinning (MAS) NMR. It narrows NMR signal substantially and improves resolution.[29] The resolution of wider peaks caused by larger distribution of information, i.e., bonding angles, was improved by the introduction of a 2-dimensional technique.[30] The technique correlates the normal isotropic spectrum with anisotropic spectrum, specifically present in polyhedral analysis.

Earlier observations on Al^{3+} coordination in alkaline earth (RO) aluminosilicate glasses indicated Al tetrahedra (A_T) in compositions with high RO, i.e., $Al_2O_3 < 1$. Octahedrally coordinated Al^{3+} (A_O) in compositions with high alumina content, i.e., $Al_2O_3 > 1$. A calcium ion can compensate for two A_T sites. In the high RO region ($Al_2O_3 < 1$) the role of Ca^{2+} ions changes from a modifier forming NBO to charge compensator when the alumina addition increased, thus reducing NBO numbers. Specifically, for $Al_2O_3 = 1$, no NBOs are present. When excess Al^{3+} ions are added, i.e., $Al_2O_3 > 1$, the A_O sites are formed with 3 NBOs. Overall, the population of NBO reduces until the alumina addition

reaches 1 Al_2O_3 ratio and increase again with any excess Al^{3+} addition with assuming that all Al^{3+} are occupied in A_O sites.[3, 4, 31] When there is excess Al_2O_3, all access Al ions are assumed to be in Octahedral sites which generate NBO. The hardness improvement, however, cannot be explained only by this simple information.

Sato performed MAS NMR work to evaluate Al^{3+} coordination in $Al_2O_3 \geq 1$.[32] Those results showed that three-fold, four-fold, five-fold, and six-fold coordination were observed as alumina additions increased from 1.0 Al_2O_3. For the data reliability, he tried to deal with noise from the quadrupolar coupling by generating data at two magnetic field strengths. The quadrupolar coupling constant was estimated and used as characteristic information because it is sensitive to the local structure. Also, spinning speed was controlled (increased) to optimize the results. These results also agreed with previous results that showed four-fold and six-fold coordination in high alumina region ($Al_2O_3 >$ 1).[33] Quantitative analysis concluded that about 15% of the aluminum were not detected due to the quadrupolar line broadening. It was suggested that some aluminum ions are placed in distorted sites that alter the chemical shift in the NMR data. This work confirmed that all Si and Al ions are tetrahedrally coordinated by oxygen and bonded by the corners when $Al_2O_3 \leq 1$. When alumina level increased, three different coordination states were observed. One additional note is that the evaluated compositions in $Al_2O_3 > 1$ region in Sato's work are not within the glass formation region, with an $Al_2O_3 > 1.2$ up to 1.5.[32] It is reasonable to assume that crystallization contributed to the results and the interpretation of Al coordination.

It was useful to find a considerable amount of NBO present at the tectosilicate composition, 1.0 Al_2O_3.[20] ^{17}O MAS NMR data was used to determine the NBO peaks which are distinguished from bonding oxygen peaks. Al-O-Al linkages are promoted by calcium which generates more Si-Al disorder. Schmucker tried to provide a way to interpret the NMR data differently using the mullite structure as a model.[34] The peak at 30ppm is known as a AlO_5 ($^{[5]}Al$) peak. He argued that the peak is related to the tricluster formation rather than $^{[5]}Al$ because the $^{[5]}Al$ is not present in the mullite structure. Thus, still it is considered that NBO formation in tectosilicate glasses are coupled with tricluster formation.

Neuville evaluated aluminum coordination over a broad range of Al_2O_3 levels using 3Q MAS NMR.[11-14] The environment of the Al tetrahedra were expressed by the interpretation of isotropic chemical shifts. It was stated that in the environments around Al tetrahedras, the number of NBOs in the vicinity of Al tetrahedras or neighboring glass forming tetrahedra, can be estimated by isotropic chemical shifts. It was confirmed that the system was depolymerized in the high CaO region, $Al_2O_3 < 1$. Al^{3+} cations in tetrahedral sites require charge balancing, and thus satisfied by charge compensating monovalent or divalent cations. Excess alkaline earth (or alkali) cations contribute to the depolymerization of the network by forming NBO. The existence of NBO was also investigated in tectosilicate glass. Two major hypotheses were considered: (1) the formation of $^{[5]}Al$ or (2) tricluster formation with NBO.

Quantitative analysis for AlO_5 ($^{[5]}Al$) species was reported in samples containing up to 2.0 Al_2O_3 (Figure I-1).[14] AlO_5 was observed not only at high alumina concentrations, but also in the high CaO region. The concentration of $^{[5]}Al$ systemically increases with increasing Al_2O_3 level. The results also indicated that AlO_6 ($^{[6]}Al$) formation was minimal. The environment around Al^{3+} ions in glass is similar to that in a crystal structure of similar chemical composition. More importantly, the results provided an explanation for the existence of NBO in tectosilicate composition with a considerable amount of $^{[5]}Al$ species (~7%). (Note that some of the tested compositions were out of the glass formation region.)

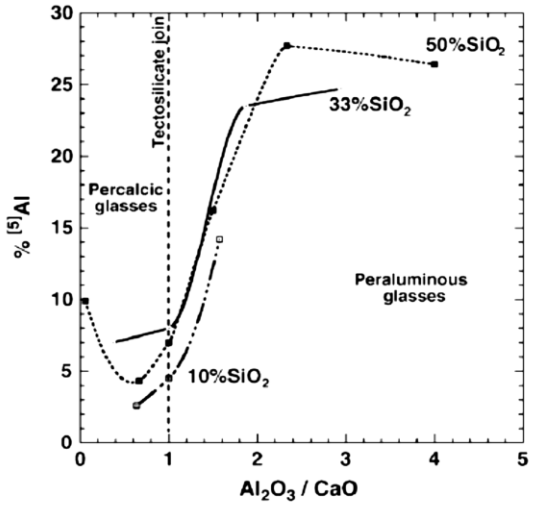

Figure II.1. Proportion of $^{[5]}Al$ as a function of Al_2O_3 level.[14]

AlO_5 in anorthite: Alumina structure in glass was compared to the one in the associated crystalline structure of anorthite and MAS-NMR results show that the local Al^{3+} environment was similar in both (Figure I-2).[25] The broad peak around 60ppm is attributed to a $^{[5]}Al$. Similar results were observed for the Si^{4+} environment. These results suggest that the structure of glasses are chemically similar to an associated mineral structure.

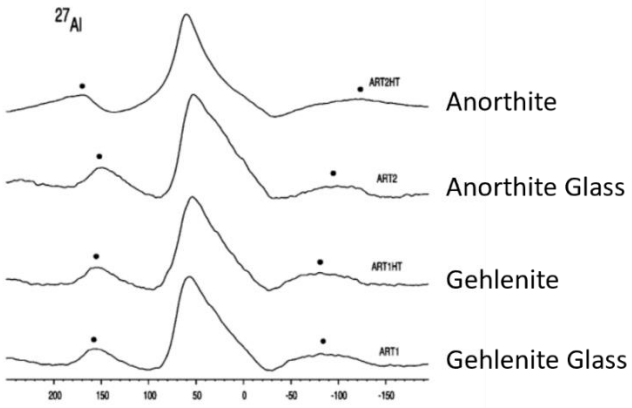

Figure II.2. ^{27}Al MAS-NMR spectra of the ART1 and anorthite (ART2) glasses and their spectra following crystallization to gehlenite and anorthite.[25] Anorthite crystalline spectrum is the top and the glass is second top. Broad peak around 60ppm is attributed to a $^{[5]}Al$. No significant changes in glass and crystalline were observed.

CFS effects on AlO_5 formation: It was reported that the $^{[5]}$Al formation is affected by cation field strength. The formation of NBO and aluminum coordination were evaluated in calcium- and barium-aluminosilicate (CAS and BAS) glasses prepared with Al_2O_3 level of 0.94 to 1.20,[21, 35] with all compositions residing within the glass formation region. Quantitative analysis for the NBO concentration shows that ~ 6% of NBO/total oxygen ions are presented in the 1.0 Al_2O_3 composition. Although the concentration of NBO reduced with increasing alumina levels, NBOs were still detected in the glasses, with levels slightly higher in CAS compared to BAS glasses. The population of $^{[5]}$Al increased with increasing alumina additions, consistent with other results.[14] The most important observation was that $^{[5]}$Al concentration in barium aluminosilicate glass was lower than that in calcium aluminosilicate glass, leading to the conclusion that the CFS influences the NBO and $^{[5]}$Al formation, a result supported by several other researchers.[6, 15, 36]

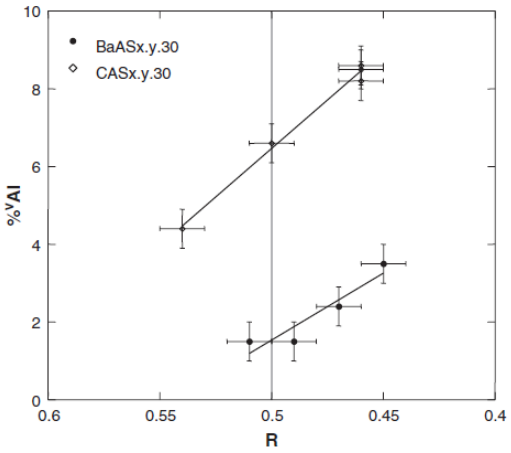

Figure II.3. The $^{[5]}$Al content of calcium and barium aluminosilicate glasses as a function of R=RO/(RO+Al_2O_3).[21]

Rare earth (RE) cation effects on AlO_5 formation: Similar results related to the CFS were reported with rare earth cations.[37, 38] In the Stevensson's work, data was collected using MAS-NMR.[37] Scandium additions generated up to ~35% $^{[5]}$Al. The mechanism for the $^{[5]}$Al increase with RE cations was referenced by previous researchers.[18, 39, 40] The brief explanation was that higher coordination improves the compactness of glasses. The effect of highly coordinated Al on the hardness was also discussed regarding the packing density and bond strength.

Reaction between AlO_5 and Tricluster: Formation of $^{[5]}$Al with tricluster oxygen was also discussed and it was proposed that the system network is stabilized with $^{[5]}$Al,[10] and that medium range order is improved by combining of $^{[5]}$Al with tricluster oxygens. In the high peraluminous region ($Al_2O_3 > 1$), results showed that Al^{3+} cations in all three coordination states were observed. In this work, the Al^{3+} coordination was evaluated at elevated temperatures. Compared to the tectosilicate composition, $^{[5]}$Al population in the peraluminous composition studied was significantly higher. For the charge balance, it was considered that $^{[5]}$Al carries oxygen triclusters. Consequently, this localization of oxygen tricluster in the $^{[5]}$Al implies the formation of structured clusters at the scale of several tetrahedras in glass. This is an interesting argument because it can provide an explanation of how $^{[5]}$Al formation improves the mechanical properties of glasses.

Alumina coordination in high temperature: Al coordination changes with temperature using *in situ* high temperature MAS NMR.[19, 22, 41, 42] This is to explain thermodynamic behavior of glasses with temperature, but these results are still compatible for quenched glasses. The population of $^{[5]}$Al increased with increasing temperature over a broad range of Al_2O_3:RO (or R_2O) ratios in aluminosilicate glasses. It is reasonable that higher Al coordinations ($^{[5]}$Al and $^{[6]}$Al) are favorable in high temperature because Al cations are larger than Si cations in high temperature, and generally possess less net positive charges, resulting in weaker Al-O bonding compared to Si-O. Thus, the bonding stretches with increasing temperature. When the bond lengthening is sufficient, then tetrahedrally coordinated Al^{3+} transform to higher coordination. The high temperature structure can be maintained by quenching. Some of the variability observed in glasses prepared through different processing methods may be explained with these observations.

II.1.2 T-O-T Bonding

Tetrahedron-O-Tetrahedron (T-O-T) bonding structure (where, T=Al_T or Si_T) have been discussed with aluminum coordination in glass structure. This information is most likely dealing with medium range glass structure and supporting local aluminum environment. The T-O-T bonds are often described based on the Al-avoidance rule which is that Al-O-Al bonds are not favored in glass structure.[43] The degree of disorder in glass forming structure, i.e., concentration of Al-O-Al, depends on the Al/Si ratio. In the alkali aluminosilicate glass, Al-O-Al bonding proportion increased with Al/Si ratio. Further, the degree of disorder increased with higher CFS cation additions and with increased temperature of the system.[44] Addition of higher CFS increases the population of Al-O-Al. In the study, controlling disorder of Si/Al can be related to the formation of species, i.e., tricluster and/or AlO_5, which can affect glass properties.

In another work it was mentioned that the Al-O-Al bonding supports the possible existence of triclusters.[45] In this study, a glass composition with Si/Al= 1 in sodium aluminosilicate was examined using 3Q MAS NMR. The results revealed that ~17% of the bonds were Al-O-Al.

Another example of the compositional dependence on the Al-O-Al formation was research conducted over a wide range of silica and alumina contents.[46] Analysis in wide range of composition showed that Al-O-Al bonding was formed in low silica range (10 mole%) and isolated Al_T were formed with Si_T generating ring structures in relatively high silica compositions. It does not directly explain, however, whether such a bonding structure proves the existence of triclusters. The polymerization degree, however, obtained by the formation of AlO_4 and AlO_5 were evaluated based on the Al_2O_3 levels. The data was argued to explain thermal properties of glasses. A similar idea was presented in the work of Kucharczyk.[47]

II.2 Hardness of Glass

Hardness of glass is commonly defined in terms of indentation hardness using a Vickers indenter. Vickers indenter is a diamond pyramid with 136° tip angle. Typical force is up to 9.8N (1kg load) for glass testing. Hardness is calculated using the applied force and indentation dimensions. The preferred unit for hardness is GPa, but the units of kgf/mm^2 were historically reported. (The unit of kgf/mm^2 is converted to GPa by multiplying by 0.0098.) The calculation is:

$$Vickers\ Hardness\ (H_v) = \frac{Force}{area} = \frac{2Fsin(\theta/_2)}{d^2} = 1.8544 \cdot \frac{F}{d^2} \qquad (1)$$

Where, F is the force in kgf, θ is the diamond pyramid angle (136°) and d is the average diagonal of the indents.

Hardness is a measure of the capability of the glass to resist deformation forces applied externally.[3] The deformation process includes elastic deformation, plastic flow (shear), and densification. Elastic deformation is a reversible process where the deformation is recovered upon unloading. Plastic deformation is irreversible and occurs when the applied force exceeds the elastic limit. Figure I-4 shows a schematic cross section of indentation, including the deformation results. Plastic flow is volume conservative process in the absence of densification and typically results in pileups. Densification is a nonreversible, non-volume conservative process resulting in permanent compaction of the structure. The volume exhibiting elastic deformation is typically larger and deeper than the volume experiencing densification.

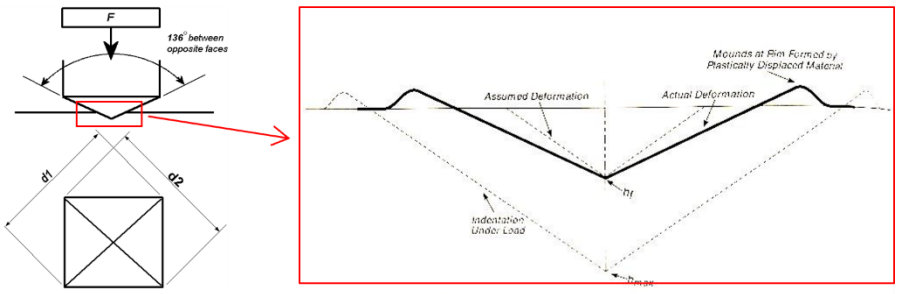

Figure II.4. Schematic of indentation on glass showing elastic deformation, plastic flow, and densification.[3]

Vickers indentation fracture (VIF): Vickers indentation is also being used to achieve the toughness information commonly called as Vickers indentation fracture (VIF).[48-50] The length of cracks extending from the corners of the indenter are measured and used to calculate fracture toughness. Januchta reviewed the effects of the measuring conditions including time and environments on the results in his dissertation.[51] Several equations have been proposed leading to some confusion in the literature, based on different assumptions regarding crack types, i.e., Palmqvist or median. The ratio of the crack length (c) and the indentation dimension (d) are important factors to calculate toughness. Several different models were reported that depend on the crack ratios. i.e., c>1.25d or c<1.25d. The most common relationship is:

$$K_c = \alpha \left(\frac{E}{H_v}\right)^n \frac{P}{c^{3/2}} \quad (2)$$

Where, α is a calibration constant and n is parameter depending on the model selected. As an example, Barlet showed similar trends of hardness and toughness on the glass structure.[48] Quinn and Bradt, however, argued that the Vickers indentation fracture test is not a reliable method from which to obtain fracture toughness.[52] Their arguments first noted that the equation is not based on an exact theory. Many of the relationships were generated with calibration factors and several were manipulations of previous equations with additional calibration factors introduced for specific materials. They also identified several problems associated with the complexity of cracking mechanism and the difficulties of accommodating these complexities with a simple equation.

Indentation size effects: Indentation procedure, especially, micro-scale, uses loads higher than 0.98N (0.1kgf) which typically generates fracture at the corners. Such cracking at the corners is not desirable as it makes the accurate measurement of the hardness difficult because of problems in correctly measuring the indent size. Nano-indentation is proposed as a solution to the cracking problems.

Indentation load affects the measured hardness values.[53-55] Hardness increases disproportionately as the size of the indentation decreases, as reported for metal, metallic glass, or crystalline ceramics.[56] While the mechanisms are different for different materials, it is common that hardness increased as indentation size is reduced.

As in definition, indentation in glass includes elastic and plastic deformation. The elastic properties are material dependent. Thus, the critical load value to generate the plastic deformation, i.e., to exceed the elastic deformation, depends on the material properties. Ideally, if the load is below a threshold level, no indentation is formed. Bull explained the indentation size effect in ceramic system by existence of "discrete elastic zone."[57] His argument was that the deformation occurs in discrete bands rather than being continuous. Although this argument was intended for crystalline materials, it applies to a certain extend to the indentation of glasses. He developed an equation to evaluate the correspondence of elastic properties and hardness.

$$H_m = H_o \left(1 + \frac{\delta}{d_m}\right)^2 \quad (3)$$

Where H_m is the measured hardness, d_m is measured diagonal dimension of the indent, H_o is hardness including elastic deformation, and δ is elastic deformation. Based on the equation, when $d_m >> \delta$ indicating a high load, $H_m \approx H_o$. However, when load is low, effect of elastic deformation band becomes critical. As a result, the measured hardness will increase with elastic deformation. To verify his hypothesis, Bull generated experimental data with the nano-indentation of sapphire.[57]

To account for, or measure, the elastic displacement, one widely used method is to measure displacement with force as the indent is formed.[58] Data is collected on both loading and unloading. The unloading data is then analyzed to achieve the contact area information at peak (maximum) load which generated both elastic and plastic deformation.

Oliver reported a method for accurate estimation of the contact area based on the measured maximum and final height of indentation.[59] The area estimation was based on the h_c in the Figure I-5a, which is the difference between total displacement (h) and the displacement of the surface at the perimeter of the contact (h_s). The determination of h_s involves the calculation from the deflection related to indenter geometry and from the load-displacement data through this equation:

$$h_s = \frac{2(\pi-2)}{\pi} \cdot \frac{P}{S} \quad (4)$$

Where, P is load and S is slope of load and displacement curve at the initial stage of unloading (Figure I-5b). The contact area (A) can be calculated from h_c (h-h_c) by solving the area function. The key was that the calculation, especially the determination of the area function, involved all possible variables, including load frame and sample compliance and the varied mechanical properties that contribute to the contact area at peak load, which also incorporates plastic and elastic deformation.

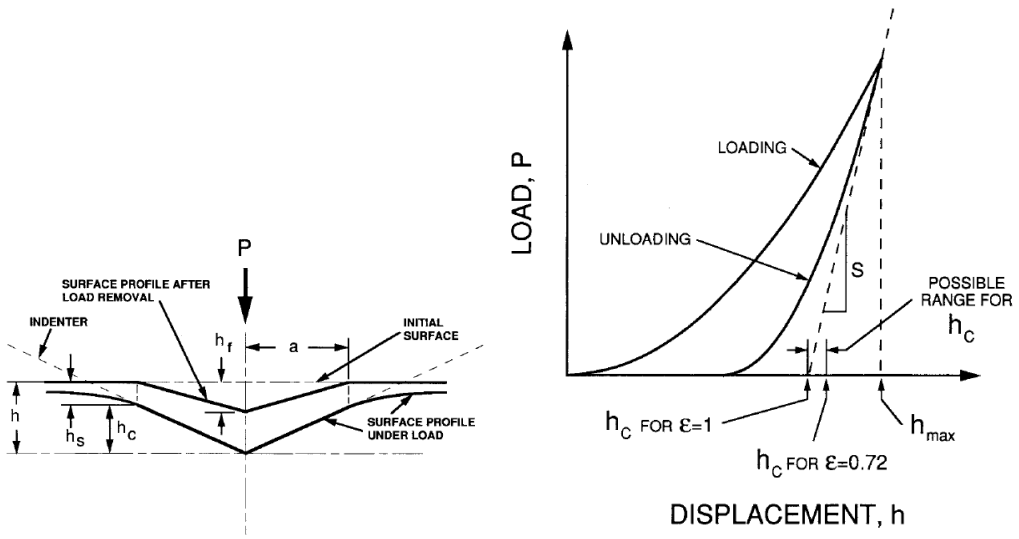

a) b)

Figure II.5. a) A schematic representation of a section through an indentation showing various quantities used in the analysis. b) A schematic representation of load versus indenter displacement showing quantities used in the analysis as well as a graphical interpretation of the contact depth.[59]

Technically, nano-indentation hardness, particularly when using the measurements of deformation as the maximum load is applied, must be the same or lower than micro-indentation hardness which is calculated with indent dimension after load removal (which

cannot accommodate elastic recovery of the indent when the load is removed). However, still it is questionable if the nano-indentation hardness can be directly compared to the micro-indentation hardness.

Knoop indentation is one of the hardness measurement methods in glass research area and often compared to the Vickers indentation data.[60-62] Knoop indenter is a lozenge-based diamond pyramid with two different semi-apex angles θ_1=86°15, θ_2=65° along the length L and the width b. Knoop hardness is calculated with applied load per contact area:

$$Hk = \frac{P}{A_p} = \frac{2 \cdot P}{L^2} \cdot \frac{tan\theta_1}{tan\theta_2} = 14.229 \cdot \frac{P}{L^2} \quad (5)$$

Where L is the measured long diagonal of the residual impression and P is applied load. In general, Knoop hardness is lower than Vickers hardness. The difference between Vickers and Knoop hardness has been reported as a gradual deviation from 1:1 relation, i.e., smaller Knoop hardness, with increasing hardness.[62-64] One of the examples is showed in Figure I-6. Hardness is an intrinsic property of materials, therefore so that the values must be same when they are measured by Vickers or Knoop indenters. The difference was explained with unusual elastic recovery of Knoop impression. Indent diagonals in Vickers indentation remain approximately unchanged after unloading. Elastic recovery occurs only along the indentation depth. However, in Knoop indentation, a radial displacement of the impression edges inside the contact impression occurs. Thus, elastic recovery occurs along the short axis and it is related to elastic modulus of the material.[64] Ghorbal demonstrated that Knoop hardness values can be aligned with Vickers hardness values by manipulating the equations to compensate for the abnormal elastic deformation observed in Knoop hardness measurements.

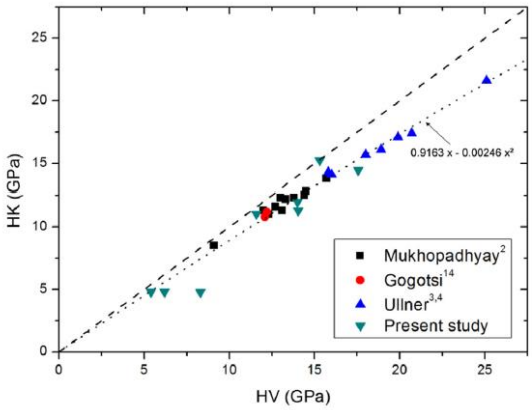

Figure II.6. Comparison between Vickers and Knoop hardness.[64]

Hardness of glasses: The mechanisms that determine the hardness of glass are plastic flow (shear) deformation and densification.[56, 65] Theory postulates that the densification is the predominant mechanism in a loosely packed network while the shear deformation is the primary mechanism in a densely packed system. Therefore, from a structural glass perspective, the chemistry of the glass is the most important factor to control the mechanism for the hardness. Rouxel, et al proposed that Poisson's ratio is an indicator of the deformation mechanism (Figure I-7).[65] In the material with a lower Poisson's ratio, deformation is controlled by densification.

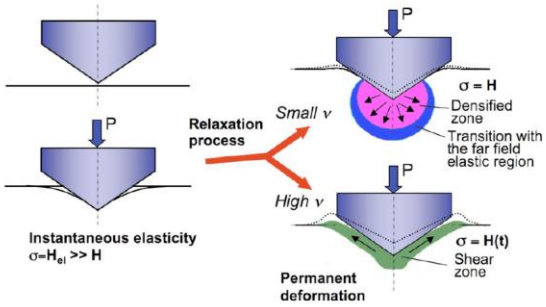

Figure II.7. Schematic sketch of the indentation deformation stages. The dashed line indicates the indentation profile after unloading. Arrows indicate matter displacement, σ is the mean contract pressure.[65]

Based on the theories proposed, the mechanisms controlling hardness can be altered by chemical composition. Thus, other glass properties dictated by chemistry should correlate with hardness. Ramberson reported that shear deformation is dominant in low silica regions while the densification mechanism dominates in high silica regions (>80%) in CAS glasses.[66] These results were explained with flowability associated with NBOs. In general, the reported hardness data increases with alumina addition in tectosilicate glasses.

The change in hardness with silica level follows the opposite trend. in the low silica region: 0.31 to 1.17 SiO_2:CaO with an Al_2O_3 level approximately 0.55.[67] A slight increase in hardness was observed with increasing silica. In these results, Vickers hardness increased linearly with elastic modulus (Figure I-8). A maximum hardness of 7.8GPa was obtained with the composition ~40wt% silica and 1.0 Al_2O_3.

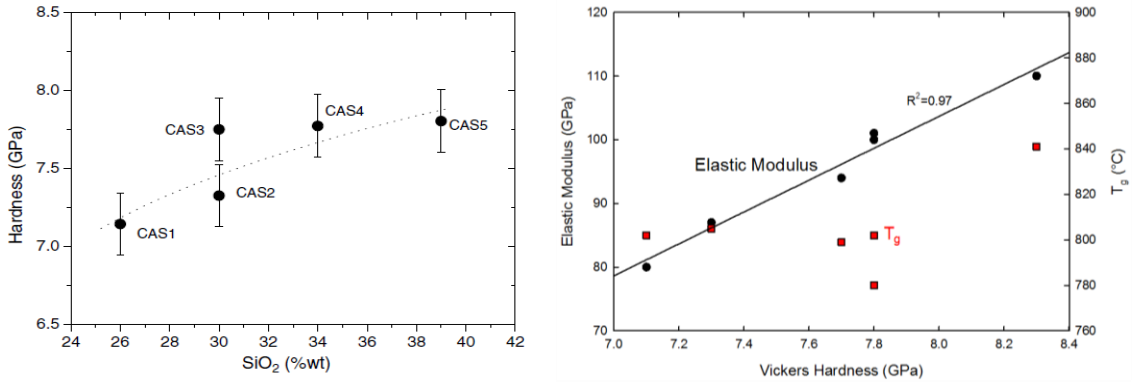

a b

Figure II.8. a) Hardness correlated to the silica contents and b) hardness vs. Elastic modulus or T_g.[67] (Second plot (b) is replotted based on the tabular data provided by Steimacher et al.)

The dependence of hardness on chemistry was reported over a more extended compositional region through the evaluation of several Al_2O_3:SiO_2 and Al_2O_3:CaO ratios (Figure I 9).[68, 69] Hardness increased linearly with increasing Al_2O_3:SiO_2 ratio of a constant Al_2O_3:CaO ratio. With increasing Al_2O_3 content, hardness was not affected significantly until 0.8 Al_2O_3 in which excess Ca^{2+} cations are available, and then hardness

increased with further alumina addition. They used the ratio (2Al/(2Al+Ca) to point out aluminum (tetrahedra) numbers based on the charge compensator numbers. In this case, calcium is the compensator. Two A_T needs one calcium. Thus, 0.5 (2Al/(2Al+Ca) is equivalent to an Al_2O_3level of 1.0. Figure I-9 uses this ratio. Also, it was noted that hardness of low silica compositions were higher than that of high silica levels over all of the Al_2O_3:CaO ratios. Elastic modulus, Poisson's ratio, and hardness correlated with the compositional changes. However, when Al_2O_3:CaO ratio changes in the vicinity of tectosilicate compositions, Poisson's ratio correlation with hardness is noticeable. It may be due to the transformation of indentation mechanism changes with compositional change.

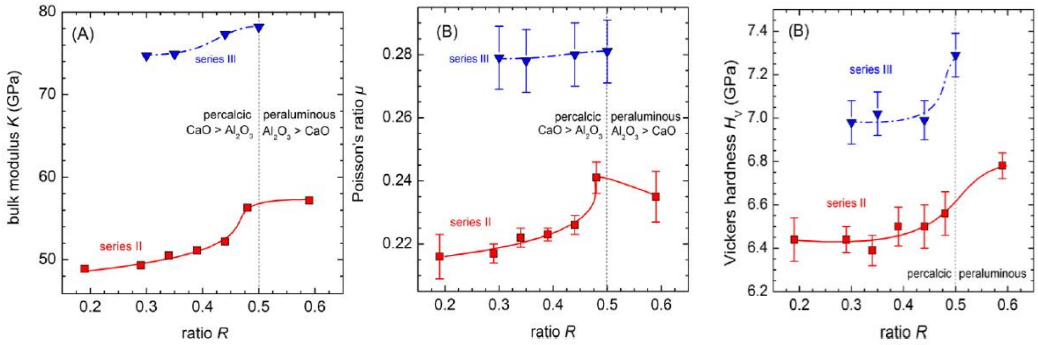

a b c

Figure II.9. a) Bulk modulus, b) Poisson's ratio, and c) Vickers hardness as a function of Al_2O_3:CaO ratio.[69]

Effects of cation field strength on glass hardness: It is clear that hardness is strongly affected by glass structure, especially when the densification is the dominant deformation mechanism.[70] Glass structure is often presented as an atomic density, via the molar volume, a measure of compactness. Simple calculations for atomic packing factor, C_g, are:

$$C_g = \frac{1}{V_m}\sum_i V_i x_i \tag{6}$$

Where,

$$V_i = \frac{4}{3}\pi N(xr_A^3 + yr_o^3) \tag{7}$$

Where, V_i is the molar volume of the *i*th constituent oxide of molar fraction x_i with A_xO_y chemical formula.

Weigel provided great examples for the charge compensator effects of alkali and alkaline earth ions on the glass structure and glass properties.[71] Higher CFS cations reduced the molar volume of glass thus increasing the atomic packing density. As an example, when Ca^{2+} cation replaces Na^+ cations, aluminosilicate frame is rearranged to maintain local charge balance because two negative charged $[AlO_4]^-$ tetrahedrons are balanced with one divalent cation. This structural rearrangement increases the elastic modulus, i.e., elastic modulus is inversely proportional to molar volume. Author pointed that dependence of molar volume was observed with cation field strength of charge compensators. In aluminosilicate glasses, the term "glass modifier" is distinguished from "charge compensator." Although no hardness data was presented, it is reasonable to state that hardness increases with CFS cation additions because the elastic modulus increases with improved packing density (and hardness increases with increasing elastic modulus).

Mixed alkaline earth effects on glass hardness: Most of the reported Vickers hardness values of MgO-CaO-Al_2O_3-SiO_2 systems can be obtained from the literature addressing Mixed Alkaline Earth Effects (MAEE). Mixed modifier effects, defined as non-linear variations of a property, are often observed in thermal or mechanical properties such as thermal expansion coefficient, glass transition temperature, elastic modulus, hardness etc.[7, 50, 72-76]

Especially, hardness can deviate either negatively or positively from the linearity when the one modifier is replaced systematically by another modifier keeping the overall molar modifier additions level constant. Although still the origin of the MAEE has not been clearly addressed, a few researchers have attempted to explain the underlying mechanism. To the best of author's knowledge, not many studies were reported regarding the MAEE of pure RO aluminosilicate systems without any alkali involved. It was known that the mechanism and results of effects the mixed modifier effects are similar in alkali/alkaline earth silicate or aluminosilicate system. Kjeldsen summarized the historical origins of the MAE or MAEE concisely.[72, 76, 77]

Kjeldsen reported work span several years.[72, 76, 77] One the studies addressed MAEE in aluminosilicate system. Hardness of CaO-MgO-Na_2O-Al_2O_3-SiO_2 system was measured using Vickers indentation and the results were compared to other mechanical, thermal, and bulk properties the system.[78] The matrix was sodium aluminosilicate system and the MgO and CaO content were changed. The MAEE was detected in the Vickers hardness data. The values of both CaO and MgO ends were ~7.0GPa. Negative deviation from the linearity was observed with 0.4 to 0.6 of MgO substitution for CaO. The minimum hardness was 6.6GPa. The origin of the MAEE was described as that the negative deviation in the hardness was related to the local structural environment around the network modifiers causing overall bond weakening. No MAEE was observed, however, in elastic modulus, thermal expansion, molar volume, density, or refractive index, but was observed in heat capacity and glass transition temperature. The results of the various measured properties did not always correlate with the same MgO substitution level. MAEE was discussed from the perspective of viscosity as a function of temperature. In a later paper, he concluded that the plastic flow (shear flow) mechanism must be invoked to explain the mixed alkaline earth effect observed in hardness data.[77]

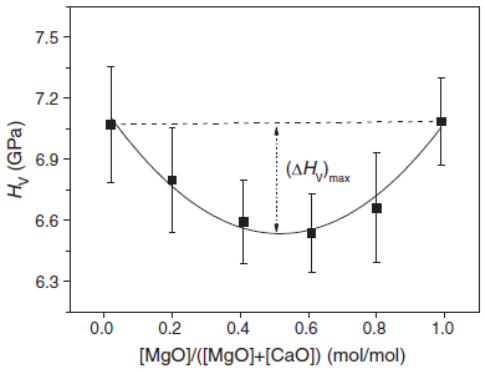

Figure II.10. Vickers hardness as a function of molar ratio [MgO]/([MgO]+([CaO]).[78, 79]

Several reports worked with different compositions. Kilinc and Hand prepared a typical soda lime silicate glasses with varied CaO and MgO ratios.[80] Most of the monovalent

and divalent cations functioned as modifiers because added Al_2O_3 levels were very low. Mechanical properties including hardness, fracture toughness, elastic modulus, and Poisson's ratio, were measured and interpretated with structural information. The glass structure was analyzed, and Raman polymerization index was calculated to compare to the mechanical property data. The Raman polymerization index is the ratio of the peak related to the Si_T bond stretching and the Si_T bond bending. The index decreases as a function of $RO:SiO_2$ increases indicating that the NBO concentration were increasing. MgO substitution for CaO only slightly affected the index. A small peak in the index was presented at 0.65 [MgO]/RO, but the authors did not interpret this as an indication of MAEE. All mechanical properties improved with deceasing Raman polymerization index as presented in Figure I-11. The results are not consistent with most of the other literature data in which mechanical properties are improve when the network is more polymerized.

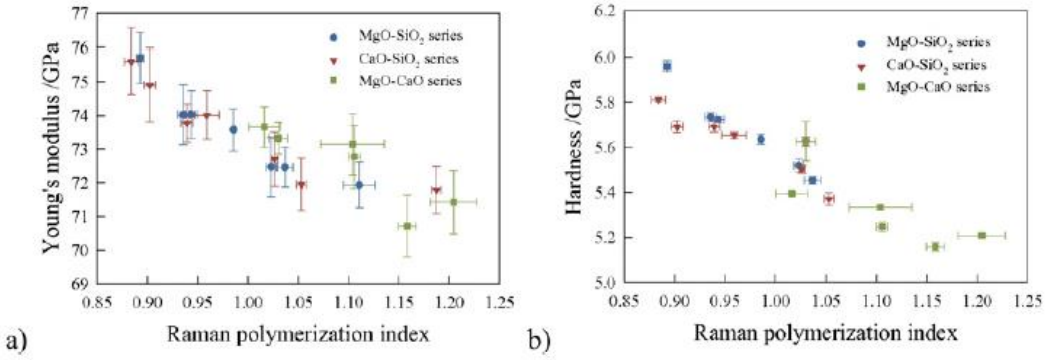

Figure II.11. Variation of selected mechanical properties with Raman polymerization index: a) Young's modulus and b) hardness.

Some researchers show positive MAEE in silicate glasses. Calahoo reported mechanical properties of $MgO\text{-}CaO\text{-}SiO_2$ system with varying CaO:MgO ratios.[73] The evaluated composition was 1.0 SiO_2:RO and [MgO]/RO ranged from 0.17 to 0.84. No alumina was added so all RO are functioning as modifiers generating NBOs. The MAEE was not observed in the NBO levels but they were reduced with increasing MgO substitution for

CaO. The positive MAEE was found in mechanical properties. A peak hardness of 7.7GPa was obtained at 0.67 [MgO]/RO ratio (Figure I-12). The hardness (MAEE) was correlated to the molar volume data in which the minimum was at a ratio of ~0.7 [MgO]/RO. The positive MAEE was also observed in activation energy and with elastic, bulk, and shear moduli with maxima similarly located at ~0.67-0.70 [MgO]/RO ratio. Glass structural explanations were proposed for the MAEE observed in the hardness data. Known Mg^{2+} characteristics, higher CFS compared to Ca^{2+} and capability as a glass former, contribute for the MAEE with balanced Ca^{2+} cations. For instance, NBO numbers are higher at the CaO rich composition end while strong bonded Mg-O exist at the other end.

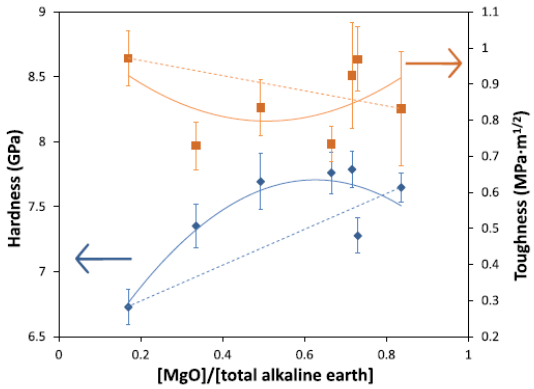

Figure II.12. Vickers hardness as a function of relative alkaline earth ratio.[73]

II.3 References

1. Seger HA, editor. The Collected Writings of Hermann August Seger: Chemical Publishing Company; 1902.

2. Carty W, Katz M, Gill J. Unity Molecular Formula Approach to Glaze Development. Ceram Eng Sci Proc. 2000;21(2):95-109.

3. Varshneya AK. Fundamentals of Inorganic Glasses. Sheffield: The Society of Glass Technology; 2006.

4. Shelby JE. Introduction to Glass Science and Technology, 2nd Edition. Chmbridge, UK: The Royal Society of Chemistry; 2005.

5. Agnello G, Youngman R, Lamberson L, Smith N, LaCourse W, Cormack AN. Bulk Structures of Cilica-Rich Calcium Aluminosulphate (CAS) Glasses Along the Molar $CaO/Al_2O_3 = 1$ Join via Molecular Dynamics (MD) Simulation. J Non-Cryst Solids. 2019;519:119450-1 - 11.

6. Kelsey KE, Stebbins JF, Singer DM, Jr. GEB, Mosenfelder JL, Asimow PD. Cation Field Strength Effects on High Pressure Aluminosilicate Glass Structure: Multinuclear NMR and La XAFS Results. Geochimi Cosmochim Acta. 2009;73:3914-33.

7. Kelsey KE, Allwarde JR, Stebbins JF. Ca-Mg Mixing in Aluminosilicate Glasses: An Anvestigation using 17O MAS and 3QMAS and ^{27}Al MAS NMR. J Non-Cryst Solids. 2008;354:4644-3653.

8. Guignard M, Cormier L. Environments of Mg an Al in $MgO-Al_2O_3-SiO_2$ Glasses: A Study Coupling Neutron and X-ray Diffraction an Reverse Monte Carlo Modeling. Chem Geol. 2008;256:111-8.

9. Arnaud Q, Caurant D, Majérus O, Lenoir M, Dussossoy J-L, Charpentier T, et al. Structural Study of a Rare Earth-Rich Aluminoborosillicate Glass. Proceedings of the XXIst International Congress of Glass. 2011.

10. Losq C, Neuville DR, Florian P, Henderson GS, Massiot D. The Role of Al^{3+} on Rheology and Structural Changes in Sodium Silicate and Aluminosilicate Glasses and Melts. Geochimi Cosmochim Acta. 2014;126:495-517.

11. Neuville DR, Cormier L, Montouillout V, Massiot D. Local Al Site Distribution in Aluminosilicate Glasses by ^{27}Al MAS NMR. J Non-Cryst Solids. 2007;353:180-4.

12. Neuville DR, Cormier L, Flank A-M, Briois V, Massiot D. Al Speciation and Ca Environment in Calcium Aluminisilicate Glasses and Crystals by Al and Ca K-edge X-ray Absorption Spectroscopy. Chem Geol. 2004;213:153-63.

13. Neuville DR, Cormier L, Massiot D. Al Environment in Tectosilicate and Peraluminous Glasses: A ^{27}Al MQ-MAS NMR Raman, and XANES Investigation. Geochimi Cosmochim Acta. 2004;68(24):5071-7079.

14. Neuville DR, Cormier L, Massiot D. Al Coordination and Speciation in Calcium Aluminosilicate Glasses: Effects of Composition Determined by ^{27}Al MQ-MAS NMR and Raman Spectroscopy. Chem Geol. 2006;229:173-85.

15. Allwardt JR, Stebbins JF, Schmidit BC, Frost DJ, Withers AC, Hirschmann MM. Aluminum Coordination and the Densification of High-Pressure Aluminosilicate Glasses. Am Mineral. 2005;90:1218-22.

16. J.F. Stebbins, J.V. Oglesby, Kroeker S. Oxygen Triclusters in Crystalline $CaAl^4O^7$ (Grossite) and in Calcium Aluminosilicate Glasses:^{17}O NMR. Am Mineral. 2001;86:1307–11.

17. Kaneshi K, Stebbins JF. In Situ High Temperature ^{27}Al NMR Study of Structure and Dynamics in a Calcium Aluminosilicate Glass Melt. J Non-Cryst Solids. 2007;353:4001-10.

18. Schaller T, Stebbins JF. The Structural Role of Lanthanum and Yttrium in Aluminosilicate Glasses: A ^{27}Al and 17O MAS NMR Study. J Phys Chem B. 1998;102:10690-7.

19. Stebbins JF, Dubinsky EV, Kanehashi K, Kelsey KE. Temerature Effects on Non-Bridging Oxygen and Aluminum Coordination Number in Calcium Aluminosilicate Glasses and Melts. Geochimi Cosmochim Acta. 2008;72:910-25.

20. Stebbins JF, Xu Z. NMR Evidence for Excess Non-Bridging Oxygen in an Aluminosilicate Glass. Nature. 1997;390(6):60-2.

21. Thompson LM, Stebbins JF. Non-Stoichiometric Non-Bridging Oxygens and Five-Coordinated Aluminum in Alkaline Earth Aluminosilicate Glases: Effect of Modifier Cation Size. J Non-Cryst Solids. 2012;358:1783-9.

22. Kanehashi K, Stebiins JF. In Situ High Temperature ^{27}Al NMR Strudy of Structure an Dynamics in a Calcium Aluminosilicate Glass and Melt. J Non-Cryst Solids. 2007;353:4001-10.

23. Kanehashi K. Structural Roles of Calcium in Alkaline and Alkaline-Earth Aluminosilicate Glasses by Solid-State ^{43}Ca, ^{17}O and ^{27}Al NMR. Solid State Nucl Magn Reson. 2017;84:158-63.

24. Kucharczyk S, Zajac M, Stabler C, Thomsen RM, Haha MB, Skibsted J, et al. Structure and Reactivity of Synthetic $CaO-Al_2O_3-SiO_2$ Glasses. Cem Concr Res. 2019;120:77-91.

25. Stamboulis A, Hill RG, Law RV. Characterization of the Structure of Calcium Alumino-Silicate and Calcium Flouro-AluminoSilicate Glasses by Magic Angle Spinning Nuclear Magnetic Resonance (MAS-NMR). J Non-Cryst Solids. 2004;333:101-7.

26. Lussier AJ, Aguiar PM, Michaelis VK, Kroeker S, Hawthorne FC. The Occurrence of Tetrahedrally Coordicated Al and B in Tourmaline: An ^{11}B and ^{27}Al MAS NMR Study. Am Mineral. 2009;94:785-92.

27. Fechtelkord M. Sepctroscopic Methods in Mineralogy. Beran A, Libowistzky E, editors. Budapest: Eotvos University press; 2004.

28. Bryce B. Calcium Binding Environments Probed by $^{43}CaNMR$ Spectroscopy. J Chem Soc Dalton Trans. 2010;39:8593.

29. Youngman R. NMR Spectroscopy in Glass Science: A Review of the Elements. Maerials. 2018;11(4):476.

30. Zhang P, Grandinetti PJ, Stebbins JF. Anionic Species Determination in $CaSiO_3$ Glass using Two-demimensional ^{29}Si NMR. J Phys Chem B. 1997;101:4004-8.

31. Doremus RH. Glsas Scinece. New York: A Wiley-Interscience Publication; 1973.

32. Sato RK, McMillan PF. A Structural Inverstigation of High Alumina Glasses in the $CaO-Al_2O_3-SiO_2$ System via Raman and Magic Angle Spinning Nuclear Magnetic Resonance Spectroscopy. Phys Chem Glasses. 1991;32(4):149-56.

33. Engelhardt G, Nofz M, Forkel K, Wihsmann FG, Magi M, Samosan A, et al. Structural Studies of Calcium Aluminosilicate Glasses by High Resolution Solid State ^{29}Si and ^{27}Al Magic Angle Spinning Unclear Magnetic Resonance. Phys Chem Glasses. 1985;26(5).

34. Schmücker M, Schnieder H. New Evidence for Tetrahedral Triclusters in Aluminosilicate Glasses. J Non-Cryst Solids. 2002;311:211-5.

35. Thompson LM, Stebbins JF. Non-bridging Oxygen and High-Coordinated Aluminum in Metaluminuous and Peraluminous Calcium and Potassium Aluminosilicate Glasses: High Resolution 17O and ^{27}Al MAS NMR Results. Am Mineral. 2011;96:841-53.

36. Allwardt JR, Stebbins JF, Terasaki H, Du L-S, Frost DJ, Withers AC, et al. Effect of Structural Transitions on Properties of High Pressure Silicate Melts: ^{27}Al NMR, Glass Densities, and Melt Viscosities. Am Mineral. 2007;92(1093-1104).

37. Stevensson B, Edén M. Structural Rationalization of the Microhardness Trends of Rare-Earth Aluminosilicate Glasses: Interplay Between the RE^{3+} Field-Strength and the Aluminum Coordinations. J Non-Cryst Solids. 2013;378:163-7.

38. Iftekhar S, Grins J, Gunwidjaja PN, Edén M. Glass Formation and Structure-Property-Composition Relations of the RE_2O_3-Al_2O_3-SiO_2 (RE = La, Y, Lu, Sc) Systems. J Am Ceram Soc. 2011;94(8):2429-35.

39. S. Tanabe, Hirao K, Soga N. Elastic Properties and Molar Volume of Rare-Earth Aluminosilicate Glasses. J Am Ceram Soc. 1992;75(3):503-6.

40. Frorian P, Sadiki N, Massiot D, Coutures JP. ^{27}Al NMR Study of the Structure of Lanthanum- and Yttrium-Based Aluminosilicate Glasses and Melts. J Phys Chem B. 2007;111:9747-57.

41. Stebbins JF, Farnan I. Effects of High Tempeature on Silicate Liquid Structure: A Multinuclear NMR Study. Science. 1992;255:586-9.

42. Hennet L, Drewitt JWE, Neuville DR, Cristiglio V, Kozaily J, Brassamin S, et al. Neutron Diffraction of Calcium Aluminosilicate Glasses and Melts. J Non-Cryst Solids. 2016;451:89-93.

43. Loewenstein W. The Distribution of Aluminum in the Tetrahedra of Silicates and Aluminates. Am Mineral. 1954;39(1-2):92-6.

44. Lee SK, Stebbins JF. Al-O-Al and Si-O-Si Sites in Framework Aluminosilicate Glasses with Si/Al = 1: Quantification of Framework Disorder. J Non-Cryst Solids. 2000;270:260-4.

45. Yildirim E, Fupree R. Investigation of Al-O-Al Sites in an Na-Aluminosilicate Glass. Bull Mater Sci 2004;27:269-72.

46. Takahashi S, Neuville DR, Takebe H. Thermal Properties, Density and Structure of Percalcic and Peraluminus CaO-Al_2O_3-SiO_2 Glases. J Non-Cryst Solids. 2015;411:5-12.

47. Kuchaeczyk S, Sitarz M, Zajac M, Deja J. The Effect of CaO/SiO_2 Molar Ratio of CaO-Al_2O_3-SiO_2 Glasses on Their Strucure and Reactivity in Alkali Activatied System. Spectrochim Acta Part A. 2018;194:163-71.

48. Barlet M, Delaye J, Charpentier T, Gennisson M, Bonamy D, Rouxel T, et al. Hardness and Toughness of Sodium Borosilicate Glasses via Vickers Indentations. J Non-Cryst Solids. 2015;417-418:66-79.

49. Hand RJ, Tadjiev DR. Mechanical Properties of Silicate Glasses as a Funtion of Composition. J Non-crystaline solids. 2010;356:2417-23.

50. Calahoo C, Zwanziger JW. The Mixed Modifier Effect in Ionic Conductivity and Mechanical Properties for $xMgO$-$(50-x)CaO$-$50SiO_2$ Glasses. J Non-Cryst Solids. 2017;460:6-18.

51. Januchta K. Structural Perspective on Fracture in Oxide Glasses [Ph. D. Thesis]: Aalborg University, Denmark; 2019.

52. Quinn GD, Bridt RC. On the Vickers Indentation Fracture Toughness Test. J Am Ceram Soc. 2007;90(3):673-80.

53. Huang Y, Zhang F, Hwang KC, Nix WD, Pharr GM, Feng G. A Model of Size Effects in Nano-indentation. J Mech Phys Solids. 2006;54:1668-86.

54. Vincent S, Murty BS, Kramer MJ, Bhatt J. Micro and Nano Indentation Studies on $Zr_{60}Cu_{10}Al_{15}Ni_{15}$ Bulk Metallic Glass. Mater Des. 2015;65:98-103.

55. Manika H, Maniks J. Size Effects in Micro- and Nanoscale Indentation. Acta Mater. 2006;54:2049-56.

56. Suzuki K, Benino Y, Fujiwara T, Komatsu T. Densification Energy during Nanoindentation of Silica Glass. J Am Ceram Soc. 2002;85(12):3102-4.

57. Bull SJ, Page TF, Yoffe EH. An Explanation of the Indentation Size Effect in Ceramics. Philos Mag Lett 1989;59(6):281-8.

58. Nix W, Gao H. Indentation Size Effects in Crystalline Materials: A Law for Strain Gradient Plasticity. J Mech Phys Solids. 1998;46(3).

59. Oliver EC, pharr GM. An Improved Technique for Determining Hardness and Elastic Modulus Using Load and Displacement Sensing Indentation Experiments. J Mater Res. 2004;19(1):3-20.

60. Ghorbal G, Tricoteauz A, Thuault A, Louis G, Chicot D. Mechanical Characterization of Brittle Materials using Instrumented Indentation with Knoop Indenter. Mech Mater. 2017;108:58-67.

61. Athanasiou V, Zervaki AD, Papamichos E, Giannakopoulos A. The Use of Knoop Indentation for the Assessment of Elastic Properties of Mortars and Natural Stones. Int J Rock Mech Min Sci. 2016;83:241-7.

62. Chicot D, Mercier D, Roudet F, Silva K, Staia MH, Lesage J. Comparison of Instrumented Knoop and Vickers Hardness Mreasurements on Various Soft Materials and Hard Ceramics. J Eur Ceram Soc. 2007;27:1905-11.

63. Gong J, Wnag J, Guan Z. A Comparison between Knoop and Vikers Hardness of Silicon Nitride Ceramics. Mater Lett. 2002;56:941-4.

64. Ghorbal GB, Tricoteauz A, Thuault A, Louis G, Chicot D. Comparion of Conventional Knoop and Vickers Hardness of Cermics Materials. J Eur Ceram Soc. 2017;37:2531-5.

65. Rouxel T, Ji H, Guin JP, Augereau F, Ruffle B. Indentation Deformation Mechanism in Glass: Densification versus Shear Flow. J Appl Phys. 2010;107:094903-1 - 5.

66. Lamberson L. Influence of Atomic Structure on Plastic Deformation in Tectosilicate Calcium-Aluminosilicate, Magnesium-Aluminosilicate, and Calcium-Galliosilicate Glasses [Ph.D. Thesis]: Cornell University; 2016.

67. Steimacher A, Astrath NGC, Novatski A, Pedrochi F, Bento AC, Baesso ML, et al. Characterization of Thermo-Optical and Mechanoical Properties of Calcium Aluminosilicate Glasses. J Non-Cryst Solids. 2006;352:3613-7.

68. Eagan R, Swearengen JC. Effect of Composition on the Mechanical Properteis of Aluminosilicate and Borosilicate Glasses. J Am Ceram Soc. 1978;61(1-2):27-30.

69. Pönitzsch A, Nofz M, Wondraczek L, Deubener J. Bulk Elastic Properties, Hardness and Fatigue of Calcium Aluminosilicate Glasses in the Intermediate-Silica Range. J Non-Cryst Solids. 2016;434:1-12.

70. Tiegel M, Hosseinabadi R, Kuhn S, Herrmann A, Russel C. Young's Modulus, Vickers Hardness and Indentation Fracture Toughness of Alumino Silicate Glasses. Ceram Int. 2015;41:7267-75.

71. Weigel C, Losq CL, Vialla R, Dupas C, Clément S, Neuville DR, et al. Elastic Moduli of $XAlSiO_4$ Aluminosilicate Glasses: Effects of Charge-Balancing Cations. J Non-Cryst Solids. 2016;447:267-72.

72. Kjeldsen J, Smedskjaer MM, Mauro JC, Yue Y. On the Origin of the Mixed Alkali Effect on Indentation in Silicate Glasses. J Non-Cryst Solids. 2014;406:22–6.

73. Calahoo C, Zwanziger JW. The Mixed Modifier Effect in Ionic Conductivity and Mechanical Properties for $xMgO-(50-x)CaO-SiO_2$ Glasses. J Non-Cryst Solids. 2017;460:6-18.

74. Griebenow K, Bragatto B, Kamitsos EI, Wondraczek L. Mixed-Modifier Effect in Alkaline Earth Metaphosphate Glasses. J Non-Cryst Solids. 2018;481:447-56.

75. Maass P. Towards a Theory for the Mixed Alkali Effect in Glasses. J Non-Cryst Solids. 1999;255:35-46.

76. Kjeldsen J, Smedskjaer MM, Mauro JC, Youngman RE, Huang L, Yue Y. Mixed Alkaline Earth Effect in Sodium Aluminosilicate Glasses. J Non-Cryst Solids. 2013:61-8.

77. Kjeldsen J, Smedskjaer MM, Potuzak Ml, Yue Y. Role of Elastic Deformation in Determining the Mixed Alkaline Earth Effect of Hardness in Silicate Glasses. J Appl Phys. 2015;117:034903-1 -7.

78. Kjeldsen J, Smedskjaer MM, Mauro JC, Youngman RE, Huang L, Yue Y. Mixed Alkaline Earth Effect in Sodium Aluminosilicate Glasses. J Non-Cryst Solids. 2013;369:61-8.

79. Zhang C, Cao W, Fan T, Zhang D. Fabrication and Formation Mechanism of in-situ AlN and Mg_2Si Particles-Reinforced Mg Matrix Composites. Key Eng Mater. 2007;351:151-5.

80. Killinc E, Hand R. Mechanical Properties of Soda-Lime-Silica Glasses with Varying Alkaline Earth Contents. J Non-Cryst Solids. 2015;429:19-197.

III THE GLASS FORMATION BOUNDARY IN ALUMINOSILICATE SYSTEMS

III.1 Abstract

The glass formation boundary defines a chemistry space within which compositions prefer to remain amorphous when cooled from a melt. Work on alkali aluminosilicates and alkaline earth aluminosilicates demonstrated that the alumina edge of the glass formation boundary was independent of cooling rate and defined by a fixed molar ratio of 1.2 (±0.1) moles of Al_2O_3 to 1.0 moles of flux – R_2O (Na_2O or K_2O) or RO (CaO or MgO) – over a broad range of silica levels. These results were consistent with the glass composition in porcelains, the grain boundary chemistry in sintered alumina, and gloss-matte boundary in whiteware glazes with mixed fluxes.

Key Words: Glass formation, aluminosilicate glasses

III.2 Introduction

The glass formation boundary (GFB) is defined as the chemistry limit for compositions that would prefer to remain amorphous on cooling rather than crystallize. Commercial glasses fall well within the glass formation region, usually located in the vicinity of eutectics to facilitate melting and fining processes. The melting temperature isotherms in flux-alumina-silica phase diagrams for pure end-point ternary systems can be used to predict the melting temperatures of the initial compositions prior to glass formation.

The concept of a GFB was originally introduced for glass-ceramic applications, where the compositions lie outside of the glass formation region.[1] The glass formation region in the MgO-Al_2O_3-SiO_2 system is shown in Figure 1. As presented this diagram would initially appear to be incorrect as it would be expected that the glass formation region would extend to the pure silica endpoint, suggesting the upper boundary may have been restricted by furnace temperature limitations, leading to the hypothesis that crystalline components present after cooling or quenching may have been unmelted batch materials. Our work, however, confirms this low alumina-high silica limit, but a second glass formation region should still exist in the high-silica (in the low MgO and Al_2O_3 region).

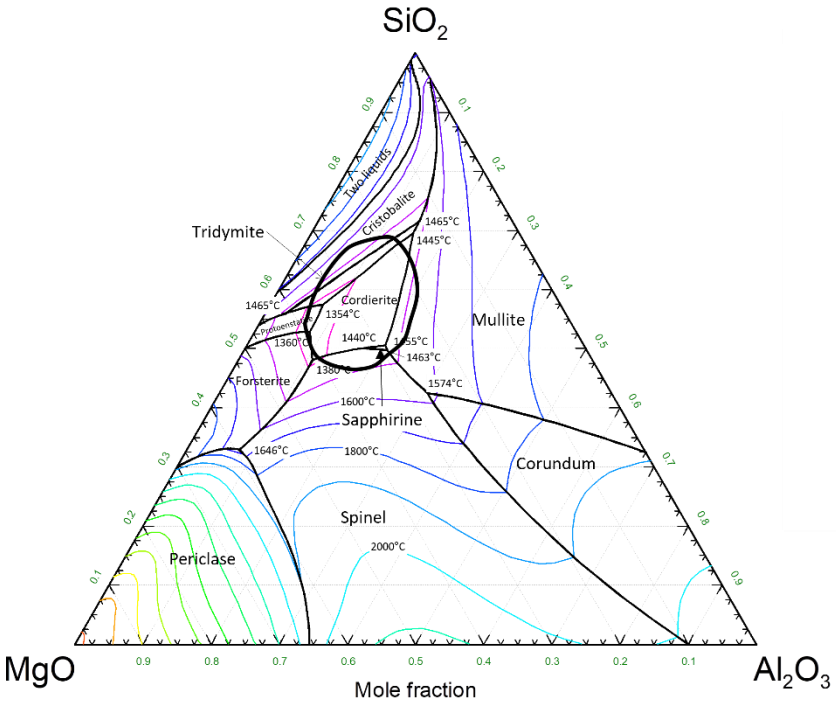

Figure III.1. The defined glass forming region (circle) for magnesium aluminosilicates (molar basis, replotted on the MgO-Al_2O_3-SiO_2 phase diagram generated using FactSage).[1]

The Seger or Unity molecular formula (UMF)

All glass compositions in this study are presented in the format of a Seger formula or Unity Molecular Formula (UMF) – a molar ratio approach for describing the chemistry of glass in which the chemistry is normalized to the moles of flux.[2, 3] Seger grouped oxides by the cation to oxygen ratio, postulating that the structure of the oxides predicted their role in glass formation. For simple aluminosilicate glasses, this approach is reasonable, with fluxes being defined as R_2O (Li_2O, Na_2O, K_2O, etc.) and RO (MgO, CaO, SrO, and BaO, as well as FeO, CuO, ZnO, etc.) and fluxes are additive on a molar basis. Intermediates are represented as R_2O_3 and include Al_2O_3 and Fe_2O_3. RO_2 represents the glass formers, specifically SiO_2. This approach breaks down for B_2O_3, which is a glass former, and for TiO_2 and ZrO_2 which are not good glass formers. Overall, Seger formulas offer an excellent format to describe aluminosilicate glass chemistry. Alumina

and silica levels are then represented by the molar ratio to flux, so a glass obtained directly from orthoclase (potassium feldspar) would have the chemistry $K_2O \cdot Al_2O_3 \cdot 6SiO_2$, or 1.0:1.0:6.0 with one mole of flux, one mole of alumina and six moles of silica.

Glass Formation in Porcelain and Whiteware Glazes

An extensive investigation of porcelains, both modern commercial compositions and ancient Asian ceramics, demonstrates that the GFB is independent of heating rate, peak temperature, and soak time at temperature. These results also indicate that the GFB is unaffected by cooling rates that range from ~0.5 K/min (for high-tension electrical insulators with an overall cycle time of 96 hours, incorporating a 3-hour soak at a peak temperature of ~1300°C) to ~60 K/min for fast-fire porcelain tile (50 minutes from cold-to-cold with a six-minute dwell at ~1250°C).[4-12] In these studies the GFB comprised a fixed alumina level that was independent of the flux chemistry. It was also demonstrated that glass formation was independent of heating rate and that quartz dissolution progresses linearly with temperature at a constant soak time, but with the logarithm of soak time at a constant temperature.[10]

Porcelain glazes commonly contain mixed fluxes, typically in the range of 0.3 R_2O + 0.7 RO and matte glaze compositions lie outside of the glass formation boundary. The glass formation boundary was consistent with a fixed ratio of flux:alumina in the high silica region, but the flux:alumina ratio reduces to eventually close off around a 1:1 flux:silica in mixed alkali + alkaline earth (R_2O + RO) systems. Glaze compositions that lie outside of the GFB crystallize on cooling in a manner similar to glass-ceramics, with the crystallization products consistent with phase diagram predictions, forming robust matte glazes that are independent of firing conditions provided the peak heat treatment temperatures are sufficient to melt the glaze composition.[13] This is consistent with early work by Stull in the mapping of glaze compositions (over a narrower chemistry range).[14]

Glass Formation in Alkali and Alkaline Earth Aluminosilicates

To verify the glass formation boundary observations in porcelains, a broad range of compositions were prepared from carbonates and oxides in the alkali and alkaline earth

aluminosilicates. In addition, work on the grain boundary chemistry of liquid-phase sintered alumina, in the CaO-Al_2O_3-SiO_2 system, demonstrated that the grain boundary chemistry resides on the GFB.[15]

When combined, these results all indicated that the alumina saturation level in aluminosilicate glasses was consistently 1.2 moles of Al_2O_3 per mole of flux and that a broad range of SiO_2 levels were observed in systems composed of alkali and CaO, but the silica range was narrower when the flux was MgO.

III.3 Experimental procedure

III.3.1 *Glass chemistry in porcelain*

Twenty-four porcelain bodies were obtained from dinnerware, electrical insulator, and sanitaryware manufacturers, and from laboratory compositions (Table I). The chemistry of each body was measured using ICP by an external lab (ICP-ES, Acme Analytical Laboratories Ltd., Vancouver, BC, Canada). These compositions all reside within the mullite phase field.

The porcelain samples were soaked at 1100°C to 1400°C, in 50K intervals, with soak times ranging from 0.1 hours (six minutes) to 100 hours at the peak temperatures. Heating rates varied from 5K/min to 60K/min, but no dependence on heating rate was observed. After the soak at peak temperature the furnace was shut off (for an uncontrolled cooling cycle). Samples were split with one half retained for chemical analysis and the other half analyzed via quantitative XRD analysis for mineralogy. The porcelain glass chemistry was determined by subtracting the amount of the crystalline species from the overall body chemistry.

Table III-i. Chemical compositions (mass %) of the evaluated bodies.

Composition	SiO_2	Al_2O_3	Na_2O	K_2O	MgO	CaO
1	21.17	3.60	0.24	0.61	0.07	0.08
2	23.73	5.50	0.22	0.59	0.11	0.08
3	15.04	2.99	0.27	0.63	0.04	0.06
4	23.52	5.28	0.22	0.60	0.10	0.08
5	23.73	5.13	0.24	0.59	0.09	0.08
6	23.72	5.25	0.24	0.57	0.10	0.09
7	20.24	3.46	0.24	0.60	0.08	0.08
8	20.03	3.44	0.23	0.58	0.09	0.10
9	17.55	3.05	0.28	0.52	0.07	0.13
10	22.65	5.01	0.22	0.58	0.10	0.10
11	14.66	2.93	0.26	0.62	0.04	0.08
12	22.97	5.10	0.22	0.59	0.10	0.09
13	20.78	3.52	0.26	0.56	0.08	0.10
14	24.60	5.45	0.20	0.62	0.10	0.09
15	17.72	2.99	0.23	0.62	0.06	0.09
16	14.97	3.83	0.25	0.61	0.05	0.09
17	12.70	3.68	0.36	0.18	0.04	0.42
18	23.69	3.64	0.51	0.27	0.05	0.18
19	10.92	7.58	0.53	0.26	0.05	0.16
20	11.17	2.58	0.69	0.23	0.04	0.05
21	19.21	5.13	0.65	0.24	0.05	0.06
22	19.33	5.18	0.65	0.24	0.05	0.06
23	18.89	5.06	0.64	0.24	0.05	0.06
24	14.97	3.83	0.25	0.61	0.05	0.09

Quantitative XRD analysis was conducted using an internal standard method with CaF_2 (Reagent grade, Fisher Scientific, Fair Lawn, NJ).[10, 16, 17] Volumetric calibration curves for mullite, quartz, and corundum, were generated using commercially available materials: mullite (Mulcoa 70, Imerys, Roswell, GA), quartz (325 Mesh Flint, Oglebay Norton Industrial Sands, Inc., Brady, TX), and corundum (HPA-0.5, Condea Vista Co., Ceralox Division). The mixing ratios of standard materials and the CaF_2 internal standard ranged from zero through 70 mass % in steps of 10% and subsequently converted to volume basis (using measured pycnometer densities). All analyses were performed using X-ray diffraction (Kristalloflex 81, D500, Siemens, Germany). The diffraction patterns were analyzed using XRD data analysis software (Jade, Version 7.1, Materials Data, Inc., Livermore, CA). Peak areas were measured and summed for three non-overlapping peaks for the crystalline phase of interest to generate calibration curves. The reliability of the

measurement was ±2% for mullite, ±3% for quartz, and ±1% for corundum (on a mass basis).[10, 16]

III.3.2 *Verification of the glass formation boundary with oxide melts.*

Alkali-Aluminosilicates:

For systematic verification of the glass formation boundary in alkali aluminosilicates, 25 compositions were prepared and melted from carbonates and oxide raw materials.[18] For alkali-aluminosilicates, twenty-five glass compositions were prepared with a 1:1 molar ratio of K_2O and Na_2O varying the molar ratios of Al_2O_3 and SiO_2. Potassium and sodium carbonates (Alfa Aesar, Tewksbury, MA) were blended with calcined alumina (A-10, Almatis, Leetsdale, PA) and quartz (Sil-co-Sil 52, U.S. Silica, Mapleton, PA) and the compositions are plotted on the R_2O-Al_2O_3-SiO_2 diagram in Figure 2a. Al_2O_3 ranged from 0.4 to 1.3 and SiO_2 from 2.0 to 8.0. For the 2.0 SiO_2 series, only 0.4 Al_2O_3 was prepared because of predicted high melting points.

Thirty-five gram batches were batched and then milled for one hour in a canister vibratory mill with alumina milling media. The compositions were melted in 40ml yttria stabilized zirconia (YSZ) crucibles at either 1400°C or 1600°C depending upon the predicted melting points from the phase diagram. All samples were heated at 3K/min to 900°C, held for one hour, then ramped up to the peak temperature at 5K/min. Melts were held for a one hour at temperature then cooled by shutting off the furnace (i.e., not quenched). Significant foaming was observed in the samples that formed glasses, so those samples were re-melted for 3 hours at 1500°C or 1700°C to improve uniformity, collapse the foam, and allow for fining. Melts that were transparent were verified to be X-ray amorphous using powder X-ray diffraction (D2 Phaser, Bruker, Madison, WI), indicating that the crystalline content must be below 0.1%.

Alkaline Earth-Aluminosilicates:

Similar to the alkali-aluminosilicates, RO-aluminosilicate batches were also prepared with $MgCO_3$ and $CaCO_3$ (Alfa Aesar, Tewksbury, MA), alumina and silica. The composition matrix is plotted in Figure 2b. To evaluate for mixed RO contributions calcium aluminosilicate (CAS) and magnesium aluminosilicate matrices (MAS) were prepared separately and blended in 20% increments. The minimum SiO_2 level was 1.0 to

avoid invert glass formation.[15] All prepared batches were melted for 2 hours at 1600°C. Glass forming compositions were identified via visual inspection and confirmed to be amorphous by XRD.

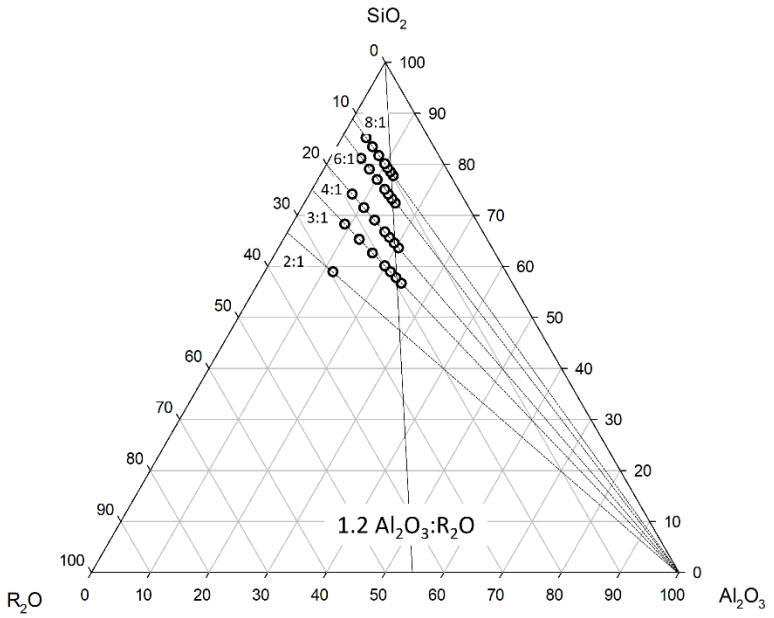

a)

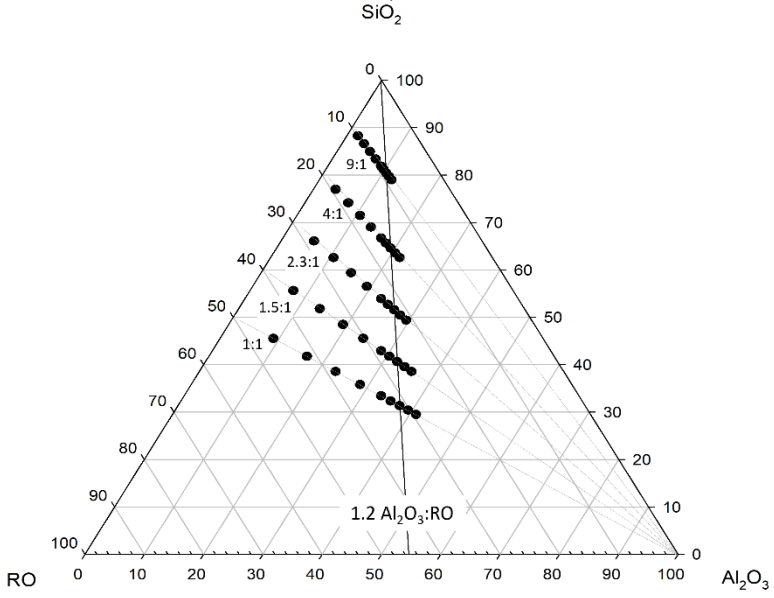

b)

Figure III.2. Compositions evaluated for glass formation within the (a) R_2O-Al_2O_3-SiO_2 and (b) RO-Al_2O_3-SiO_2 systems (mole-based). For RO-Al_2O_3-SiO_2 systems, CAS and MAS glasses were also blended.

III.4 Results and Discussion

III.4.1 Glass Chemistry in Porcelain

In the early stages of porcelain heat treatment, primary mullite forms in the relics of kaolinite particles around 1000°C.[19] Primary mullite crystallites nucleate secondary mullite that grows into the feldspar relicts as alkali diffuses from the melting feldspar particles into the eutectic liquid leaving behind a alumina-rich aluminosilicate melt.[20, 21] Mullite crystallizes simply because both meta-kaolin and all porcelain compositions reside in the mullite phase field. Quartz, added as a raw material, dissolves into the melt during heat treatment, initially slowly and rapidly at temperatures above 1200°C.[3, 10, 22]

The quartz found in heat treated porcelain bodies is unreacted quartz from the batch; it cannot be formed as a devitrification product. As temperature increases, quartz dissolution proceeds linearly with increasing temperature at a constant soak time. The dissolution of quartz at a constant temperature, however, progresses logarithmically with time, not linearly.[10] Interestingly, cristobalite is occasionally observed in porcelains, but tridymite, the predicted thermodynamically stable phase over the range of porcelain heat treatment temperatures, has never been reported in the literature nor found in any of our experimental results.

Above 1150°C the feldspar grains are completely dissolved and as the only source for flux in the system, control liquid formation in the body. Quantitative XRD analysis demonstrates that mullite starts precipitating slowly as low as 1100°C, but forms rapidly ≥1200°C.[10-12] A constant mullite level indicates that the alumina level in the glass must be constant. In this work the mullite composition is assumed to be $3Al_2O_3 \cdot 2SiO_2$.

As quartz dissolves the amount of liquid increases with the increase in silica in the melt. Subtracting the crystalline content from the overall body chemistry provides the chemistry of the glass phase. The glass chemistries for 24 commercial porcelain bodies fired at 8 temperatures are plotted on a ternary sub-system along with the overall body compositions. (Figure 3)

The silica level in the glass increases linearly with increasing temperature for commercial porcelain, a consequence of quartz dissolution.[12] Over the temperature range of 1200-1400°C the alumina level remains constant and is narrowly distributed at 1.2 ±0.1. The

silica level in the porcelain glass ranges from a minimum of ~10 to a maximum of ~17 over the temperature range of 1200°C to 1350°C.

Because the raw materials are produced directly from mined and beneficiated clay, feldspar and quartz, porcelains frequently contain small amounts of several oxide impurities. The largest contaminants are Fe and Ti oxides. Iron oxide is the most interesting as it can be present in either Fe^{2+} or Fe^{3+}, and thus is incorporated into the glass phase when Fe^{2+}, functioning as a flux (similar to Ca^{2+}), or as Fe^{3+} behaving similar to Al^{3+}, even to the point of substituting for Al^{3+} in mullite.[7] The measured impurity levels for Fe_2O_3 and TiO_2 in industrial porcelain bodies, however, are typically <1% and <0.5%, respectively, and can therefore be ignored with regards to their contribution to glass formation.

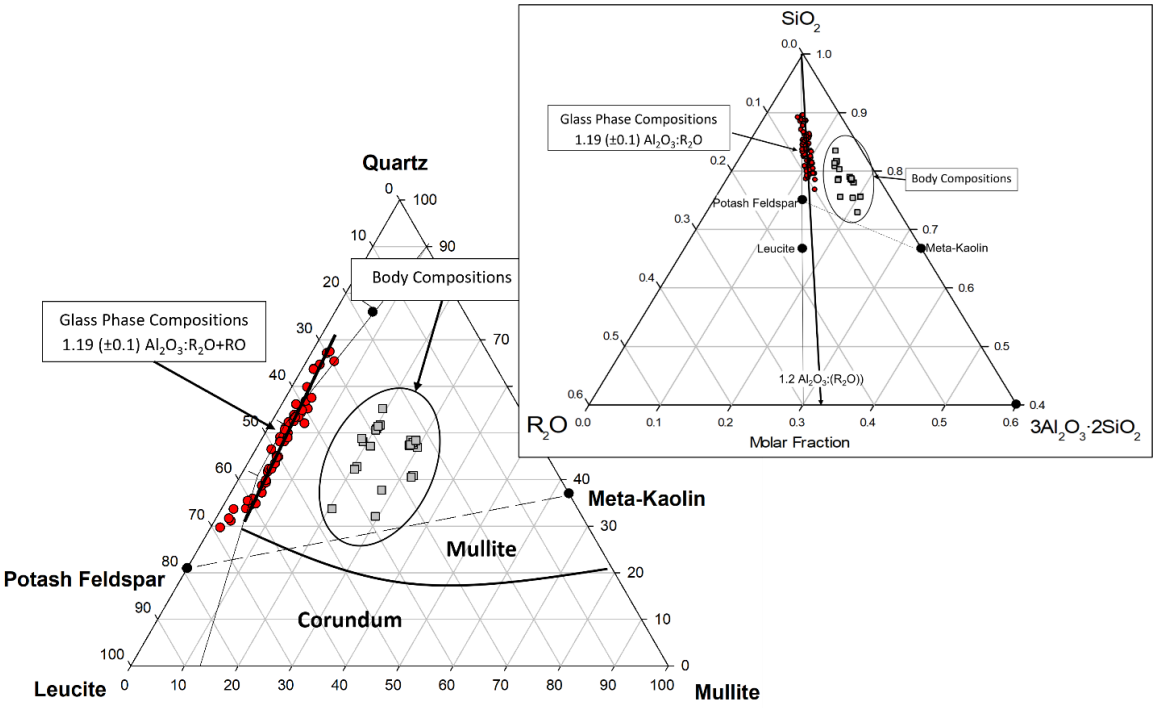

Figure III.3. The measured glass compositions in porcelain (circles), residing on the GFB, plotted on a modified subsection of the K_2O-Al_2O_3-SiO_2 phase diagram (weight based) and all contain ≥75 mole % SiO_2 (inset).[23] The chemical compositions of the porcelain bodies (squares) are identified.

III.4.2 The glass formation boundary in alkali aluminosilicates

The GFB was verified in R_2O-aluminosilicate compositions as plotted in Figure 4.[18] Melts that were transparent were verified to be X-ray amorphous using powder X-ray diffraction (D2 Phaser, Bruker, Madison, WI). Similar to the results observed for the porcelain glass phase, the GFB was consistently at an alumina level of 1.2 ±0.1. Samples with 1.3 Al_2O_3:RO all exhibited crystallization consistent with the phase diagram.

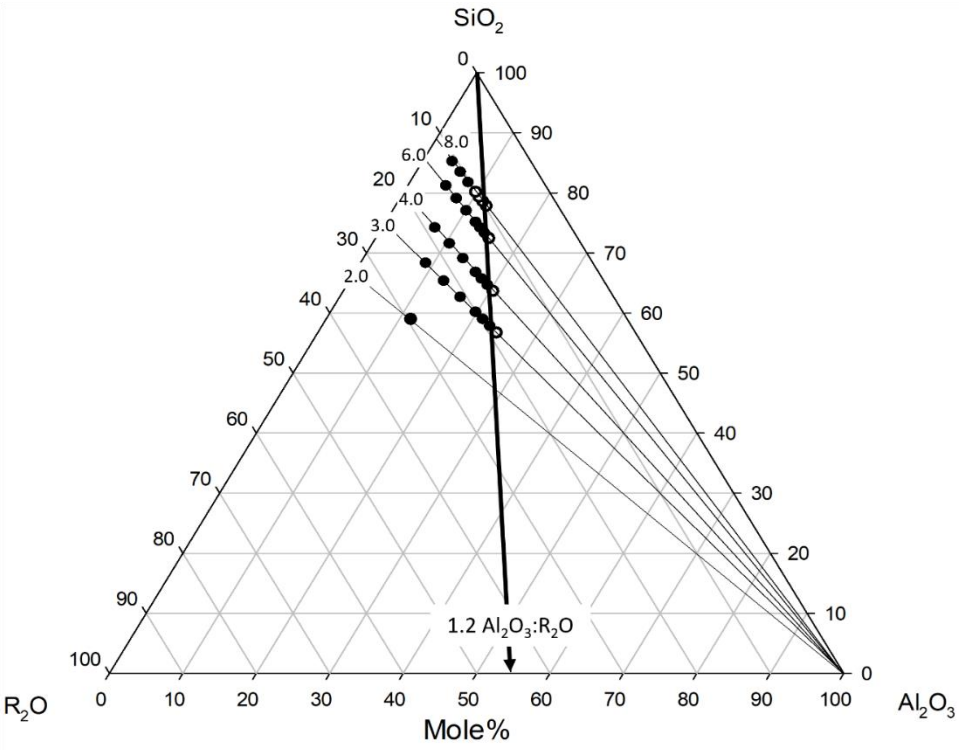

Figure III.4. Composition matrix evaluated and compositions which formed glass (filled circles).[18]

III.4.3 The glass formation boundary in alkaline earth aluminosilicates

The glass formation regions in alkaline earth aluminosilicate glasses were examined in CaO-Al_2O_3-SiO_2 (CAS) and MgO-Al_2O_3-SiO_2 (MAS) systems separately, and then over a range of CaO:MgO ratios. Overall, the glass formation region in CAS was significantly broader than that observed in the MAS system. The blending of the CAS and MAS resulted in a progressive reduction in the glass formation region with increasing MgO

content. Figure 5 shows the experimental compositions resulting in glass formation in each matrix. Compositions with silica levels of 9.0 did not melt within the temperature range employed in this study and were thus omitted. In the CAS system glass formation was observed in all compositions up to 1.2 Al_2O_3 over the silica range of 1.5-4.0. The range of silica levels observed to form glass in the MAS system was narrower, with a range of 2.3-4.0, but the alumina limit remained 1.2 Al_2O_3. An example of an XRD pattern and SEM image of precipitated mullite in the composition of $MgO{\cdot}1.3Al_2O_3{\cdot}4SiO_2$ is presented in Figure 6.

The glass formation boundary in the MAS system is significantly smaller than that of the CAS system in terms of SiO_2 levels. Perhaps as a consequence of more limited glass formation tendencies, exhibited as restricted stabilization temperature range (difference between T_g and T_c), the MAS system is widely used as a foundation for glass-ceramics with various crystallization agents.[24-26] A structural argument for the reduction in the glass formation region may be related to the oxygen coordination of magnesium ions within aluminosilicate glasses. Magnesium is proposed to sometimes exhibit tetrahedral oxygen coordination,[27-29] but more preferably 5-fold coordination, due to the size of Mg^{2+}. Ca^{2+} is too large however to exhibit either 4- or 6-fold coordination, preferring 8-fold coordination. When aluminum ions are presented in the system with magnesium ions, the tendency to form 4-fold coordinated Mg^{2+} is apparently enhanced indicated by the reduced average oxygen coordination number.[27, 30] In addition, the resulting structures are proposed to be more ordered, promoting crystallization over a broader range of compositions compared to the CAS system. The tendency towards crystallization minimizes the glass formation region, specifically constricting the silica GFB limit. Magnesium functions as a modifier in the vicinity of NBO in the eutectic compositions. When the melt composition moves away from the eutectic, $[MgO_4]^-$ tetrahedras distort the system resulting in stress that is accommodated by the formation of higher coordination Al.[30] The magnesium tetrahedra and $^{[5]}$Al bonding lead to less stability at high temperature and a reduction in the stabilization temperature. In addition to an increase in tetrahedrally coordinated Mg, the melting points increase with an increase in the alumina level.

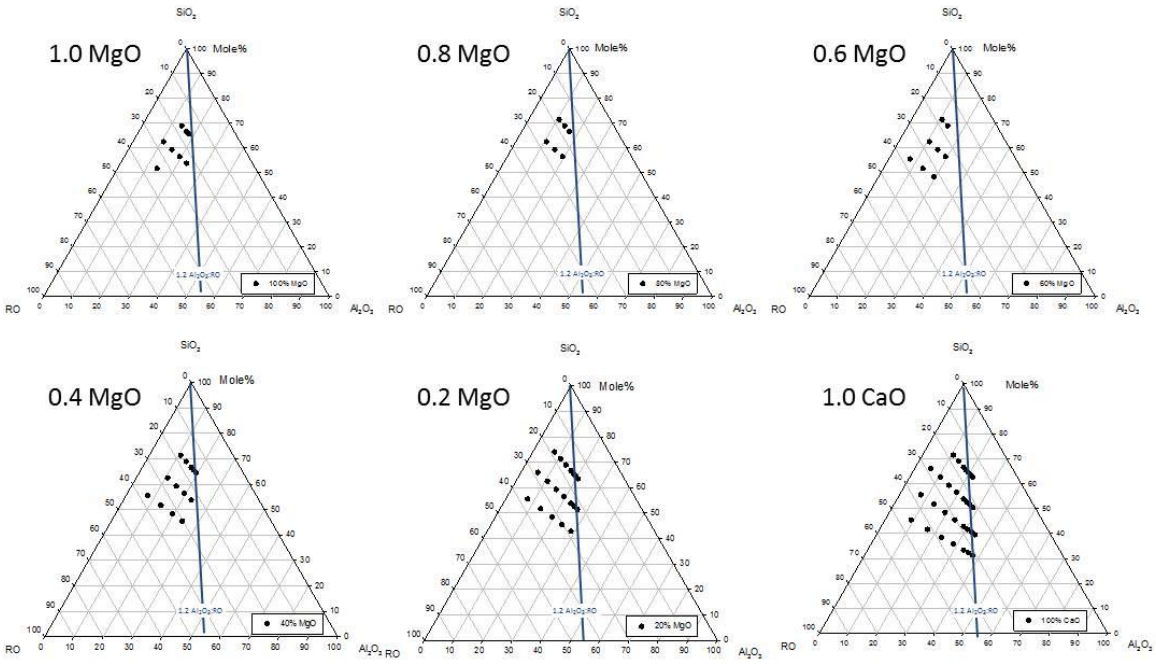

Figure III.5. Glass formation regions represented by experimental compositions that formed glasses in the CAS and MAS systems and their blends. Evaluated composition range was 1 to 9 SiO_2 and 0.2 to 1.4 Al_2O_3.

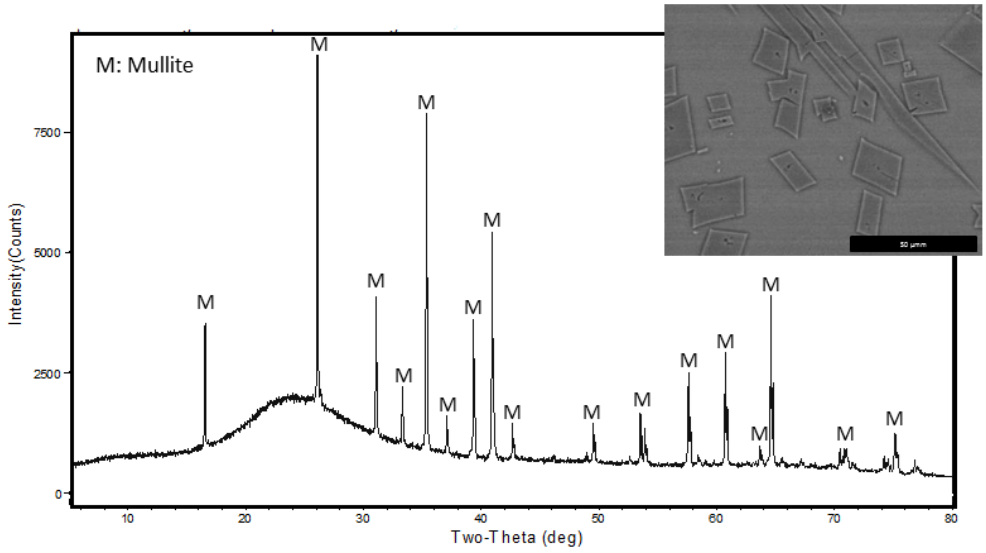

Figure III.6. XRD pattern of the sample $MgO:1.3Al_2O_3:4SiO_2$. SEM-BSE image showing precipitated mullite.

Work on the grain boundary chemistry for liquid-phase sintered alumina, in which the dopants were introduced over a range of CaO and SiO_2 levels, demonstrated that alumina will rapidly dissolve into the grain boundary.[5, 15] If the sintering temperature is sufficiently high, as predicted by the phase diagram, so that the grain boundary liquid composition lies outside of the glass formation region, the liquid in the grain boundary will crystallize as predicted by the phase diagram, but the remaining liquid will remain amorphous on cooling when the composition reaches the GFB. These results, and the GFB chemistry, were verified by TEM analysis, as summarized in Figure 7.[15] In the normal glass formation region, the GFB alumina level is consistently 1.2 at high silica levels (CaO<SiO_2). As the CaO:SiO_2 level approaches 1.0, decreasing from high SiO_2 levels, invert glasses form in which the amorphous phase is primarily composed of an amorphous calcium-aluminate matrix.[15]

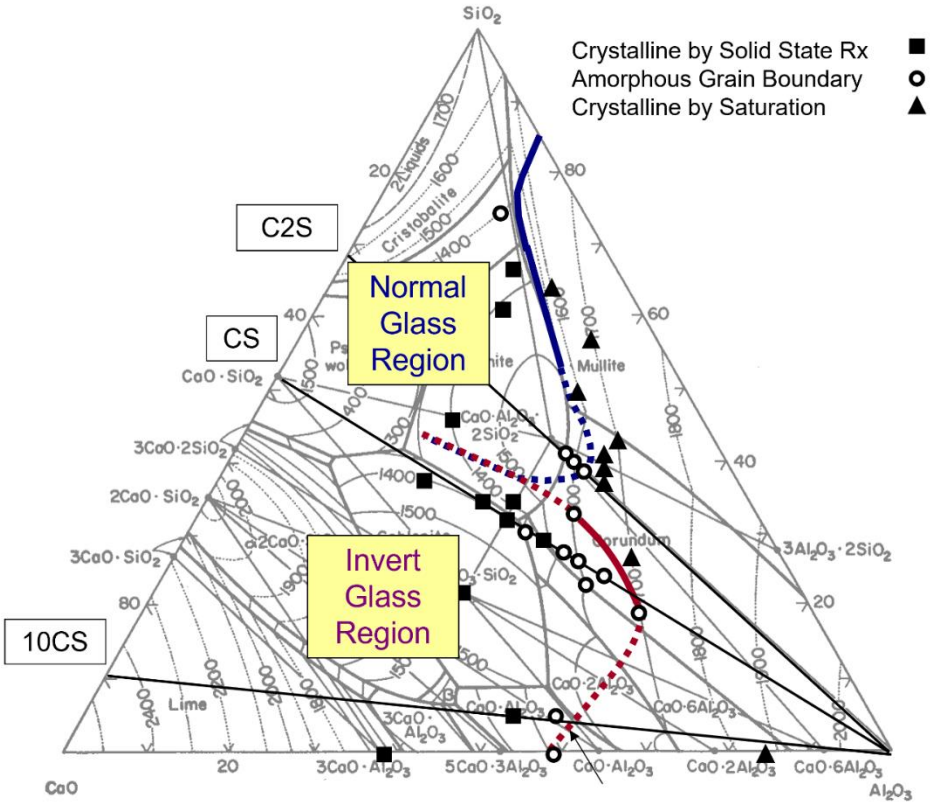

Figure III.7. Proposed glass formation boundary as observed in sintered alumina showing the normal and invert glass formation regions. [15]

Glass phase boundary in mixed alkali and alkaline earth aluminosilicates

Porcelain glazes are mixed flux systems containing both R_2O and RO. To understand crazing better, Stull mapped texture and crazing as a function of the molar ratios of silica and alumina, creating a map of glaze behavior (Figure 8).[14, 31] His results also showed a glass formation limit at a SiO_2:Al_2O_3 ratio of 5:1, represented as the boundary between bright glazes (gloss) and semi-mattes.

Subsequently, Quinlan revisited a portion of Stull's diagram to verify glaze behavior and to further define the glass formation boundary.[32] In his study, porcelain glazes were prepared, as indicated by the inset box in Figure 8, over the range of 0.2-0.6 Al_2O_3 and 1.8-5.0 SiO_2. Stull, however, only investigated glaze compositions up to 1.0 Al_2O_3, but his results show that mixed flux systems follow trends similar to that described previously for alkali and alkaline earth aluminosilicates. Both the observations of Stull and Quinlan support the idea that R_2O and RO fluxes are additive on a molar basis and can thus be combined when mapping the glass formation boundary for aluminosilicate glasses.

High alumina glazes, however, with SiO_2:Al_2O_3 ratios <5:1, are now referred to as "robust matte glazes" as the glaze textures are independent of firing conditions, provided peak temperature is sufficient to melt the applied glaze. These compositions lie outside of the glass formation boundary, and therefore crystallize on cooling to provide the matte surface texture, in a manner similar to glass-ceramics.[3, 32]

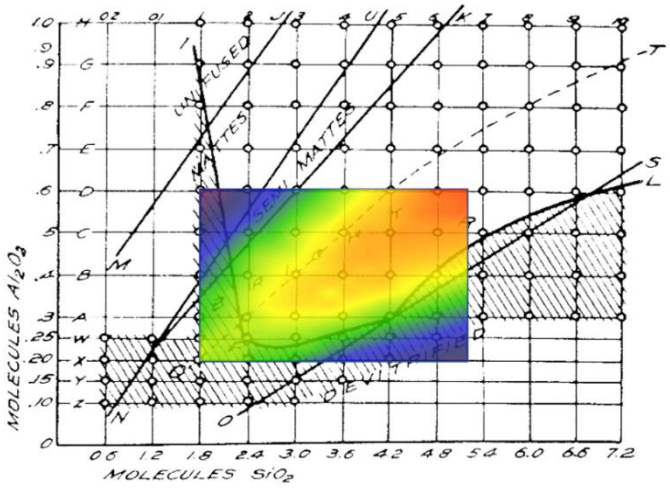

Figure III.8. A glaze texture map, at Cone 11 (~1315°C),based on the Seger formula approach with the fluxes composed of 0.3 K_2O:0.7 CaO) .[31] The "Semi Mattes"-"Bright" boundary (5:1 SiO_2:Al_2O_3) is the glass formation boundary in this system. The high silica mattes (bottom right quadrant of the diagram) are identified as "Devitrified", but these glazes are under-fired (partially melted). The experimental matrix of Quinlan is represented by the inserted box. The colors represent gloss meter data with red exhibiting the greatest reflectance (gloss glazes) and blue exhibiting poor reflectivity (i.e., matte glazes.)

To better interpret Stull's results, a ternary phase diagram of (0.3K_2O-0.7CaO)-Al_2O_3-SiO_2 system was generated using thermodynamic software (FactSage, version 8.0, Phase diagram module, FTOxid database, Thermfact and GTT-Technologies, Montreal, Quebec, Canada) as shown in Figure 9. When Stull's results are plotted on this diagram, the results map the glass formation boundary, as shown in Figure 9. Most of the glaze compositions are located in the tridymite, anorthite, wollastonite and leucite phase fields. The eutectic melt temperature at the intersection of feldspar, wollastonite, and tridymite phase fields is calculated to be 1171°C at the intersection of the anorthite, wollastonite, and tridymite phase fields. Stull, understandably for the time, mis-labeled the high silica glaze region, with SiO_2:Al_2O_3 ratios exceeding ~12:1, as "devitrified," indicating crystallization from the melt. Evaluation of glazes in that region indicated that these glazes were incompletely melted, as evidenced by the presence of quartz, which could not have resulted from devitrification – quartz can only be present as an unmelted batch

material. Replotting Stull's results on the phase diagram confirms that these compositions are refractory possessing high melting temperatures.

In Quinlan's work, the GFB in the mid-silica region, illustrated as the dotted line in Figure 10, could not be precisely defined because of the continuous anorthite–albite solid solution series ($CaO{\cdot}Al_2O_3{\cdot}2SiO_2$–$Na_2O{\cdot}Al_2O_3{\cdot}6SiO_2$) and the variation in silica level in the feldspar endpoints.

The glass formation regions for alkali, alkaline earth, and mixed alkali-alkaline earth fluxes are presented in Figure 11. The GFB for alumina was 1.2 in both R_2O aluminosilicate and RO aluminosilicate glasses over a broad silica range. The silica levels for glass formation, however, varied depending on the flux composition, with the broadest range of silica levels observed in the CAS system (1 to 4.3) and the narrowest range in the MAS system (2.3 to 4.0). In mixed alkali-alkaline earth fluxed compositions, glass formation extended over a broad range of silica levels similar to that observed with CAS.

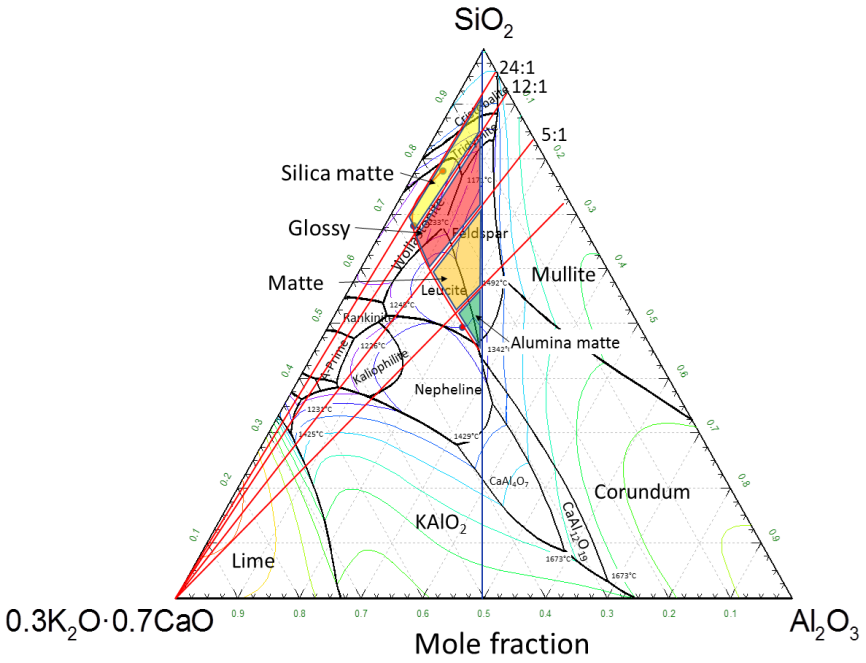

Figure III.9. The results of glaze tests, based on Figure 5, replotted on the $0.3K_2O{\cdot}0.7CaO$-Al_2O_3-SiO_2 phase diagram.

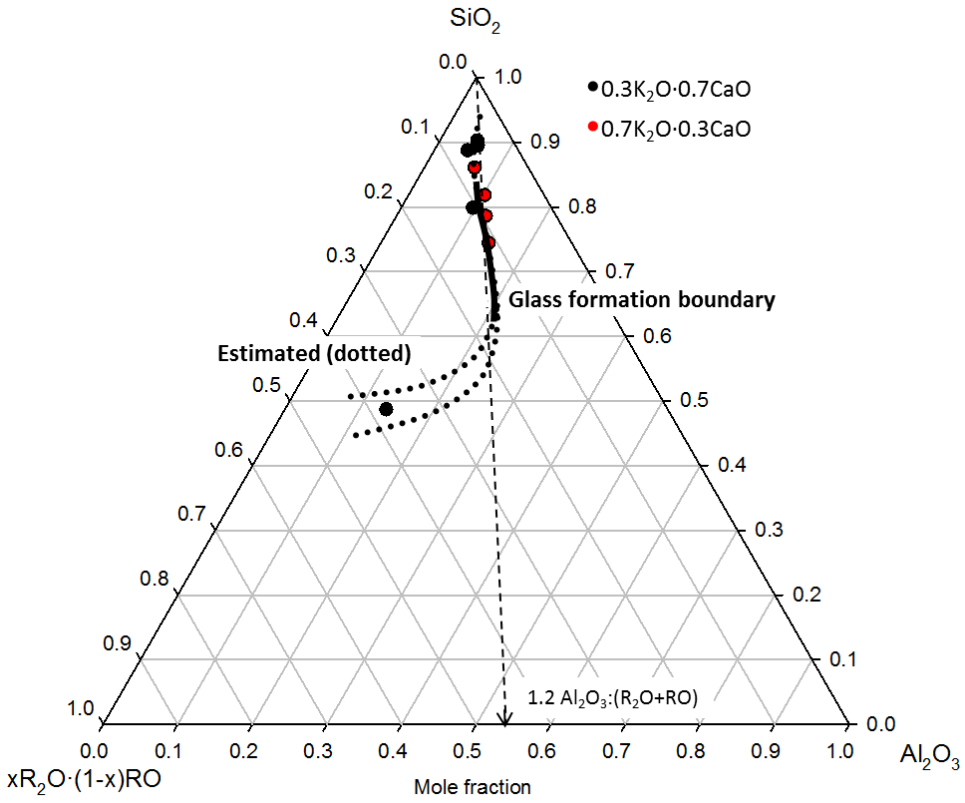

Figure III.10. Measured and calculated glass formation boundary replotted from work on porcelain glazes.[32]

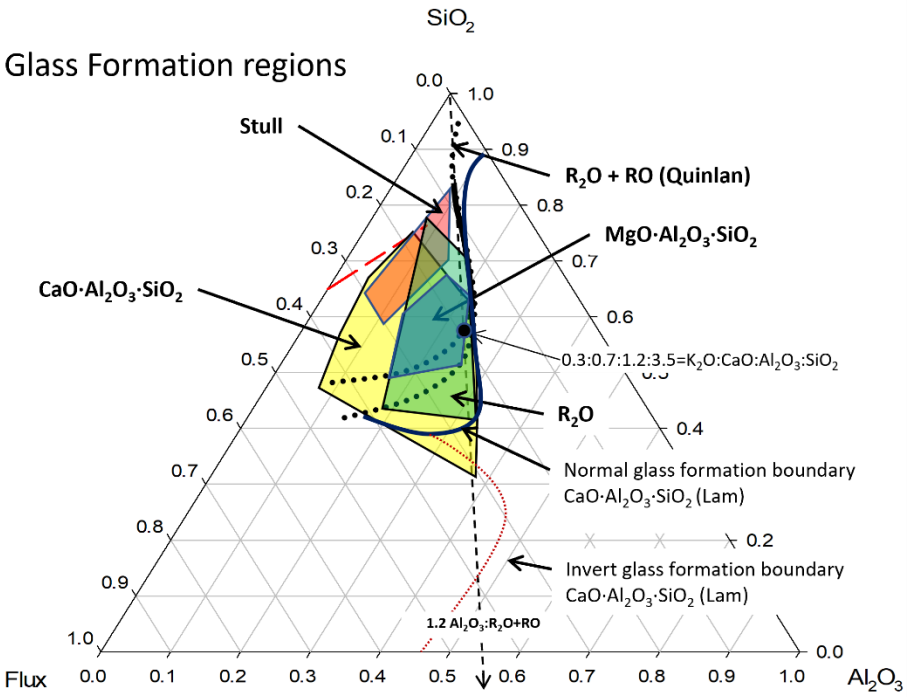

Figure III.11. Compiled glass formation regions of $R_2O{\cdot}Al_2O_3{\cdot}SiO_2$ (green), $MgO{\cdot}Al_2O_3{\cdot}SiO_2$ (blue), Stull (red)[31], and R_2O+$RO{\cdot}Al_2O_3{\cdot}SiO_2$ (line)[32], $CaO{\cdot}Al_2O_3{\cdot}SiO_2$ (yellow), and invert GFB in $CaO{\cdot}Al_2O_3{\cdot}SiO_2$ (dotted line)[15].

III.5 Conclusion

Glass formation in aluminosilicate glasses was found to uniformly be limited to 1.2 moles of alumina per mole of flux for alkali, alkaline earth, and mixed flux systems. This limit was observed for porcelain bodies, glasses prepared from conventional raw materials, whiteware glazes, and the grain boundaries in sintered alumina. This fixed alumina level extended over a range of silica levels that were dictated by the fluxes in the system. In the RO-fluxed systems, MgO was significantly restrictive compared to CaO aluminosilicates. Similar to the results observed for CaO-fluxed melts, mixed alkali and alkaline earth fluxes exhibited a broad silica range at the alumina saturation limit. These results extend the range of alumina saturation level by 20% from the 1:1 molar ratio to flux level commonly reported for alumina-containing glasses.

III.6 References

1. McMillian PW. Glass Ceramics. London Academic Press; 1979.

2. Seger HA, editor. The Collected Writings of Hermann August Seger: Chemical Publishing Company; 1902.

3. Carty W, Katz M, Gill J. Unity Molecular Formula Approach to Glaze Development. Ceram Eng Sci Proc. 2000;21(2):95-109.

4. Carty WM. Observation on the Glass Phase Composition in Porcelains. Ceram Eng Sci Proc. 2002;23(2):79-94.

5. DeCarlo K, Lam T, Carty W. Dissolution of Alumina in Silicate Glasses and the Glass Formation Boundary. Olevsky E, editor: American Ceramic Society; 2010. 61-8 p.

6. Lee H, Carty WM. Determination of Sintering Temperature of Korean Celadon. Pacrim 2011;9:125-32.

7. Lee H, Carty WM. Determining the Firing Conditions of Ancient Korean Celadons. Asian Ceramic ware technology symposium. 2013.

8. B. Pinto. The Effect of Quartz Particle Size on Percelain Strength [M.S Thesis]. Alfred NY: Alfred University; 2001.

9. Juthapakdeeprasert P. The Translucency of Porcelain [M.S. Thesis]. Alfred: Alfred University; 2011.

10. Lerdprom W. Firing of Porcelain [M.S. Thesis]. Alfred, NY: Alfred University; 2014.

11. Colorado V. Fast Firing of Porcelain [M.S. Thesis]. Alfred, NY: Alfred University; 2014.

12. Ouyang R. Determining the Firing Condition of Ancient Chinese Porcelain. Alfred, NY: Alfred University; 2015.

13. Pavlish AE, Mockrin I. Development of Hard Glasses. J Am Ceram Soc. 1947;30(2):54-63.

14. Seger H. The Collected Writings of Hermann August Seger. Easton, PA: Chemical Publishing Company; 1902.

15. Lam T. Glass Formation Boundary Approach to the Sintering of Alumina [Ph.D. Thesis]. Alfred, NY: Alfred University; 2010.

16. Modugno M. Mechanical Behavior of Porcelain [M. S. Thesis]. Alfred, NY: Alfred University; 2021.

17. Seymour D. Phase Evolution in Elctrical Porcelains during Firing [M.S. Thesis]. Alfred, NY: Alfred University; 2000.

18. Dudka M. Glass Formation in Alkali Aluminosilicates [B.S. Thesis]. Alfred, NY: Alfred University; 2020.

19. Carty WM, Senapati U. Porcelain- Raw Materials, Processing, Phase Evolution, and Mechanical Behavior. J Am Ceram Soc. 1998;81(1):3-20.

20. Lundin ST. Sudies on Triaxial Whiteware Bodies. Stockholm: Almqvist & Wiksell; 1959 1959.

21. Iqbal Y, Lee WE. Microstructural Evolution in Triaxial Porcelain. J Am Ceram Soc. 2000;83(12):3121-27.

22. Martin-Marquez M, Rincon JM, Romero M. Effect of Firing Temperature on Sintering of Porcelain Stoneware Tiles. Ceram Int. 2008;34:1867-73.

23. Kingery W, Bowen H, Ullmann D. Introduction to Ceramics. New York: John Wiley & Sons; 1976.

24. Beall GH. Refractory Glass-Ceramics based on Alkaline Earth Aluminosilicates. J Eur Ceram Soc. 2009;29:1211-9.

25. Han L, Song H, Lin C, Liu J, Liu T, Zhang Q, et al. Crystallization, Structure and Properties of $MgO-Al_2O_3-SiO_2$ Highly Crysalline Transparent Glass-Ceramics Nucleated by Multiple Nucleating Agents. J Eur Ceram Soc. 2018;38:4533-42.

26. Zalapa-Garibay MA, Torres-Torres D, Arizmendi-Morquecho AM, Reyes-Lopez SY. Effect of Nio and MoO_3 Addition on the Crystallinity and Mechanical Properties of alfa-cordierite and beta-cordierite in the $MgO-Al_2O_3-SiO_2$ system. Results Phys. 2019;13:102227.

27. Solvang M, Jensen SL. The Effects of Mg-Ca and Fe-Mg Substitution on Rheological and Thermodynamic Properties of Aluminosilicate Melts. J Non-Cryst Solids. 2004;345&346:782-6.

28. Neuville DR, Cormier L, Montouillout V, Florian P, Millot F, Rifflet J, et al. Structure of Mg-and Mg/Ca Aluminosilicate Glasses: ^{27}Al NMR and Raman Spectroscopy Investigations. Am Mineral. 2008;93:1721-31.

29. Shannon RD, Prewitt CT. Effective Ionic Radii in Oxides and Fluorides. Acta Cryst. 1969;B25:925-645.

30. Guignard M, Cormier L. Environments of Mg an Al in $MgO-Al_2O_3-SiO_2$ Glasses: A Study Coupling Neutron and X-ray Diffraction an Reverse Monte Carlo Modeling. Chem Geol. 2008;256:111-8.

31. Stull R. Influences of Variable Silica and Alumina on Porcelain Glazes of Constant R O. Trans Amer Ceram Soc. 1912;XIV:62-70.

32. Quinlan B. The Unity Molecular Formula Approach to Glaze Development [M.S. Thesis]. Alfred, NY: Alfred University; 2002.

IV POTENTIAL CORRELATION OF THE HARDNESS OF CaO-Al_2O_3-SiO_2 GLASSES WITH MELTING BEHAVIOR

IV.1 Abstract

It is proposed that the hardness of aluminosilicate glasses correlates with the melting temperature as predicted by the phase diagram. To evaluate this hypothesis, a broad range of CaO-Al_2O_3-SiO_2 compositions were evaluated, verifying the glass formation region, and allowing for a systematic comparison of Vickers indentation hardness with melting temperature. Candidate glass forming compositions were restricted to the normal glass formation region (SiO_2>CaO) and ranging from SiO_2:CaO ratios of 1:1 to 9:1 and Al_2O_3:CaO ratios ranging from 0.2:1.0 to 1.3:1.0. Glass forming compositions were X-ray amorphous. The correlation of hardness was non-linear but showed reasonable correlation with the melting behavior, with the lowest hardness glass obtained for the eutectic composition. The maximum hardness was obtained in the narrow glass chemistry range of 1.0:1.0:1.5 to 1.0:1.2:1.5 (CaO:Al_2O_3:SiO_2) in the vicinity of anorthite ($CaO \cdot Al_2O_3 \cdot 2SiO_2$).

Key Words: calcium aluminosilicate glasses, Vickers hardness, liquidus temperatures

IV.2 Introduction

High hardness glasses, especially within the alkaline earth aluminosilicate (RO-Al_2O_3-SiO_2) system, have broad potential applications but the role of chemistry on glass hardness has only been studied to a limited extent.[1-4] Most of the previous studies have focused on the role of modifiers on hardness and but few studies have evaluated the role of alumina.[5, 6] Hardness is linked to the compressibility of the atomic network and increases with increasing atomic density in the glass.[7, 8] To explain the increase in hardness with composition, the modifier cation field strength hypothesis was proposed, with an increase in cation field strength accounting for the observed increase in hardness, due to the formation of higher density and thus a more compact glass structure.[1, 2, 9-11] Since the focus was modifier substitution the balance of the glass chemistry was held constant. Reported glass forming compositions in the CaO-Al_2O_3-SiO_2 system are

summarized in Figure 1, typically obtained by quenching.[3, 5, 12-15] Most of the studies restricted the Al_2O_3:CaO ratio to 1:1 based on a tetrahedrally-coordinated Al^{3+} charge compensation assumption and were limited to tectosilicate glass compositions, i.e., normal glasses. These glasses exhibit Vickers hardness values ranging from 6 to 9 GPa.[3, 5, 12] Only two studies evaluated hardness as a function of alumina level.[12, 16] In contrast, many studies that have investigated the structure of alumina within aluminosilicate glasses with NMR, but these studies have not been linked to indentation hardness.[17-34]

In Figure 1, the results presented by Shelby indicated that glass formation was also observed at low silica levels, where the CaO molar level exceeded the SiO_2 level.[13] Glasses having CaO levels greater than SiO_2 levels are referred to as invert glasses and are typically fragile melts. The glass formation boundary in the CAS system was also confirmed by TEM results evaluating the grain boundary glasses in sintered alumina.[15]

In this study, glass forming compositions were mapped in the CaO-Al_2O_3-SiO_2 system and then hardness was measured on glass forming compositions. Glass formation is proposed to be intrinsic in that it is independent of cooling rate within the range of normal industrial cooling rates (0.5 - 60K/min), i.e., not quenched.[14] All glass compositions are represented on a molar ratio basis, normalized to the moles of CaO, following the form CaO:Al_2O_3:SiO_2. In this format, anorthite, $CaO \cdot Al_2O_3 \cdot 2SiO_2$, is 1:1:2. The glass formation region was observed over a broad SiO_2 range with Al_2O_3 levels ranging from 0.2 to 1.2. A correlation of hardness with glass structure is proposed incorporating the structural information presented in the literature.

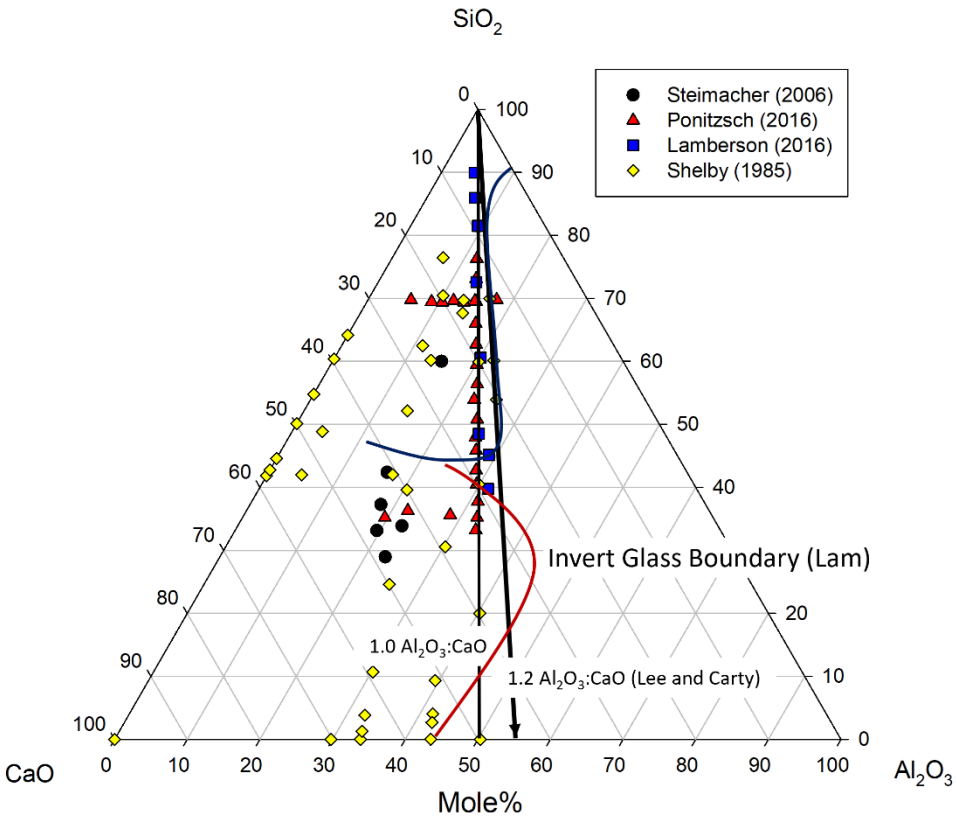

Figure IV.1. Compositions evaluated in previous studies.[3, 5, 12-15] Lee and Carty defined the maximum alumina saturation level in aluminosilicate glasses[14] and Lam reported the normal-invert glass boundary.[15]

IV.3 Experimental procedure

Forty-five compositions were batched within the CaO-Al_2O_3-SiO_2 system as mapped in Figure 2. The SiO_2 levels range from 1.0 to 9.0 with specific ratios of 1.0, 1.5, 2.3, 4.0, and 9.0. Each series consisted of nine alumina levels: 0.2, 0.4, 0.6, 0.8, 1.0, 1.1, 1.2, 1.3, and 1.4. Of particular interest is the alumina range of 0.8-1.2.

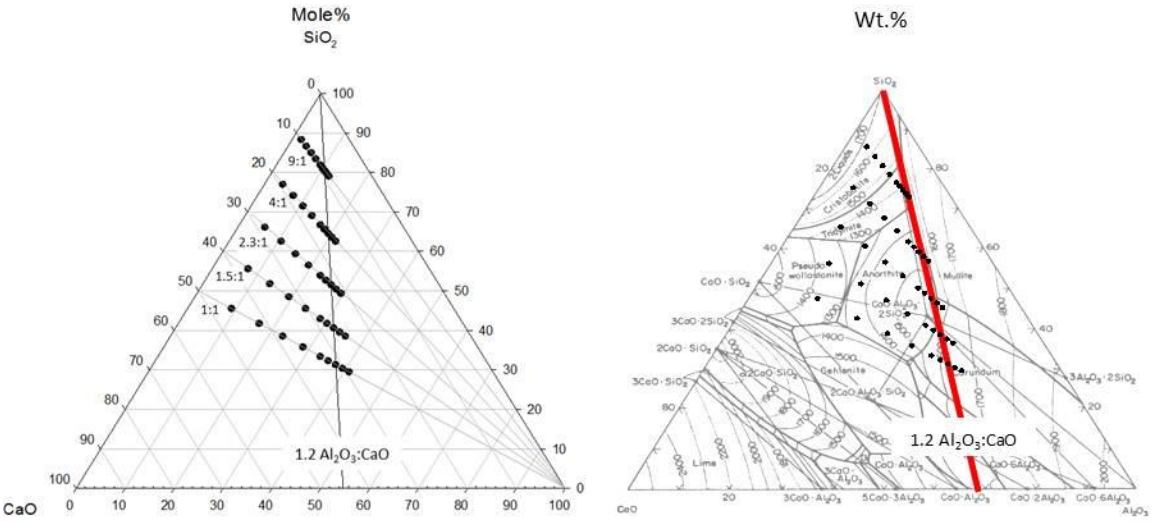

Figure IV.2. Glass compositions in mole% (left) and mass% (right) prepared in this study. The matrix is constructed with 1.0-9.0 SiO_2:CaO and 0.2-1.4 Al_2O_3:CaO molar ratio.

Alumina and silica in the glass batch were introduced as calcined alumina (A10, Almatis, Leetsdale, PA) and ground quartz (Sil-Co-Sil 52, U.S. Silica, Mapleton, PA) with measured mean particle sizes of ~5 µm and ~23 µm, respectively. Calcium carbonate ($CaCO_3$) (Castle Carb 18, Oldcastle Industrial Minerals, Inc., Thomasville, PA) was the calcium source (D_{50} ~42µm). Ten gram batches were prepared and blended via dry milling for 2 hours in polypropylene (Nalgene) bottles with alumina media. No particle size reduction was observed. Two gram batch specimens were melted in silica crucibles at 1600°C for one hour and were not quenched, but were furnace cooled (by shutting off the furnace) without a specific annealing step. Two grams of batch produce approximately 0.7 cm^3 of solid glass, which is sufficient for analyzing glass formation and indentation hardness. Several compositions were duplicated with larger specimen size and annealed on cooling with a hold at 600°C. The measured hardness values of annealed and unannealed specimens showed generally good agreement, with a slight increase in hardness (~0.3 GPa) observed in un-annealed samples.

After cooling the crucibles were sectioned and polished for Vickers indentation hardness measurements. The other half of the crucible was used to confirm chemistry using

energy dispersive x-ray spectroscopy (EDS, EDAX Inc., Mahwah, NJ) in the SEM (Quanta 200F, FEI, Hillsboro, OR), glass formation (confirmed to be X-ray amorphous), glass melting temperature (T_m), and density.

Vickers hardness was measured using a micro hardness instrument at a load of 500 grams (V-100-A2, Leco, Japan) applied for 15 seconds. The indenter was calibrated against an NIST traceable standard (Standard 2831, NIST, Gaithersburg, MD). Relative humidity in the lab was controlled at less than 50% during measurements. Dimensions of the indents were measured using optical microscopy (Polyvar, Leica, Buffalo, NY). The densities of ground glass samples were measured using a pycnometer method (AccuPyc II TEC (He-pycnometer), Micromeritics, Norcross, GA). Molar volumes were calculated using the measured densities and glass chemistries.

IV.4 Results and Discussion

Glass formation is observed over a wide range of compositions. Due to furnace limitations, all compositions in the 9.0 SiO_2 series (the highest silica level) were expected to form glasses but did not melt properly. In the series 4.0 SiO_2 series, the two lowest alumina compositions exhibited phase separation and were thus excluded from further analysis. Consistent with previous studies, compositions with high alumina levels, i.e., 1.3 Al_2O_3:CaO, showed mullite precipitation at intermediate and high silica levels and in the two lowest silica levels, corundum was observed consistent with the phase diagram.[14]

The compositions of the resulting glass specimens were verified using energy dispersive spectroscopy (EDS).[35] Independent EDS calibration curves were generated that mimicked the compositions of interest. It was found that all glass compositions shifted to higher silica contents due to melt interaction with the crucible. All data points were corrected and mapped as a quadrilateral in Figure 3 with Vickers hardness data.

For illustration purposes, an orthogonal x-y hardness contour plot was deformed to match the bounded quadrilateral composition matrix shape. 28 data points were used to compose the contour plot employing a spline fit (SigmaPlot, v.*12.5*, StatEase, Inc., Minneapolis, MN). The y-axis presents the SiO_2:CaO ratios (i.e., 1.0, 1.5, 2.3, 4.0, and 9.0). To avoid increments in step size in the y-axis, SiO_2 values were divided by sum of

SiO_2 and CaO in molar basis. Therefore 1.0 SiO_2:CaO equates to 0.5 on the axis, shifted from 0.55 due to the chemistry shift during melting. Improved hardness was observed in the compositions of 1.0 to 1.2 Al_2O_3 and 1.0 to 1.5 SiO_2. A second hardness peak was observed at low alumina and high silica levels. The variation in the hardness trends as a function of composition do not appear to follow a logical or predictable pattern with regards to either alumina or silica level.

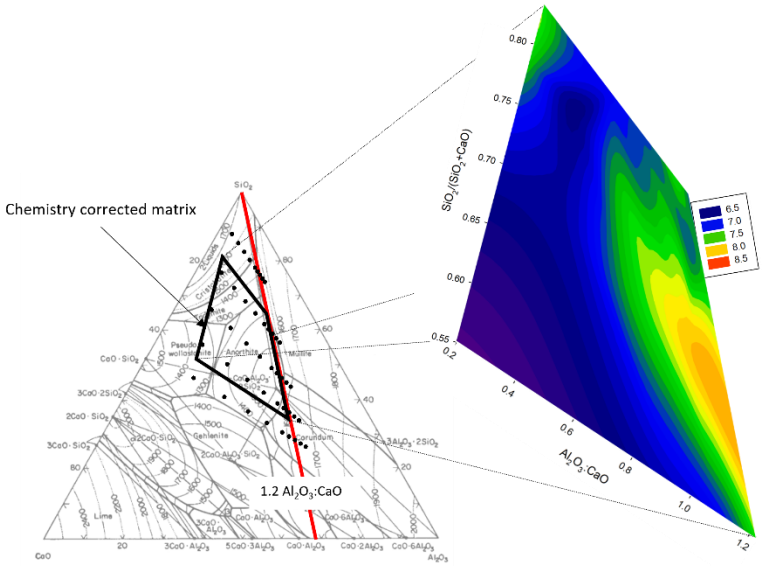

Figure IV.3. Vickers hardness of the CaO-Al_2O_3-SiO_2 system (mass%) showing maximum hardness in the range of 1.0-1.2 Al_2O_3:CaO and 1.0-1.5 SiO_2:CaO [0.5-0.6 SiO_2:(SiO_2+CaO)]. Some improvement in hardness with lower alumina with increased silica (right top) was observed.

Additionally, the hardness trends did not correlate with the physical properties of glasses (density and molar volume of the glasses). The molar volume increased with increasing alumina and silica content. The density of the glasses increases with alumina content at lower silica levels – a trend that is less distinct at higher silica levels. Figure 4 compares density, molar volume, and Vickers hardness, illustrating no discernable correlation.

Hardness, when compared to thermal behavior, i.e., T_g and melting temperature, supports the hypothesis that the melt structure mimics the structure of the solid below the liquidus, as observed by Navrotsky.[32, 36] The correlation of hardness and T_g has been reported in

borate glasses,[37] and alkali aluminoborate glasses,[38] However, no correlation of mechanical properties to T_g has been reported in alkaline earth aluminosilicate glasses.[1] It is proposed that the melting behavior represented by the liquidus surfaces in the phase diagram correlates to the hardness data measured on the glasses in this study. Melting temperatures of the evaluated compositions were extrapolated from the liquidus lines in the phase diagram.[39]

The indentation hardness trends with melting behavior as presented in Figure 5. The lowest hardness is observed for the eutectic composition: $CaO{:}0.4Al_2O_3{:}1.5SiO_2$. Hardness then increases as the alumina level moves away from the eutectic, with both increasing and decreasing alumina additions. The large standard deviations observed in glasses with high hardness values can be partially attributed to cracking at the corners of the indents. This phenomena has been addressed in the literature with the observation that cracks were most often generated at higher loads (1.0 kgf).[40] It is difficult to explain these results solely by proposed glass structure models.

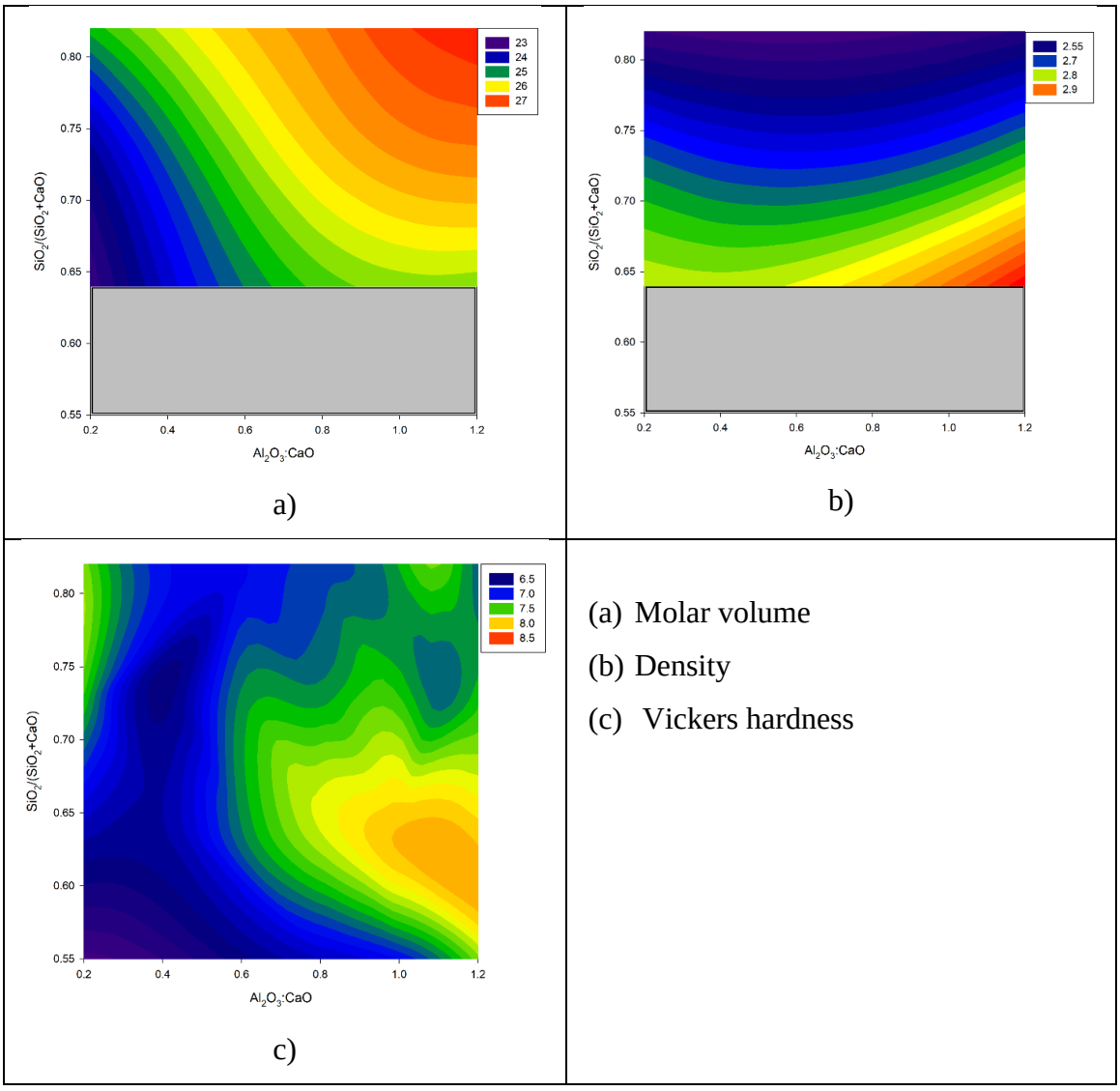

Figure IV.4. (a) Molar volume and (b) density of the CaO-Al_2O_3-SiO_2 system. Their trends are compared to the Vickers hardness (box in c).

The measured liquidus temperatures of the compositions of 1.5, 2.3, and 4.0 SiO_2 series were compared to the melting temperatures calculated using FactSage (version 8.0, Phase diagram module, FTOxid database, Thermfact and GTT-Technologies, Montreal, Quebec, Canada). The composite and calculated high silica levels of the CAS phase diagram are compared in Figure 6 (mass %) showing the major mineral phases of anorthite, mullite, cristobalite, and tridymite. The calculated and published phase

diagrams are similar except for the crystalline silica phase field intersection of tridymite and cristobalite and the intersection of the anorthite and mullite phase fields.

Figure 7 compares the liquidus temperatures from the composite and calculated phase diagrams. When the temperatures are compared, the compositions generally fit the 95% confidence band indicating good agreement with the composite phase diagram. [39] As expected, the differences noted above accounted for the deviation of the composite and calculated phase diagrams as identified in Figure 7.

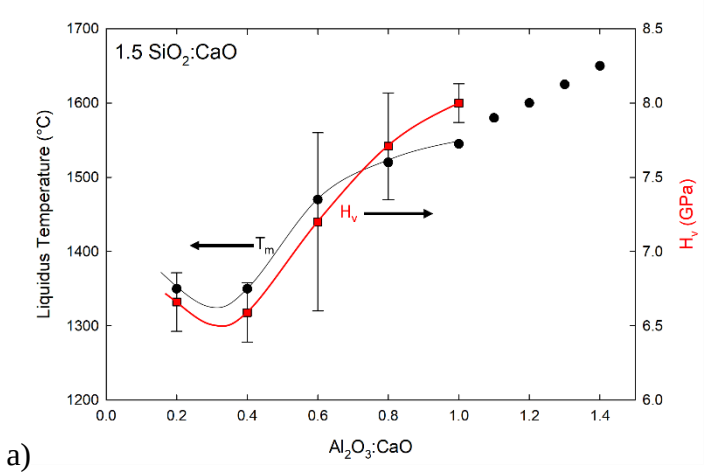

a)

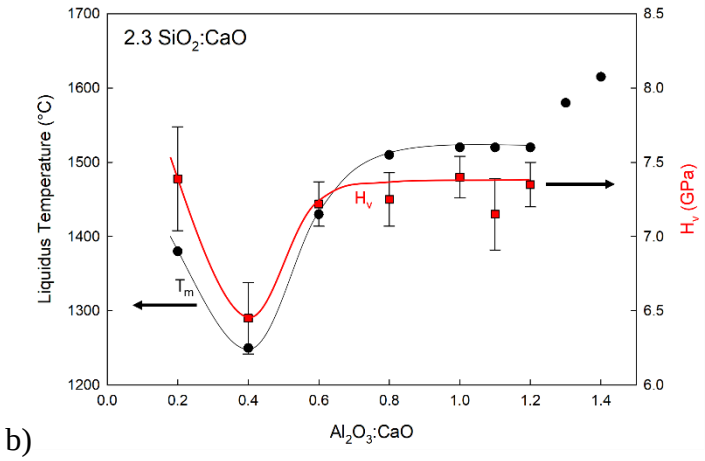

b)

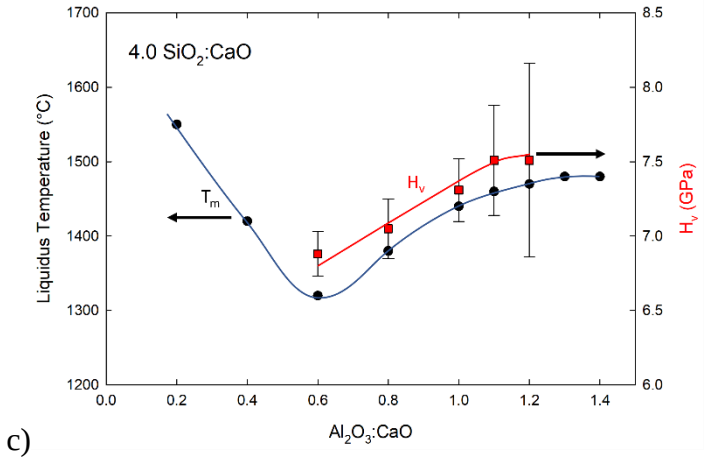

c)

Figure IV.5. Vickers hardness of glasses in the series (a)1.5, (b) 2.3, and (c) $4SiO_2$:CaO compared to liquidus lines of the associated compositions. The liquidus temperatures were extracted from the phase diagram.

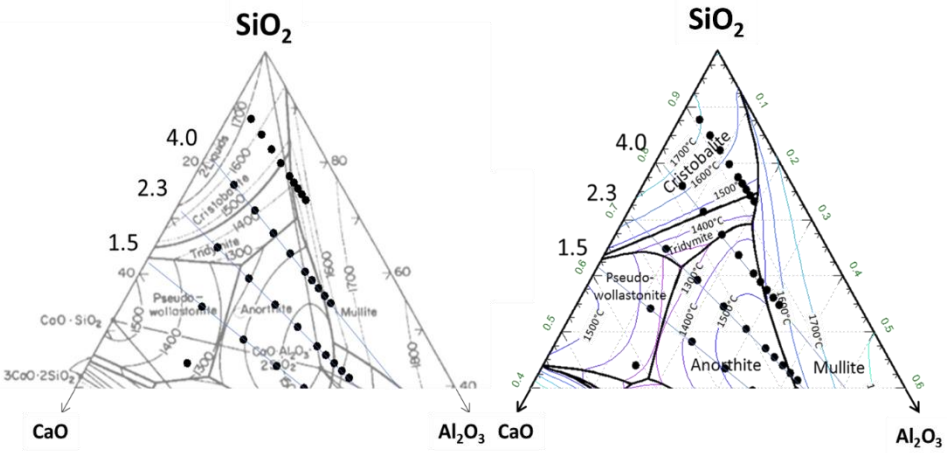

Figure IV.6. Comparison of CaO-Al_2O_3-SiO_2 phase diagram (left) to the calculated phase diagram using FactSage (right).

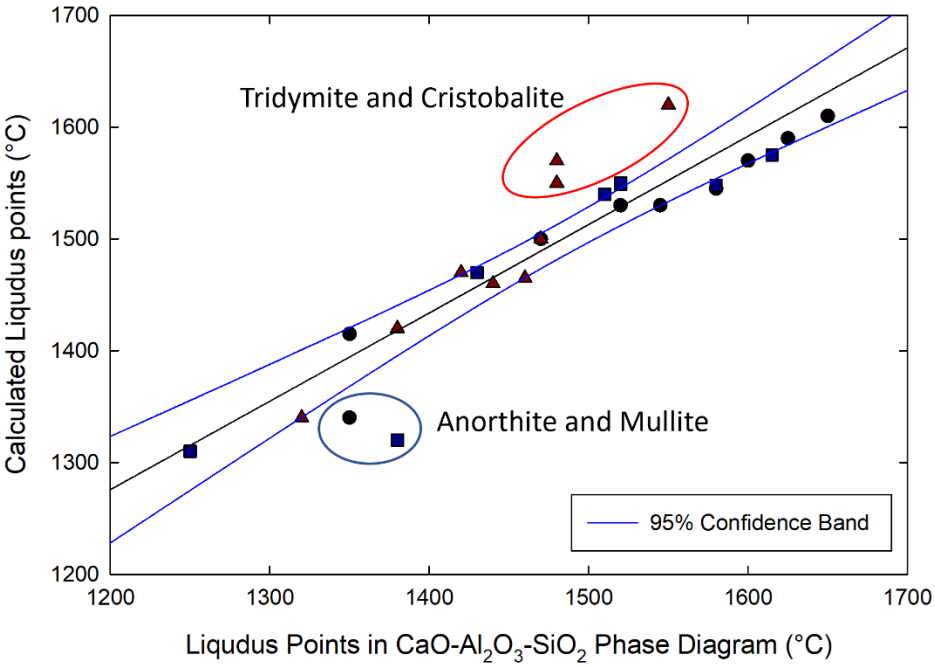

Figure IV.7. Comparison of measured liquidus temperature to the calculated temperatures.

The 2.3 SiO_2 series passes through three phase fields: anorthite in the high alumina region, and tridymite and cristobalite in the low alumina region. Anorthite ($CaO{\cdot}Al_2O_3{\cdot}2SiO_2$) is within the feldspar tectosilicate group.[41] Aluminum ions substitute for 50% of silicon tetrahedral sites in the feldspar lattice. Calcium ions function as charge compensators in the vicinity of $[AlO_4]^-$ tetrahedra adhering to Pauling's rules for oxygen coordination. The most stable composition in the vicinity is anorthite with a melting point of 1553°C and a 1:1 $CaO:Al_2O_3$ ratio. Aluminum and silicon ions are in highly ordered tetrahedral sites and each $[AlO_4]^-$ tetrahedra is coordinated by four $[SiO_4]^-$ tetrahedra.[32]

During melting the long-range structure dissociates and distorts to an amorphous form while maintaining short range order (i.e., $[SiO_4]^-$ and $[AlO_4]^-$ tetrahedra). This structure is proposed to be similar to the structure of the parent mineral phase. It is therefore predicted that the glass structure of stoichiometric anorthite will produce the highest temperature melt, the most rigid network on cooling, and thus the greatest hardness.

In the anorthite phase field, the degree of aluminum and silicon ordering is reduced as the composition moves away from anorthite, due to the formation of non-bridging oxygen (NBO). The reduction in melting point also portends a reduction in the network rigidity. The classic theory states that Al^{3+} ions occupy tetrahedral sites when the ratio of Al_2O_3:RO is less than one.[20] Under this condition, the R^{2+} compensates for the charge deficiency associated with Al^{3+} substituting for Si^{4+} in the tetrahedrally coordinated oxygen positions. When the Al_2O_3 >1 (the Peraluminous glass region), the formation of five- and six-fold coordinated Al^{3+}, $[AlO_5]^-$ or $[AlO_6]^-$, is more favorable.[42] At 1.0 Al_2O_3 (tectosilicate) no NBO formation is expected because the charge of the modifier cations is equivalent to the number of aluminum ions with each charge compensating for one AlO_4^- tetrahedron.

It has been proposed that hardness is affected by several glass structural factors including network connectivity, cross-linking strength and atomic packing density, which are often manipulated by changing the composition.[1, 8, 38] However, based on the results of this study, it is proposed that the coordination of aluminum ions in the glass network formation is the most important factor contributing to indentation hardness. The highest

hardness glasses were obtained from compositions with alumina levels at or above saturation, from 1.0 to 1.2 Al_2O_3 (in the tectosilicate to Peraluminous glass region). Key information regarding this transition region is the formation of five-fold coordinated aluminum $[AlO_5]^-$ within the compositional range of 0.5 to 1.4 Al_2O_3. Details on the differences in aluminum coordination have been determined using FTIR,[17] Raman,[17, 22] neutron diffraction,[24] X-ray absorption spectroscopy,[43] and NMR.[17, 21, 22, 33, 34, 44-46] From these studies, it is evident that the formation of five-fold Al depends on the Al_2O_3:CaO ratio and is related to Si/Al disorder (i.e., Al-O-Al formation) at Al_2O_3 levels above 1.0. It was reported that the population of $[AlO_5]$ species increased at Al_2O_3 levels >1.0, due to a deficit of charge compensating modifier ions.[22, 34]

Additional information is needed to explain the high hardness in the range of 1.0 to 1.2 Al_2O_3. NMR data has demonstrated that there is NBO in tectosilicate glass.[27] One hypothesis is the formation of NBO is associated with five-fold Al or tricluster formation (Al_2SiOx in the CAS) in this composition range. This model may explain the observation of property maximums in the peraluminous region. Another possible explanation is the formation of combined AlO_5 species and Al-Si triclusters (i.e., Al_2SiOx or $AlSi_2Ox$). The Al_2SiOx tricluster requires a charge compensator but the $AlSi_2Ox$ tricluster is neutral and charge balanced. Formation of these two types of triclusters depends on the ratio of silicon and aluminum and, necessarily, the availability of charge compensators (R^{2+}). With this explanation the formation of AlO_5 is not strictly limited to compositions with high Al_2O_3 content (i.e., Al_2O_3>CaO). The formation of triclusters, combined with AlO_5 or the tricluster itself, then improve network connectivity.

It has been also proposed that AlO_5 species form over the entire composition range and that the concentration of AlO_5 species change with Al_2O_3:CaO ratio.[22] Previously reported data is re-plotted in the Figure 8. The AlO_5 level is at a minimum at 0.5 Al_2O_3 and increases as the ratio shifts away from 0.5 Al_2O_3. The minimum resides in the vicinity of the eutectic composition which is at the anorthite—tridymite—pseudo-wollastonite invariant point, where the highest concentration of four-fold coordinated Al^{3+} is predicted. In general, although the concentration AlO_x species is affected by the ratio of Al_2O_3:CaO in the system, the overall glass polymerization degree can be

maintained by $[AlO_5]^-$ formation when combined with NBO or Al-Si triclusters. This argument predicts that $[AlO_5]^-$ concentration tracks similarly to the liquidus line in the system and is consistent with the proposed hypothesis that melt structure will correlate with liquidus surface and thus also with measured hardness values.

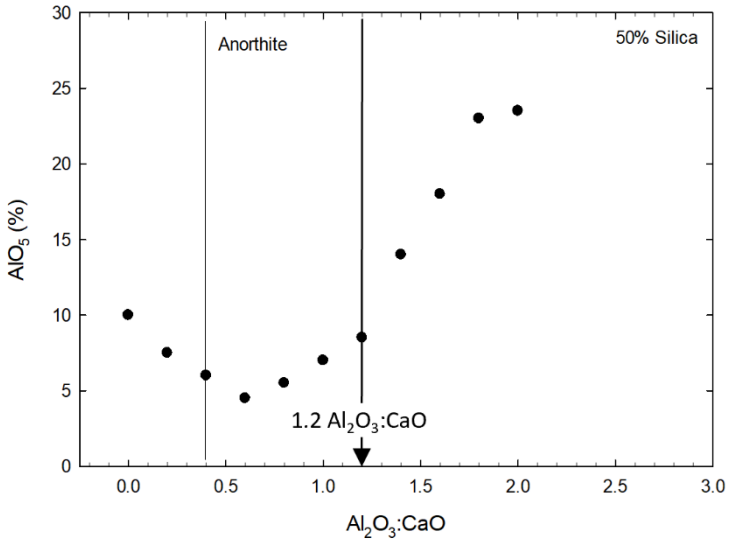

Figure IV.8. AlO_5 site changes as a function of Al_2O_3/CaO ratios.[22] The ratio for anorthite is indicated, as well as the glass formation limit at 1.2 Al_2O_3:CaO.

The glasses of maximum hardness are located in the anorthite phase field in the range of 1.0-1.2 Al_2O_3, with hardness decreasing with a reduction in Al_2O_3 to 0.6, then increasing with the further reduction in alumina (Figures 3 and 5). Under these conditions, the concentration of NBO is reduced indicating improved network connectivity, and the established association with Al coordination in aluminosilicate glasses, dictate the hardness of these glasses. The formation of AlO_5, which is directly coupled to RO level, increases both melting temperature and mechanical properties.[2, 22] One of the explanations for the improvement of properties is that AlO_5 formation may increase the structural order of the network[47], thereby stiffening the structure. Also, the distribution of bridging oxygen, resulting from the generation of triclusters, promotes medium range

order of glass. This improvement in network complexity is proposed to correlate with increased hardness.

It is thus concluded that hardness data in this study can be interpreted based on the glass structure, especially, $AlO_{5,}$ tricluster formation and NBO reduction. Glass structure is evidently closely related to the mineral structure and thus correlates well with the melting behavior, as described by the phase diagram.

IV.5 Conclusions

It was demonstrated that glass hardness correlates with the melting behavior over the experimental range evaluated, exhibiting a maximum in the vicinity of the composition of the stable ternary compound, anorthite. As the composition moves away from the ternary compound anorthite, the hardness decreases. In addition, glasses can be readily formed with excess alumina, above 1.0:1.0 Al_2O_3:CaO due to the formation of 5-fold and 6-fold Al-O polyhedral creating structures that promote high hardness. Specifically, the prediction of AlO_5 structures, the formation of Al-Si triclusters, and the elimination of NBO, are all consistent with the correlation of hardness and melting behavior. The formation of varied AlO_x sites align with melting behavior as predicted by the phase diagram, thus showing a correlation of hardness with melting temperature in the CaO-Al_2O_3-SiO_2 system.

IV.6 References

1. Weigel C, Losq CL, Vialla R, Dupas C, Clément S, Neuville DR, et al. Elastic Moduli of $XAlSiO_4$ Aluminosilicate Glasses: Effects of Charge-Balancing Cations. J Non-Cryst Solids. 2016;447:267-72.

2. Stevensson B, Edén M. Structural Rationalization of the Microhardness Trends of Rare-Earth Aluminosilicate Glasses: Interplay Between the RE^{3+} Field-Strength and the Aluminum Coordinations. J Non-Cryst Solids. 2013;378:163-7.

3. Steimacher A, Astrath NGC, Novatski A, Pedrochi F, Bento AC, Baesso ML, et al. Characterization of Thermo-Optical and Mechanoical Properties of Calcium Aluminosilicate Glasses. J Non-Cryst Solids. 2006;352:3613-7.

4. Baesso ML, Andrade AA, Catunda T, Sampaio JA, Gama S. Neodymium Concentration Dependence of Thermo-Optical Properties in Low Silica Calsium Aluminosilicate Glasses. J Non-Cryst Solids. 1997;219:165-9.

5. Pönitzsch A, Nofz M, Wondraczek L, Deubener J. Bulk Elastic Properties, Hardness and Fatigue of Calcium Aluminosilicate Glasses in the Intermediate-Silica Range. J Non-Cryst Solids. 2016;434:1-12.

6. Eagan R, Swearengen JC. Effect of Composition on the Mechanical Properteis of Aluminosilicate and Borosilicate Glasses. J Am Ceram Soc. 1978;61(1-2):27-30.

7. Macedo G, Sawamura S, Wondraczek L. Lateral Hardness and the Scratch Resistance of Glasses in the Na_2O-CaO-SiO_2 System. J Non-Cryst Solids. 2018;492:94-101.

8. Aakermann KG, Januchta K, Pedersen JAL, Svenson MN, Rzoska SJ, Bockowski M, et al. Indentation Deformation Mechanism of Isostatically Compressed Mixed Alkali Aluminosilicate Glasses. J Non-Cryst Solids. 2015;426:175-83.

9. Backhouse DJ, Corkhill CL, Hyatt NC, Hand RJ. Investigation of the Role of Mg and Ca in the Structure and Durability of Aluminobrosilicate Glass. J Non-Cryst Solids. 2019;512:41-52.

10. Kjeldsen J, Smedskjaer MM, Potuzak Ml, Yue Y. Role of Elastic Deformation in Determining the Mixed Alkaline Earth Effect of Hardness in Silicate Glasses. J Appl Phys. 2015;117:034903-1 -7.

11. Iftekhar S, Grins J, Gunwidjaja PN, Edén M. Glass Formation and Structure-Property-Composition Relations of the RE_2O_3-Al_2O_3-SiO_2 (RE = La, Y, Lu, Sc) Systems. J Am Ceram Soc. 2011;94(8):2429-35.

12. Lamberson L. Influence of Atomic Structure on Plastic Deformation in Tectosilicate Calcium-Aluminosilicate, Magnesium-Aluminosilicate, and Calcium-Galliosilicate Glasses [Ph.D. Thesis]: Cornell University; 2016.

13. Shelby JE. Formation and Properties of Calcium Aluminosilicate Glasses. J Am Ceram Soc. 1985;68(3):155-8

14. Lee H, Carty WM. The Glass Formaiton Boundary in Aluminosilicate Systems. In process. 2021.

15. Lam T. Glass Formation Boundary Approach to the Sintering of Alumina [Ph.D. Thesis]. Alfred, NY: Alfred University; 2010.

16. Amma S, Luo J, Kim SH, Pantano CG. Effect of Glass Composition on the Hardness of Surface Layers on Aluminosilicate Glases Formed through Reaction with Strong Acid. J Am Ceram Soc. 2017;101:657-65.

17. Okuno M, Zotov N, Schmücker M, Scheider H. Structure of SiO_2-Al_2O_3 Glasses: Combined X-ray Diffraction, IR and Raman Studies. J Non-Cryst Solids. 2005;351:1032-8.

18. Schmücker M, Schnieder H. New Evidence for Tetrahedral Triclusters in Aluminosilicate Glasses. J Non-Cryst Solids. 2002;311:211-5.

19. Varshneya AK. Fundamentals of Inorganic Glasses. Sheffield: Society of Glass Technology; 2006.

20. Shelby JE. Introduction to Glass Science and Technology, 2nd Edition. Chmbridge, UK: The Royal Society of Chemistry; 2005.

21. Neuville DR, Cormier L, Massiot D. Al Environment in Tectosilicate and Peraluminous Glasses: A ^{27}Al MQ-MAS NMR Raman, and XANES Investigation. Geochimi Cosmochim Acta. 2004;68(24):5071-7079.

22. Neuville DR, Cormier L, Massiot D. Al Coordination and Speciation in Calcium Aluminosilicate Glasses: Effects of Composition Determined by ^{27}Al MQ-MAS NMR and Raman Spectroscopy. Chem Geol. 2006;229:173-85.

23. Henderson GS, Neuville DR, Cormier L. An O *K*-Edge XANES Study of Glasses and Crystals in the CaO-Al_2O_3-SiO_2 (CAS) System. Chem Geol. 2009;259:54-62.

24. Hennet L, Drewitt JWE, Neuville DR, Cristiglio V, Kozaily J, Brassamin S, et al. Neutron Diffraction of Calcium Aluminosilicate Glasses and Melts. J Non-Cryst Solids. 2016;451:89-93.

25. Jakse N, Bouhadja M, Kozaily J, Drewitt JWE, Hennet L, Neuville DR, et al. Interplay Between Non-Bridging Oxygen, Triclusters, and Fivefold Al Coordination in Low Silica Content Calcium Aluminosilicate Melts. Appl Phys Lett. 2012;101.

26. Atila A, Ghardi E, Hasnaoui A, Ouaskit S. Alumina Effect on the Structure and Properties of Calcium Aluminosilicate in the Percalcic Region: A Molecular Dynamics Investigation. J Non-Cryst Solids. 2019;525:119470.

27. Stebbins JF, Xu Z. NMR Evidence for Excess Non-Bridging Oxygen in an Aluminosilicate Glass. Nature. 1997;390(6):60-2.

28. Cormier L, Neuville DR, Calas G. Structure and Properties of Low Silica Calcium Aluminosilicate Glasses. J Non-Cryst Solids. 2000;274:110-4.

29. Gambuzzi E, Pedone A, Menziani MC, Angeli F, Florian P, Charpentier T. Calcium Environment in Silicate and Aluminosilicate Glasses Probed by ^{43}Ca MQMAS NMR Experiments and MD-GIPAW Calculations. J Non-Cryst Solids. 2015;68-69(31-36).

30. Kanehashi K, Stebiins JF. In Situ High Temperature ^{27}Al NMR Strudy of Structure an Dynamics in a Calcium Aluminosilicate Glass and Melt. J Non-Cryst Solids. 2007;353:4001-10.

31. Kucharczyk S, Zajac M, Stabler C, Thomsen RM, Haha MB, Skibsted J, et al. Structure and Reactivity of Synthetic CaO-Al_2O_3-SiO_2 Glasses. Cem Concr Res. 2019;120:77-91.

32. Stamboulis A, Hill RG, Law RV. Characterization of the Structure of Calcium Alumino-Silicate and Calcium Flouro-AluminoSilicate Glasses by Magic Angle Spinning Nuclear Magnetic Resonance (MAS-NMR). J Non-Cryst Solids. 2004;333:101-7.

33. Thompson LM, Stebbins JF. Non-Stoichiometric Non-Bridging Oxygens and Five-Coordinated Aluminum in Alkaline Earth Aluminosilicate Glases: Effect of Modifier Cation Size. J Non-Cryst Solids. 2012;358:1783-9.

34. Takahashi S, Neuville DR, Takebe H. Thermal Properties, Density and Structure of Percalcic and Peraluminus CaO-Al_2O_3-SiO_2 Glases. J Non-Cryst Solids. 2015;411:5-12.

35. Goldstein J, Newbury D, Echlin P, Joy D, Fiori C, Lishin E. Scanning Electron Microscopy and X-ray Microanalysis New york: Plenum Press; 1981.

36. Newton RC, Navrostsky A, Wood BJ, editors. Thermodynamics of Minerals and Melts: Springer-Verlag; 1981.

37. Möncke D, Kamitsos EI, Palles D, Limbach R, Winterstein-Beckmann A, Honma T, et al. Transition and Post-Transition Metal Ions in Borate Glasses: Borate Ligand Speciation, Cluster Formation, and Their Effect on Glass Transition and Mechanical Properties. J Chem Phys. 2016;145:124501.

38. Januchta K, Bauchy M, Youngman RE, Pzoska SJ, Bockowski M, Smedskyaer MM. Modifiers Field Strengh Effecs on Densification Behvior and Mechanical Properties of Alkali Alumnoborate Glasses. Phys Rev Mater. 2017;1:063603.

39. Levin EM, Robbins CR, McMurdie HF. Phase Diagram for Ceramists, Vol. 1. Reser MK, editor. Columbus, OH: American Ceramic Society; 1969.

40. Quinn GD, Bridt RC. On the Vickers Indentation Fracture Toughness Test. J Am Ceram Soc. 2007;90(3):673-80.

41. Goldsmith JR. The Melting Breakdown Reactions of Anorthite at High Pressures and Temperatures. Am Mineral. 1980;65:272-84.

42. Varshneya AK, Bihuniak PP. Cover Screens for Personal Electronic Devices: Strengthened Glass or Saphire? Am Ceram Soc Bull. 2017;96(5):20-5.

43. Neuville DR, Cormier L, Flank A-M, Briois V, Massiot D. Al Speciation and Ca Environment in Calcium Aluminisilicate Glasses and Crystals by Al and Ca K-edge X-ray Absorption Spectroscopy. Chem Geol. 2004;213:153-63.

44. Atila A, Ghardi E, Hasnaoui A, Ouaskit S. Alumina Effect on the Structure and Properties of Calcium Aluminosilicate in the Percalcic Region: A Molecular Dynamics Investigation. J Non-Cryst Solids. 2019;525:119470-1 - -14.

45. Neuville DR, Cormier L, Montouillout V, Massiot D. Local Al Site Distribution in Aluminosilicate Glasses by ^{27}Al MAS NMR. J Non-Cryst Solids. 2007;353:180-4.

46. Agnello G, Youngman R, Lamberson L, Smith N, LaCourse W, Cormack AN. Bulk Structures of Cilica-Rich Calcium Aluminosulphate (CAS) Glasses Along the Molar $CaO/Al_2O_3 = 1$ Join via Molecular Dynamics (MD) Simulation. J Non-Cryst Solids. 2019;519:119450-1 - 11.

47. Losq C, Neuville DR, Florian P, Henderson GS, Massiot D. The Role of Al^{3+} on Rheology and Structural Changes in Sodium Silicate and Aluminosilicate Glasses and Melts. Geochimi Cosmochim Acta. 2014;126:495-517.

V CORRELATION OF VICKERS HARDNESS OF RO-Al_2O_3-SiO_2 GLASSES WITH PREDICTED LIQUIDUS TEMPERATURES

V.1 Abstract

Vickers hardness of RO-Al_2O_3-SiO_2 glasses were measured over a broad range of compositions, ranging from ternary endpoints to mixed ratios of RO (CaO with MgO, SrO, or BaO), with systematic variation of Al_2O_3 and SiO_2 levels. The hardness of CAS and MAS glasses are similar, ranging from 6.7 GPa to 7.2 GPa, with the replacement of CaO with MgO producing only a marginal increase in hardness. The blending of CaO with SrO and BaO generally resulted in a decrease in hardness down to 4.5 GPa with BaO. The sensitivity to alumina and silica levels, however, was much greater ranging from 4.5 to a maximum of ~8.2 GPa. The correlation of Vickers hardness with melting temperature was observed in the CAS but not in the MgO glasses, nor in the blends of BAS and SAS with CAS glasses. In the latter cases, the combined cation field strength of modifiers determined the hardness above the critical RO blending ratio.

Key Words: CFS, Hardness, Glass formation, aluminosilicate glasses

V.2 Introduction

The glass formation regions were defined for alkali and alkaline earth aluminosilicates and demonstrated that the alumina saturation limit extended up to 1.2 moles of alumina per mole of flux.[1] The hardness of these glasses appears to be strongly linked to the formation of five-fold coordinated aluminum ($[AlO_5]^-$) species, the formation of Si_2AlOx and $SiAl_2Ox$ triclusters, and the elimination of non-bridging oxygen (NBO). It was demonstrated that hardness also increased with the extension of the alumina saturation level from 1.0 to 1.2 in aluminosilicate glasses. In addition, a correlation between liquidus temperature and hardness was observed with the lowest hardness glasses observed in the vicinity of the eutectic. The highest hardness glasses observed with chemistry similar to stable crystalline phases, specifically anorthite in the CaO-Al_2O_3-

SiO_2 (CAS) system.[2] That work postulated that hardness trends could be predicted from the liquidus surface on the phase diagram.

In this study, melts in the MgO-Al_2O_3-SiO_2 system (MAS) were evaluated for glass formation boundary and Vickers indentation hardness. And then several ratios of CaO:MgO were evaluated with the goal of identifying high hardness glasses in the CaO-MgO-Al_2O_3-SiO_2 system, and to determine if the mixed RO affect extended also to hardness. CaO-SrO-Al_2O_3-SiO_2 and CaO-BaO-Al_2O_3-SiO_2 blends were also evaluated.

All glass chemistries in this work are represented on a molar ratio basis normalized to the sum of the fluxes (R_2O+RO) or specifically in this case the molar sum of the RO fluxes (MgO+CaO+SrO+BaO = 1.0). Alumina and silica levels are then represented as a molar ratio, with a glass having the composition $0.2MgO{\cdot}0.8CaO{\cdot}1.2Al_2O_3{\cdot}2.5SiO_2$ composed of 1.0 moles of RO (0.2MgO + 0.8 CaO), 1.2 moles Al_2O_3, and 2.5 moles of SiO_2.

Hardness of $CaO{\cdot}MgO{\cdot}Al_2O_3{\cdot}SiO_2$ glasses

Glass hardness is characterized as resistance to mechanical compaction with the mechanism related to densification, elastic deformation, and plastic deformation within the glass structure.[3] When Al_2O_3 is added to RO-SiO_2 glasses, network connectivity is improved by reducing number of NBO which affects the hardness of glass. The compactness of $RO{\cdot}Al_2O_3{\cdot}SiO_2$ glasses can be manipulated by changing the cation field strength (CFS) of the modifier cations. Modifier CFS scales in this manner, Mg>Ca>Sr>Ba, with Mg having the greatest CFS and Ba the lowest. Specifically, in the CaO-MgO system, the higher CFS of magnesium compared to calcium is proposed to increase the hardness of the system by improving bonding energy. It is known that oxygen coordination number of Mg^{2+} is lower than that of Ca^{2+} which creates possible structural changes including an increase in five-fold Al^{3+} and edge sharing between AlO_4 and AlO_5. The addition of MgO therefore increases the rigidity and connectivity of the glass network which may result in improvement of hardness. Inversely, this concept can be extended to SAS and BAS glasses, with the lower CFS of Sr^{2+} and Ba^{2+} resulting in a corresponding reduction in local bond density compared to CAS glasses. When the balance of the glass composition is kept constant, the hardness should order with CFS. Vickers hardness of some RO aluminosilicate glasses with different CFS was reported in

the Tiegel's work.[4] The hardness of RO-Al_2O_3-SiO_2 glasses ranged from ~6.0 - ~7.2 GPa, increasing with increasing CFS.

Vickers hardness values have been reported for MgO-CaO-Al_2O_3-SiO_2 glasses addressing the Mixed Alkaline Earth Effects (MAEE). Mixed modifier effects, defined as non-linear property variations, are frequently observed in measured properties such as thermal expansion coefficient, glass transition temperature, elastic modulus, and hardness.[5-10]

Hardness can deviate either negatively or positively from linearity when the one modifier is replaced systematically by another modifier keeping overall addition levels constant. Calahoo and Zwanziger measured a maximum hardness, between 7.5 to 8.0 GPa, at approximately 0.3:0.7 CaO:MgO, while a minimum in hardness was reported by Kielsden at 1:1 CaO:MgO, decreasing from 7.1 to 6.5 GPa.[5, 10-12]

V.3 Experimental Approach

The experimental matrix consisted of CaO- and MgO-aluminosilicates with fixed alumina and silica levels were blended in 20% increments. 45 compositions were evaluated each consisting of five SiO_2 levels: 1.0, 1.5, 2.3, 4.0, and 9.0 (as mapped in Figure 1) and nine Al_2O_3 levels: 0.2, 0.4, 0.6, 0.8, 1.0, 1.1, 1.2, 1.3, and 1.4. For the blending of CAS and MAS, the silica level extremes (1.0 and 9.0) were excluded because 1:1 RO:SiO_2 borders the invert glass region and SiO_2 levels of 9.0 did not form glasses when melted in the MAS system. The remaining 27 compositions of CAS and MAS in the series 1.5, 2.3, and 4.0 SiO_2:RO were blended in steps of 20% generating 108 compositions. The batching and melting processes are described elsewhere.[2]

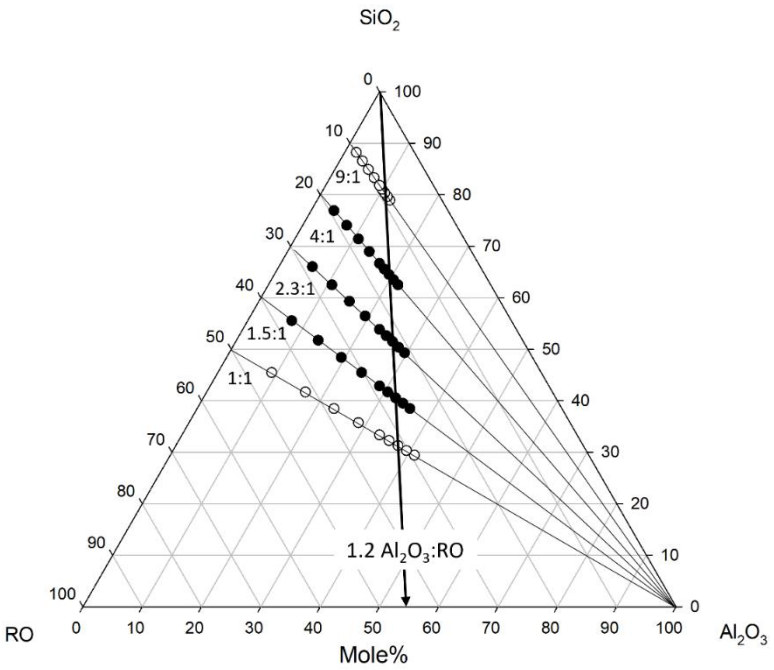

Figure V.1. Evaluated matrix of MAS system and blending of CAS and MAS system. The Al_2O_3:RO ratio ranged from 0.2:1.0 to 1.4:1.0. The SiO_2:RO ratios were at 1:1, 1.5:1.0, 2.3:1.0, 4.0:1.0, and 9.0:1.0. For the blending of two systems, only the 1.5:1.0, 2.3:1.0, and 4.0:1.0 compositions (filled) were evaluated because of the restricted glass formation region in MAS.

To further assess the role of CFS and melting behavior, a similar series was created with CaO + BaO and CaO + SrO with similar alumina and silica levels. Two compositions; the eutectic, $CaO{\cdot}0.4Al_2O_3{\cdot}2.3SiO_2$, and a composition in cordierite or anorthite phase fields, $CaO{\cdot}0.6{\cdot}Al_2O_3{\cdot}2.3SiO_2$ were selected for RO blending. CaO was replaced by SrO or BaO in steps of 20 mol% with constant Al_2O_3 and SiO_2 levels. The melting points were calculated in both systems and compared to the hardness.

Simultaneous Thermogravimetric Analyzer/Differential Thermal Analyzer (TGA/DTA, SDT-Q600, TA Instruments, New Castle, Delaware) was used to obtain melting temperatures. Vickers hardness (V-100-A2, Leco, Japan) was measured at a load of 500 grams applied for 15 seconds and indent dimensions measured with optical microscopy (Polyvar, Leica, Buffalo, NY). A NIST standard was used to calibrate the indenter (NIST Standard 2831, NIST, Gaithersburg, MD).

V.4 Results and discussion

V.4.1 CaO + MgO Aluminosilicates

The glass formation region systematically shrinks when CaO is replaced by MgO as shown in Figure 2. For all of the blended systems, the alumina edge of the glass formation boundary remained at 1.2 Al_2O_3 but the range of silica systematically narrowed from the CAS endpoint to the MAS endpoint.[13] The linearity of this shift suggests that the MAEE does not impact the glass formation region for high alumina glasses.

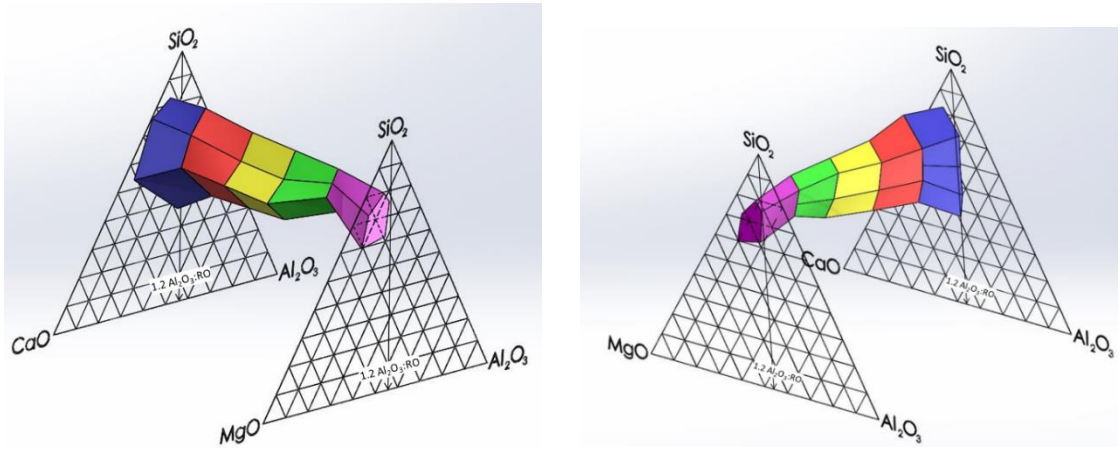

Figure V.2. Glass formation region of $xCaO{\cdot}(1\text{-}x)MgO{\cdot}Al_2O_3{\cdot}SiO_2$ system (mole%, x=0 through 1.0 in steps of 0.2). Glass formation boundary was determined based on optical observation and XRD analysis.[13]

The hardness of CAS and MAS glasses ranged from 5.8 to 8.2 GPa (Figure 3). In the MAS system (Figure 3b), several of the samples used to create the contour plot also included crystalline inclusions such as cristobalite and corundum. But within the glass formation boundary, the glasses were clear and X-ray amorphous. In samples that exhibited crystallization, however, the hardness did not measurably increase. Superimposed on the contour plot, outlined in grey, is the glass formation region. The maximum hardness in the glass formation region was obtained at Al_2O_3 and SiO_2 levels of 1.0 and 2.3, respectively. The lowest hardness values were measured in the vicinity of the cordierite-tridymite-enstatite eutectic and along the cordierite-tridymite join. Unlike

the improvement in hardness observed in the CAS system as the composition moves into the cristobalite phase field (Figure 3a),[2] there is no recuperation of hardness in the MAS system (Figure 3b).

One hypothesis proposed that hardness in aluminosilicate glasses follow a trend predicted by the liquidus temperatures in the phase diagram. In the CAS system, Vickers hardness aligned well with the liquidus surface, and appeared to be relatively independent of composition, with the exception of the clear increase in hardness with increasing alumina level. In the MAS system, however, Vickers hardness does not appear to align with melting temperature, but still shows a correlation with alumina level.

Liquidus temperatures of compositions located in the cordierite phase field increase as the composition approaches cordierite. In the MAS system, cordierite, unlike anorthite in the CAS system, is incongruently melting and lies outside of both the cordierite phase field and the glass formation region. Since the most stable composition is located outside of the phase fields, the isotherms align accordingly. The solid solution exhibited by the mullite deficiency extending away from cordierite extends into the cordierite phase field indicating that compositions deficient in alumina and silica (in a ratio of 3:2) would promote congruent melting of the solid solution mullite-deficient cordierite endpoint. Interestingly, there appears to be evidence for an increase in glass hardness along this line, based on the extrapolated hardness contours presented in Figure 3b.

The roll of the magnesium ions in the system is separated into two categories thus providing an explanation for the poor correlation of hardness data with melting temperature such as observed for glasses in the CAS system. In the MAS system, alumina level is the dominant contributor with hardness increasing as the composition approaches the ternary compound cordierite.

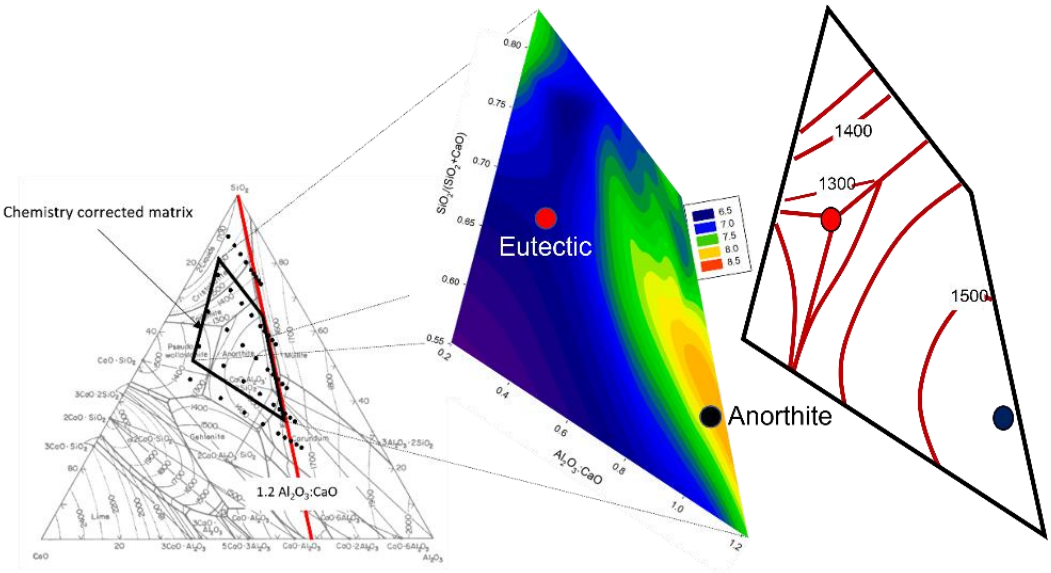

a)

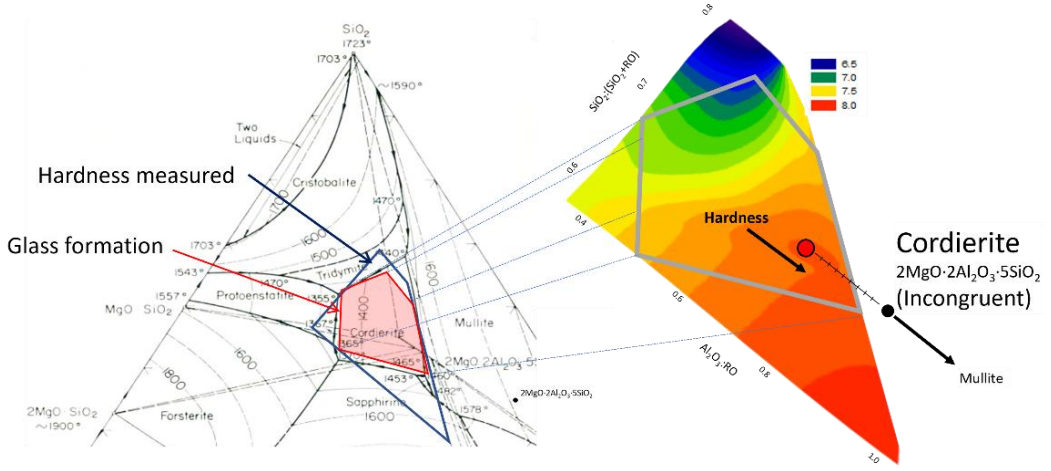

b)

Figure V.3. Vickers hardness of (a) $CaO{\cdot}Al_2O_3{\cdot}SiO_2$ system and (b) $MgO{\cdot}Al_2O_3{\cdot}SiO_2$ system. In the MAS system, all glass forming compositions reside in the cordierite phase field as indicated with the grey outline. The railroad tracks in the inset denote solid-solution for "mullite-deficient" cordierite extending into the Cordierite phase field.

Cation field strength (CFS) theories indicate that the substitution of Mg for Ca should increase indentation hardness due to the increase in modifier CFS with the substitution of Mg for Ca. Two compositions; the MgO eutectic, $MgO{\cdot}0.4Al_2O_3{\cdot}2.3SiO_2$, and the corresponding composition in the CAS system, $CaO{\cdot}0.4Al_2O_3{\cdot}2.3SiO_2$, were blended to create four intermediate MgO-CaO glasses. The melting points were measured and calculated to compare the hardness values with melting temperatures.

For the evaluation of melting behavior of corresponding phases, it would have been logical to select the highest measured hardness CAS composition, $CaO{\cdot}1.2Al_2O_3{\cdot}1.5SiO_2$, and then systematically substitute MgO for CaO, but the glass formation region in MAS did not extend to $MgO{\cdot}1.2Al_2O_3{\cdot}1.5SiO_2$. As an alternative, a composition in cordierite or anorthite phase fields, $RO{\cdot}0.6{\cdot}Al_2O_3{\cdot}2.3SiO_2$ was selected. The results of Mg substitution for Ca are presented in Figure 4. The substitution of MgO for CaO resulted in a nearly linear increase in hardness in both glasses, consistent with the literature.[14, 15] The MAS endpoint exhibited the maximum hardness of 7.2 GPa (±0.34) for both MAS glasses.

The hardness of glasses consisting of both CaO and MgO is commonly used to illustrate mixed alkaline earth effects (MAEE), which are discussed with several different hypotheses, mostly related to structural arguments. However, it is not apparent that the MAEE is observed in this hardness data possibly because of the high alumina levels in these glasses.

To assess the potential correlation of hardness with melting behavior, melting temperatures were measured using differential thermal analysis (DTA). The DTA trace, shown in Figure 5, shows an exothermic peak for beta-cordierite crystallization at ~1080°C and an endothermic peak for melting at 1360°C on heating.

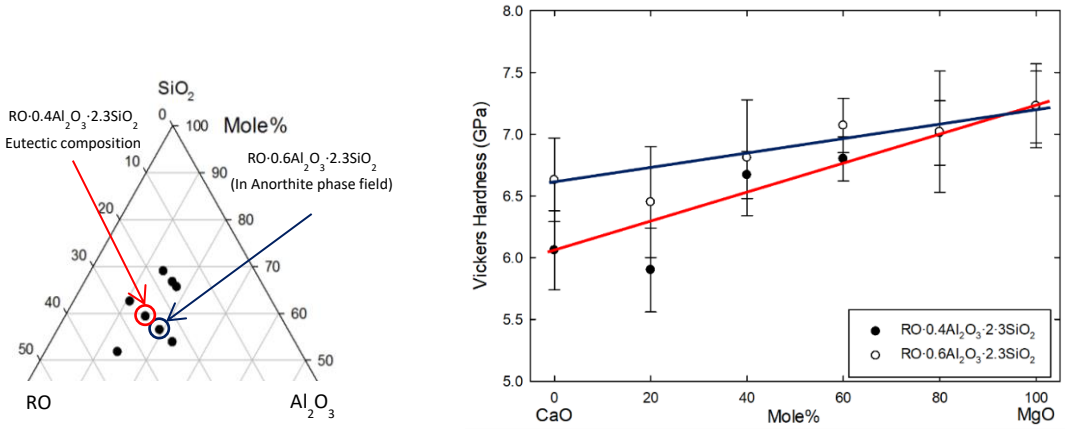

(a) (b)

Figure V.4 The location of the two compositions, $RO{\cdot}0.4Al_2O_3{\cdot}2.3SiO_2$ (eutectic) and $RO{\cdot}0.6Al_2O_3{\cdot}2.3SiO_2$ in the mole% ternary diagram (a). Vickers hardness of the two compositions as a function of CaO:MgO ratios (b) showing that hardness increases in both compositions as calcium is replaced by magnesium.

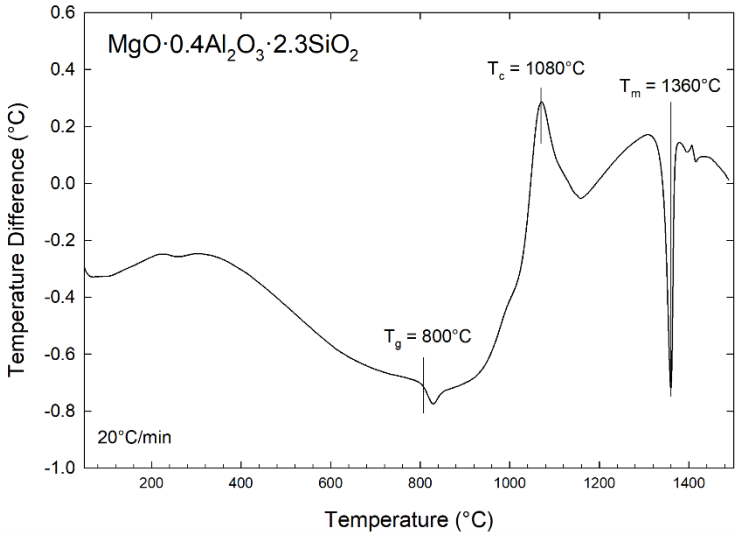

Figure V.5. Example of DTA data showing glass transition temperature (T_g), crystallization temperature (T_c), and melting temperature (T_m) of $MgO{\cdot}0.4Al_2O_3{\cdot}2.3SiO_2$ glass.

Figure 6 compiles the measured melting temperatures (liquidus temperatures) of the two systems as a function of CaO:MgO ratios for two alumina levels (0.4 and 0.6). For the eutectic composition, the melting point of the $CaO{\cdot}0.4Al_2O_3{\cdot}2.3SiO_2$ glass was 1215°C compared to that of the $MgO{\cdot}0.4Al_2O_3{\cdot}2.3SiO_2$ glass at 1360°C. Overall, the melting points of MAS compositions are greater than that of similar CAS compositions. The melting points of blended CAS and MAS compositions, however, were lower than the CaO endpoints and compositions with higher alumina levels exhibit a greater difference in melting temperatures. In the substitution mid-range, with the blending of 40-60% RO, the melting temperatures showed the greatest deviation, decreasing by >100K to ~1220°C.

The liquidus surfaces, however, of the two systems are different, indicating compositional sensitivity, and identifies compositions that possess melting temperature minima. The maximum temperature change observed with the substitution of MgO was 145K at the eutectic composition. In the $RO{\cdot}0.6Al_2O_3{\cdot}2.3SiO_2$ composition set, however, the maximum variation was considerably greater at 235K.

The compositional range for reduced melting temperatures was much narrower in eutectic range of $0.4Al_2O_3{\cdot}2.3SiO_2$ system and was essentially flat from 100% to 40% CaO, showing almost no melting point depression with mixed RO.

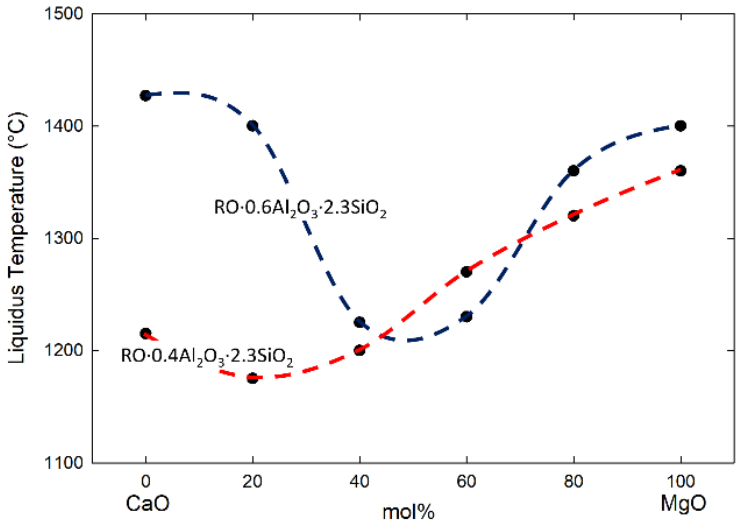

Figure V.6. Demonstration of the significant change in melting temperature behavior with a small shift in composition.

To confirm the measured melting point information, melting points were calculated using thermodynamic software. For this modeling, solid solution models and a Quasichemical approach that minimized Gibbs free energy were used to execute the calculations.[16-18] These calculations were incorporated into FactSage (version 8.0, Phase diagram module, FTOxid database, Thermfact and GTT-Technologies, Montreal, Quebec, Canada) with the needed thermodynamic values included in the FTOxid database.[19]

Liquidus lines for two systems, $CaO{\cdot}0.4Al_2O_3{\cdot}2.3SiO_2$—$MgO{\cdot}0.4Al_2O_3{\cdot}2.3SiO_2$ and $CaO{\cdot}0.6Al_2O_3{\cdot}2.3SiO_2$—$MgO{\cdot}0.6Al_2O_3{\cdot}2.3SiO_2$ were calculated and are presented in Figure 7. This shows that the minimum in melting point shifts with the substitution of Mg for Ca from 0.33 Mg:0.66 Ca for 0.4 Al_2O_3 to 1:1 Mg:Ca for 0.6 Al_2O_3.

Since the alumina and silica levels are held constant in these compositions, the change in melting behavior is solely due to the exchange of Mg^{2+} for Ca^{2+}, an indication of a change in configurational entropy and internal interaction energy which may related to changed aluminum coordination and number of NBO by this substitution.

this substitution.

Since FactSage was introduced for ceramic systems, several aluminosilicate related studies have been published[20-23] and in one case with direct comparison to experimental data.[24] For the compositions studied here, the measured melting temperatures, obtained from DTA, are compared to the calculated melting temperatures, as presented in Figure 8. In all cases the measured temperatures were lower than the calculated temperatures but generally showed good agreement. Table I lists the calculated and measured melting points and the difference.

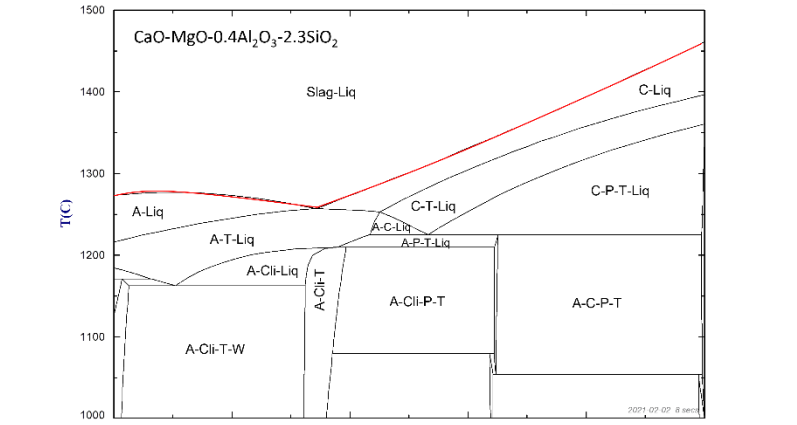

a)

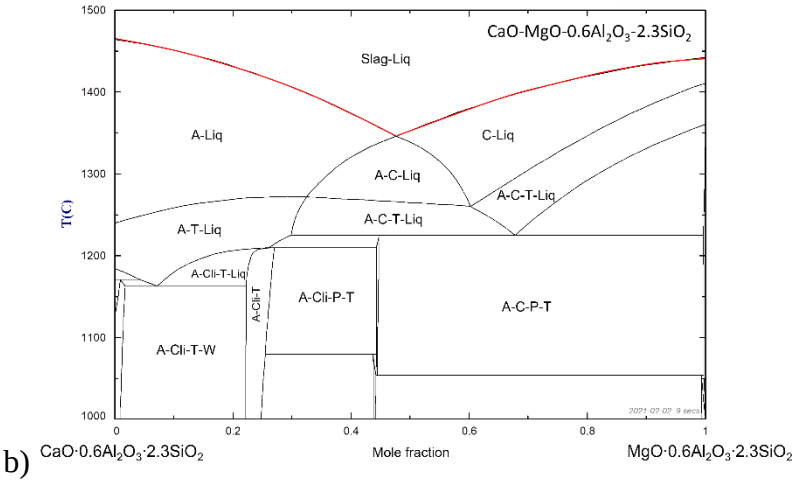

b)

Where, Where, A=Anorthite, C=Cordierite, Cli=Clinopyroxene, P=Protopyroxene, PW=Pseudo-Wollastonite, T=Tridymite, S=SiO_2, W=Wollastonite, and Liq = liquid.

Figure V.7. Calculated phase diagrams for (a) $CaO{\cdot}0.4Al_2O_3{\cdot}2.3SiO_2$—$MgO{\cdot}0.4Al_2O_3{\cdot}2.3SiO_2$ and (b) $CaO{\cdot}0.6Al_2O_3{\cdot}2.3SiO_2$—$MgO{\cdot}0.6Al_2O_3{\cdot}2.3SiO_2$.

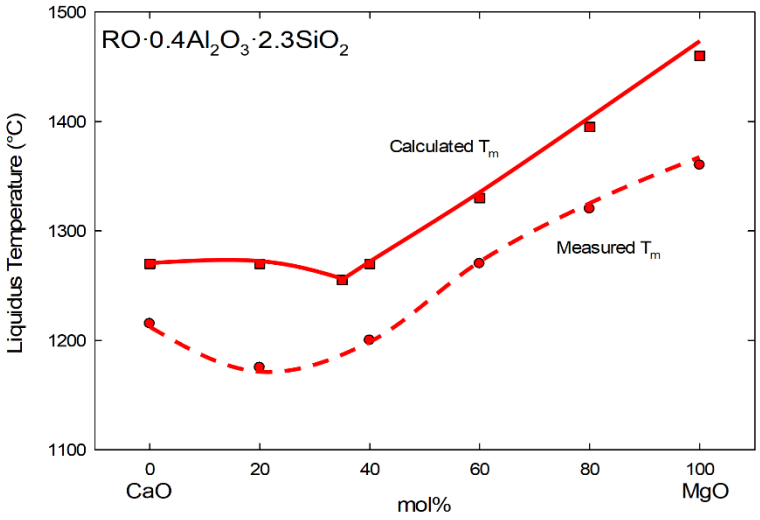

(a)

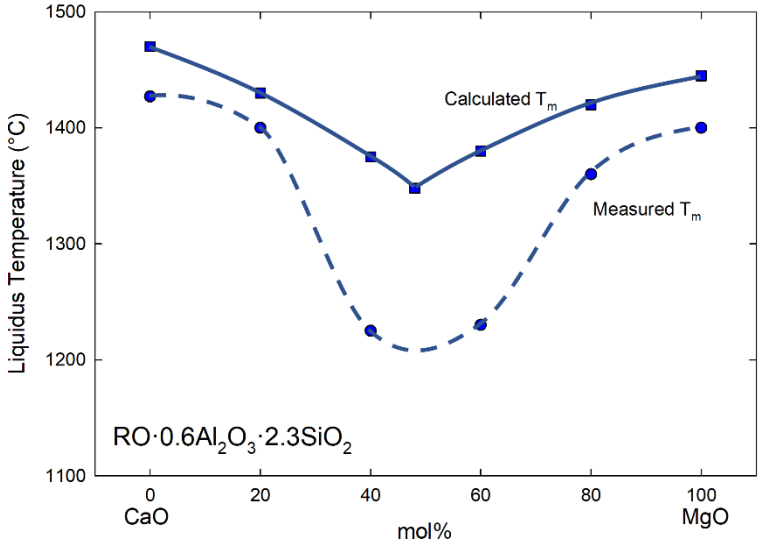

b)

Figure V.8. Comparison of calculated liquidus lines to the measured liquidus lines in the systems of (a) $RO{\cdot}0.4Al_2O_3{\cdot}2.3SiO_2$ glass and (b) $RO{\cdot}0.6Al_2O_3{\cdot}2.3SiO_2$ glass. DTA was used to measure the melting points of the compositions.

Table V-i. Measured and calculated melting points for the compositions used in this study.

Composition ($RO{\cdot}0.4Al_2O_3{\cdot}2.3SiO_2$)	Measured T_M (K)	Calculated T_M (K)	ΔT_M (%)
CaO (endpoint)	1488	1543	3.56
0.8CaO:0.2MgO	1448	1543	6.16
0.6CaO:0.4MgO	1473	1543	4.54
0.4CaO:0.6MgO	1543	1603	3.74
0.2CaO:0.8MgO	1593	1668	4.50
MgO (endpoint)	1633	1733	5.77
($RO{\cdot}0.6Al_2O_3{\cdot}2.3SiO_2$)	Measured T_M	Calculated T_M	ΔT_M (%)
CaO (endpoint)	1700	1743	2.47
0.8CaO:0.2MgO	1673	1703	1.76
0.6CaO:0.4MgO	1498	1648	9.10
0.4CaO:0.6MgO	1503	1653	9.07
0.2CaO:0.8MgO	1633	1693	3.54
MgO (endpoint)	1673	1718	2.62

In the eutectic compositions, the deviation increases with Mg substitution, but in the higher alumina system, the deviation is greater in the vicinity of the lowest temperature. In general, the experimental data agrees well with the calculations.

The Vickers hardness of the calcium and magnesium aluminosilicate glasses are plotted in Figure 9 as a function of the measured melting temperatures. As the plots indicate, the hardness tracks reasonably well with the $0.4Al_2O_3$ glasses (the eutectic glasses) but not with the $0.6Al_2O_3$ glasses. This observation appears to support the structural hypothesis that the degree of network disorder increased with the increase in cation field strength, specifically with the substitution of MgO for CaO.[25] However, for liquidus temperatures, the eutectic compositions appeared to be sensitive to the CFS mechanism while the 0.6 alumina compositions appear to indicate a MAEE.

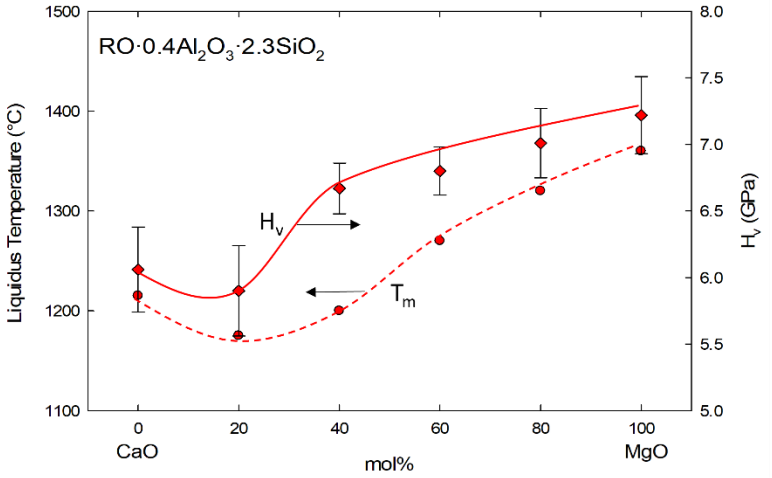

a)

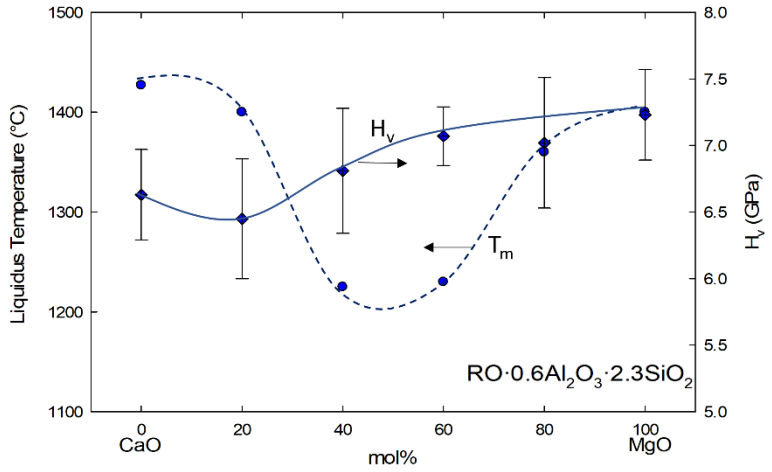

b)

Figure V.9. Measured melting points (T_m) and Vickers hardness of the a) $RO{\cdot}0.4Al_2O_3{\cdot}2.3SiO_2$ and b) $RO{\cdot}0.6Al_2O_3{\cdot}2.3SiO_2$.

V.4.2 CaO + BaO or CaO + SrO Aluminosilicates

In the $BaO\text{-}Al_2O_3\text{-}SiO_2$ (BAS) system, the Ba-feldspar, Celsian, is congruently melting and the 0.6 alumina composition resides within the celsian phase field. The calculated binary phase diagram shows that there is the minimum point in liquidus line with BaO substitution for CaO. There are no stable ternary phases in the $SrO\text{-}Al_2O_3\text{-}SiO_2$ (SAS) system, so the congruent melting hypothesis cannot be evaluated. The calculated CAS-SAS binary phase diagram shows a continuous increase in melting temperature with increasing SrO. These two systems can provide additional data to assess the congruently melting correlation with hardness hypothesis: glass hardness correlates with melting behavior provided the most stable compound is congruently melting and resides within the glass formation region.

Figure 10 shows the calculated liquidus lines of $CaO{\cdot}0.6Al_2O_3{\cdot}2.3SiO_2$—$BaO{\cdot}0.6Al_2O_3{\cdot}2.3SiO_2$ and $CaO{\cdot}0.6Al_2O_3{\cdot}2.3SiO_2$—$SrO{\cdot}0.6Al_2O_3{\cdot}2.3SiO_2$. The minimum in the CAS-BAS system was observed when Ba replaced ~25% of the CaO, but the temperature deviation was less than that observed in the in the CAS-MAS system. Minimal temperature depression was observed in the CAS-SAS system essentially increasing linearly with increasing SrO content. Overall, the melting temperature of the CAS-SAS and CAS-BAS blends were significantly greater than measured in the CAS-MAS system exhibiting similar trends. Only calculated values are employed here as there is limited information published on the BAS and SAS systems.

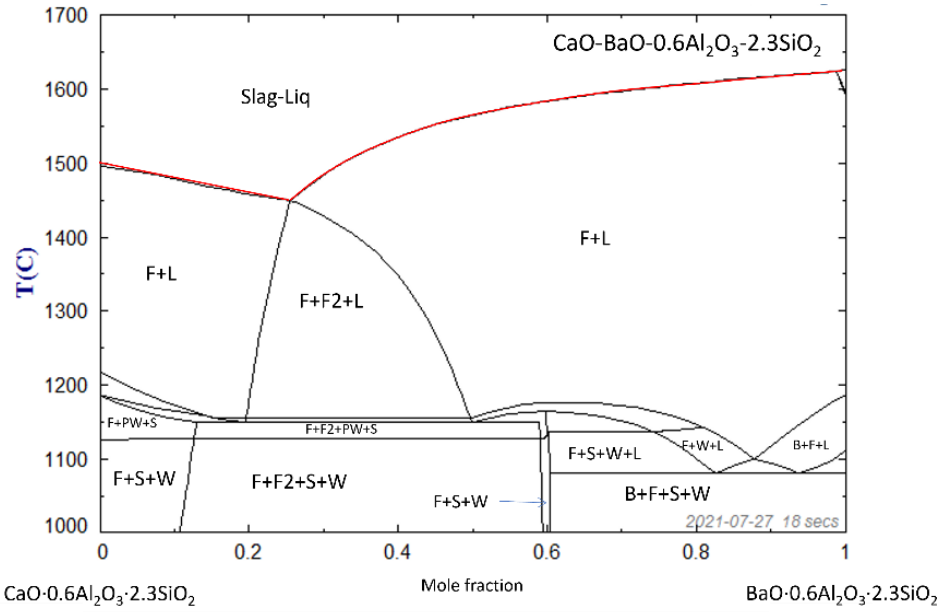

a)

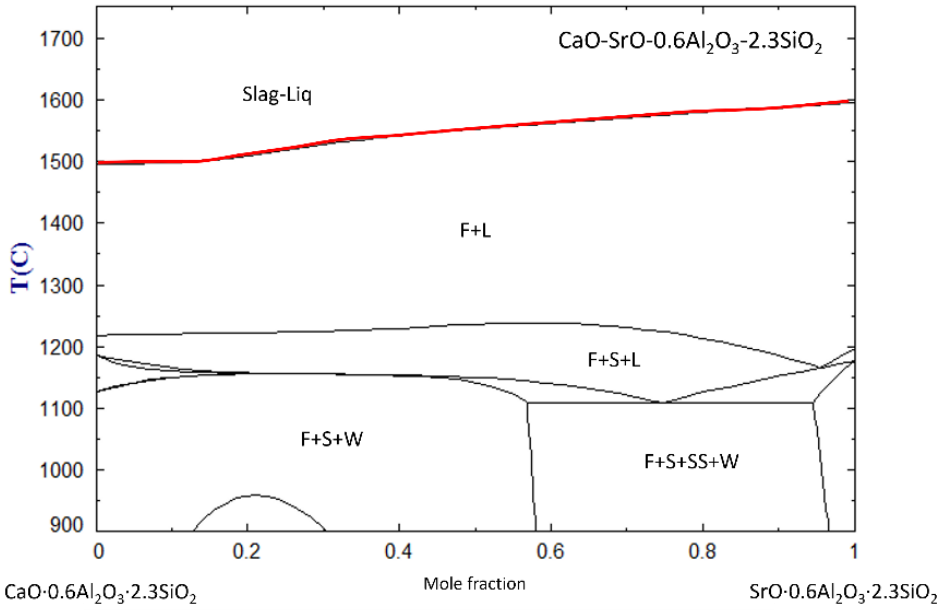

b)

Where, B=$BaSiO_5$, C=Cordierite, Cli=Clinopyroxene, F and F2= Mixed RO Feldspar, PW=Pseudo-Wollastonite, S=SiO_2, SS=$SrSiO_3$, W=Wollastonite, and L=Liq=liquid.

Figure V.10. Calculated phase diagram of (a) $CaO{\cdot}0.6Al_2O_3{\cdot}2.3SiO_2$—$BaO{\cdot}0.6Al_2O_3{\cdot}2.3SiO_2$ and (b) $CaO{\cdot}0.6Al_2O_3{\cdot}2.3SiO_2$—$SrO{\cdot}0.6Al_2O_3{\cdot}2.3SiO_2$. Red lines emphasize the shape of liquidus lines.

For the CAS-BAS and CAS-SAS systems, hardness was compared to calculated liquidus temperatures for the compositions $RO{\cdot}0.6Al_2O_3{\cdot}2.3SiO_2$. It was observed, however, that measured Vickers indentation hardness does not correlate with melting behavior in the systems, as presented in Figure 11. The measured hardness values in both systems exhibited a maximum at 40% CaO. Substitution of RO for CaO above 60% resulted in a dramatic decrease in hardness, but this does correlate with the minimum liquidus temperature observed at ~25% BaO substitution and 100% BaO produced the highest melting point ~1600°C, which also does not correlate with hardness data. No minimum temperature is present in the CAS-SAS system. Observation on the three systems including CaO + MgO, CaO + SrO, and CaO + BaO at $0.6Al_2O_3{\cdot}2.3SiO_2$, indicated that the hardness variation does not correlate with melting temperatures.

In the evaluated systems, one of the systematic variables was the cation field strength of modifier cations. Figure 12 compiles the hardness data of all three substitution systems. It appears clear that hardness is nearly independent of RO substitution for CaO up to approximately 60%. This suggests that RO substitution shows a critical level at 60% and then hardness decreases linearly with additional substitution of RO for CaO with decreased CFS. Above 60%, the hardness increases with MgO addition but decreases with SrO and BaO additions. This would appear to strongly support the CFS argument for alkaline earth cations in aluminosilicate glasses, as shown in Figure 13.

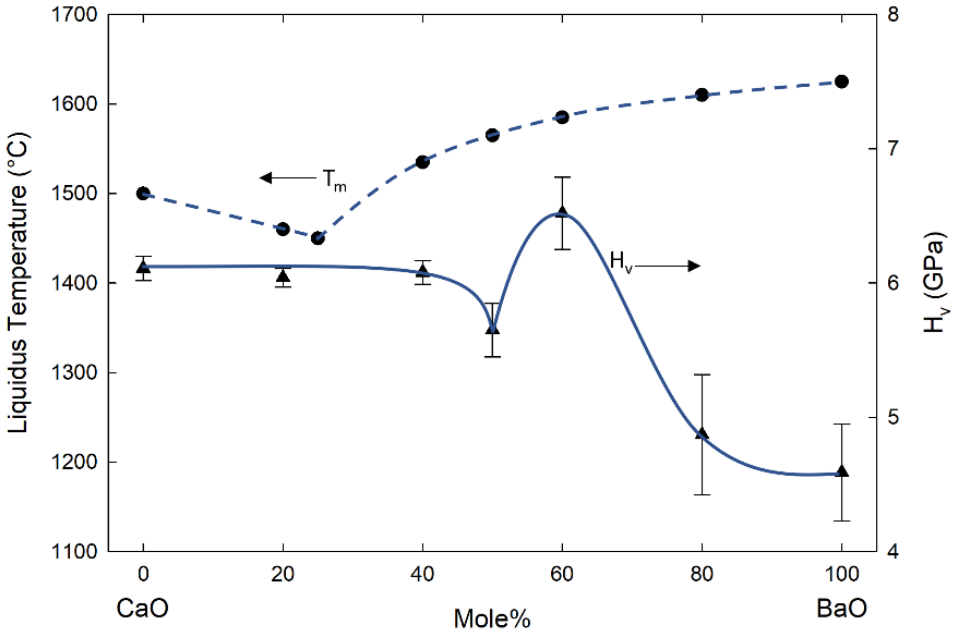

(a)

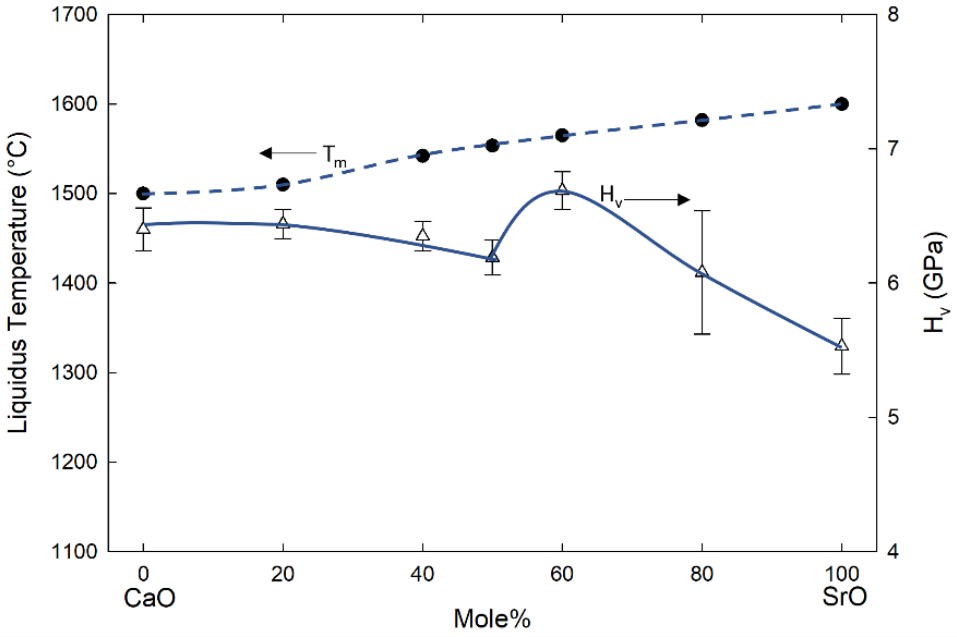

(b)

Figure V.11. Calculated melting points (T_m) and measured Vickers hardness of the $RO{\cdot}0.6Al_2O_3{\cdot}2.3SiO_2$: (a) $xCaO+(1-x)SrO{\cdot}0.4Al_2O_3{\cdot}2.3SiO_2$ and (b) $xCaO+(1-x)BaO{\cdot}0.4Al_2O_3{\cdot}2.3SiO_2$.

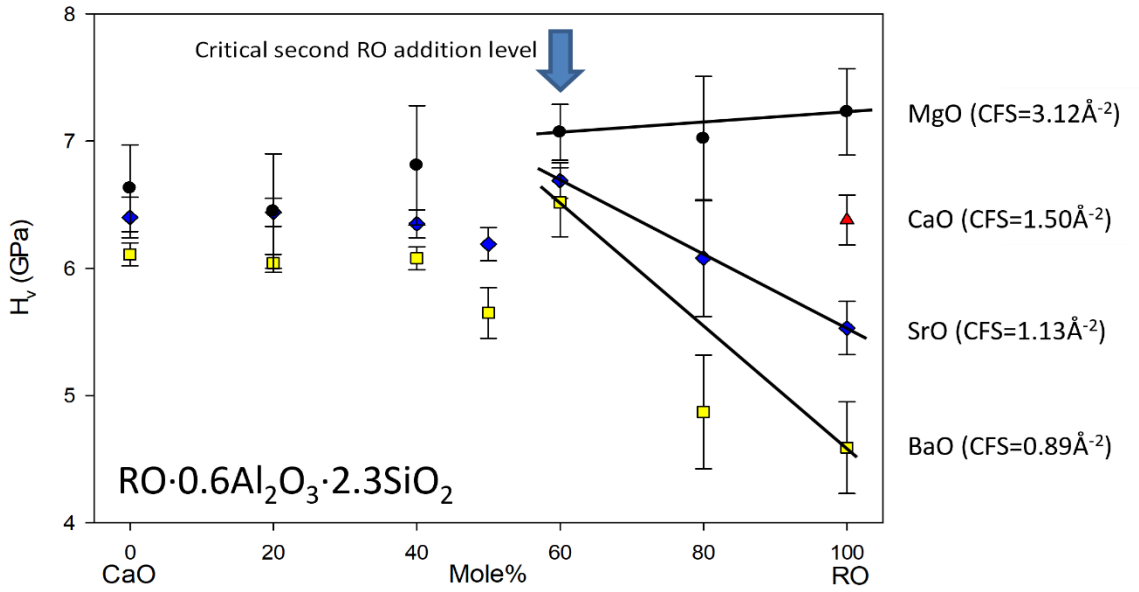

Figure V.12. Vickers hardness of three aluminosilicate glass systems (CaO-MgO, -SrO, and -BaO) as a function of RO substitution.

It was proposed that CFS follows a Rule of Mixtures (ROM) on a molar fraction basis. The composite CFS, CFS_{comp}, is calculated using Equation 1:

$$\left(f_{a,mol} \cdot CFS_a\right) + \left(f_{b,mol} \cdot CFS_b\right) + \cdots + \left(f_{n,mol} \cdot CFS_n\right) = CFS_{comp} \quad (1)$$

Where,

$$f_{a,mol} + f_{b,mol} + \cdots + f_{n,mol} = 1.0 \quad (2)$$

Vickers hardness was plotted as a function of the calculated composite CFS in Figure 13. The results have two distinct slopes, steeply dependent at low CFS (when Ca is blended with Sr and Ba) and one for higher CFS (when Mg substitutes for Ca).

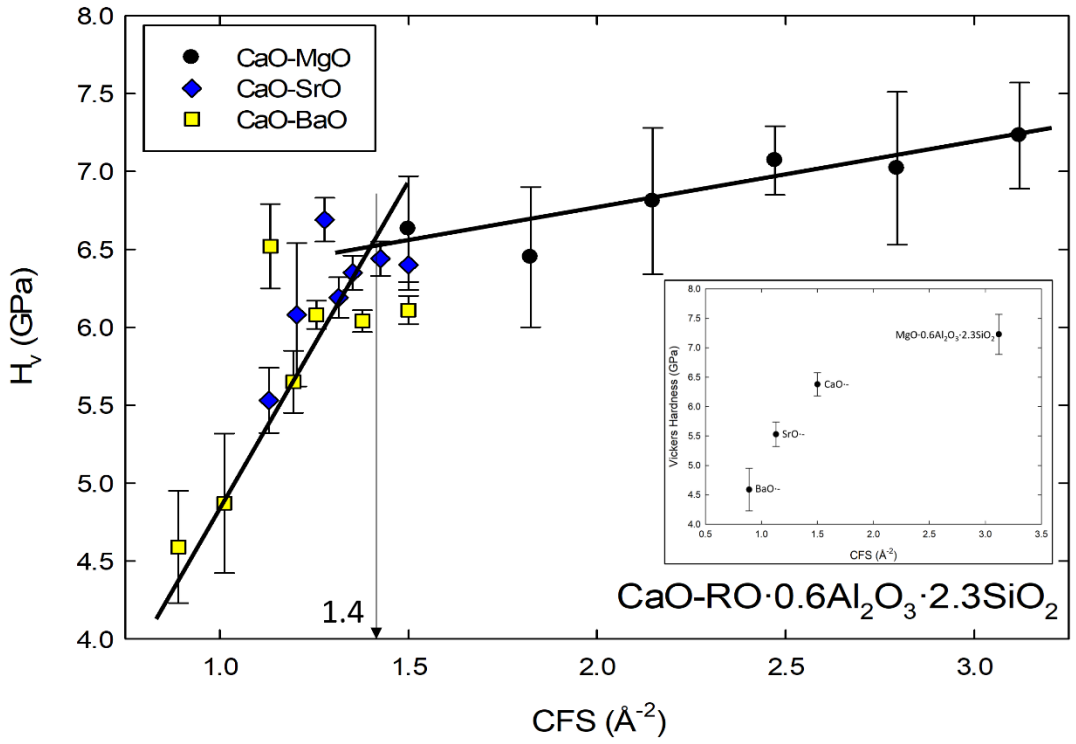

Figure V.13. H_v of the glasses as a function of the combined CFS. Insert: H_v of four endpoint glasses as a function of cation field strength of added modifiers.

Finally, the correlation of the Vickers hardness and liquidus (melting) temperatures were analyzed in Figure 14. Overall, it was demonstrated that the hardness linearly increased with increasing melting temperatures of the 0.4 alumina series in the CAS-MAS system. The linearity supports the hypothesis that hardness scales with melting temperature.

This behavior did not appear to be exhibited by the 0.6 alumina series, however. However, the mechanism is proposed to be similar to the behavior observed in the CAS-BAS and CAS-SAS systems. The hardness increased linearly with increasing melting temperatures up to a point. As shown in Figure 12, the slope changed abruptly, flipping from positive to negative, at approximately 1570°C. It is not proposed that this is a critical temperature, but that at a 60% level of the second RO for CaO, the behavior becomes dominated by the second RO.

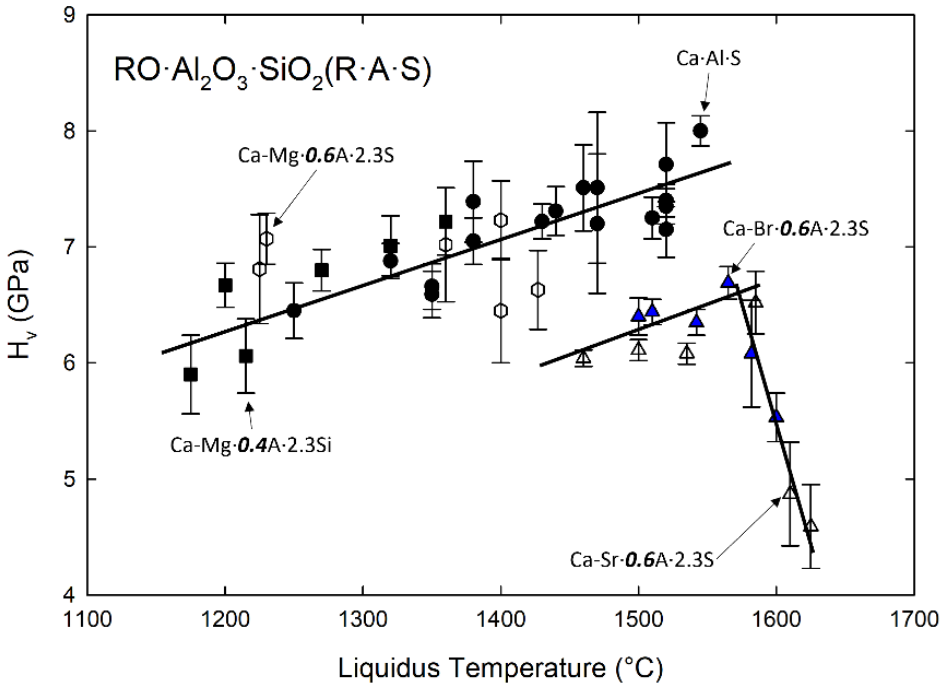

Figure V.14. Correlation of the liquidus temperatures and the Vickers hardness of $RO{\cdot}Al_2O_3{\cdot}SiO_2$ glasses: $CaO{\cdot}Al_2O_3{\cdot}SiO_2$ (●), $CaO\text{-}MgO{\cdot}0.4Al_2O_3{\cdot}2.3SiO_2$ (■), $CaO\text{-}MgO{\cdot}0.6Al_2O_3{\cdot}2.3SiO_2$ (⬡), $CaO\text{-}BaO{\cdot}0.6Al_2O_3{\cdot}2.3SiO_2$ (▲), and $CaO\text{-}SrO{\cdot}0.6Al_2O_3{\cdot}2.3SiO_2$ (△).

For the substantial decrease in hardness in this region, it is proposed that this correlates with the modifier CFS. It is supported that the hardness was ranked based on the CFS of modifiers. The melting temperature in the region was based on the thermodynamic calculation which assumes that the systems are uniform. Overall, the hardness of the RO aluminosilicate glasses is associated with melting temperatures when compositions reside in the eutectic region. When compositions move away from the eutectic, the correlation appears to be linked to the melting behavior of the system (i.e., congruent or incongruent melting). Above the critical addition level of the second RO, the hardness is determined by average CFS of modifiers.

V.5 Conclusion

The effects of MgO substitution for CaO appeared to create melts that differ both structurally and thermodynamically, but the effect was limited to a narrow range of glass chemistry. It was also noted that the glass formation region for MgO-aluminosilicate glasses is significantly smaller than that observed for CaO-aluminosilicate glasses, which consequently limits the range of RO blending. In general, the glass formation boundary deviated linearly with the blending of CaO and MgO.

The correlation of Vickers hardness with melting temperature was observed in the CAS but not in the MAS glasses, nor in the blends of BAS and SAS with CAS glasses. In general, Vickers hardness correlates most strongly with the alumina level. The hardness was marginally improved when CaO was replaced by MgO, but the results deviated linearly. Minimum melting temperatures were measured when MgO and CaO were blended 50:50, consistent with thermodynamic calculations. Different melting behaviors were observed between glasses in the vicinity of the eutectic compared to glass compositions located away from the eutectic. For hardness improvement, there is limited improvement above 40% MgO substitution for CaO, but the melting temperatures decrease significantly.

Above the critical RO blending ratio, Vickers hardness strongly depends on the CFS of the majority RO. The greatest improvement of the hardness was observed when the alumina level is the glass is saturated at 1.2 Al_2O_3.

V.6 References

1. Lee H, Carty WM. Potential Correlation of the Hardness of $CaO-Al_2O_3-SiO_2$ Glasses with Melting Behavior. In process. 2021.

2. Lee H, Carty WM. Correlation of Vickers Hardness of $RO-Al_2O_3-SiO_2$ Glssses with Predicted Liquidus Temperatures. In process. 2021.

3. Varshneya AK. Fundamentals of Inorganic Glasses. Sheffield: Society of Glass Technology; 2006.

4. Tiegel M, Hosseinabadi R, Kuhn S, Herrmann A, Russel C. Young's Modulus, Vickers Hardness and Indentation Fracture Toughness of Alumino Silicate Glasses. Ceram Int. 2015;41:7267-75.

5. Calahoo C, Zwanziger JW. The Mixed Modifier Effect in Ionic Conductivity and Mechanical Properties for $xMgO-(50-x)CaO-50SiO_2$ Glasses. J Non-Cryst Solids. 2017;460:6-18.

6. Kjeldsen J, Smedskjaer MM, Mauro JC, Yue Y. On the Origin of the Mixed Alkali Effect on Indentation in Silicate Glasses. J Non-Cryst Solids. 2014;406:22–6.

7. Kelsey KE, Allwarde JR, Stebbins JF. Ca-Mg Mixing in Aluminosilicate Glasses: An Anvestigation using 17O MAS and 3QMAS and ^{27}Al MAS NMR. J Non-Cryst Solids. 2008;354:4644-3653.

8. Griebenow K, Bragatto B, Kamitsos EI, Wondraczek L. Mixed-Modifier Effect in Alkaline Earth Metaphosphate Glasses. J Non-Cryst Solids. 2018;481:447-56.

9. Maass P. Towards a Theory for the Mixed Alkali Effect in Glasses. J Non-Cryst Solids. 1999;255:35-46.

10. Kjeldsen J, Smedskjaer MM, Mauro JC, Youngman RE, Huang L, Yue Y. Mixed Alkaline Earth Effect in Sodium Aluminosilicate Glasses. J Non-Cryst Solids. 2013:61-8.

11. Kjeldsen J, Smedskjaer MM, Potuzak Ml, Yue Y. Role of Elastic Deformation in Determining the Mixed Alkaline Earth Effect of Hardness in Silicate Glasses. J Appl Phys. 2015;117:034903-1 -7.

12. Kjeldsen J, Smedskjaer MM, Mauro JC, Youngman RE, Huang L, Yue Y. Mixed Alkaline Earth Effect in Sodium Aluminosilicate Glasses. J Non-Cryst Solids. 2013;369:61-8.

13. Lee H, Carty WM. The Glass Formaiton Boundary in Aluminosilicate Systems. In process. 2021.

14. Lee SK, Stebbins JF. Extent of Intermixing Among Framework Units in Silicate Glassses and Melts. Geochimi Cosmochim Acta. 2002;66(2).

15. Thompson LM, Stebbins JF. Non-Stoichiometric Non-Bridging Oxygens and Five-Coordinated Aluminum in Alkaline Earth Aluminosilicate Glases: Effect of Modifier Cation Size. J Non-Cryst Solids. 2012;358:1783-9.

16. Pelton AD, Eriksson GA. Thermodynamic Database Computing System for Multicomponent Glasses. Westerville, OH: Amecian Ceramic Society; 1988.

17. Pelton AD, Blander M, editors. Computer-Assisted Analysis of the Thermodynamic Properties and Phase Diagram of Slags. Proceedings of the Second International Symposium on Metallurgical Slags and Fluxes; 1984; Warrendale, PA: RMS-AIME.

18. Pelton AD, Blander M. Thermodynamic Analysis of Ordered Liquid Solutions by a Modified Quasi-Chemical Approach Application of Silicate Slags. Metall Trans B. 1986;17B:805-15.

19. Bale CW, Bellisle E, Chartrand P, Decterov SA, Eriksson G, Gheribi AE, et al. FactSage Thermochemical Software and Database, 2012-2016. Calphad. 2016;54:35-53.

20. Kim Y, Kashiwara Y, Chung Y. Effect of Varying Al_2O_3 Contents of CaO-Al_2O_3-SiO_2 Slags on Lumped MgO Dissolution. Ceram Int. 2020;46:6205-11.

21. Pei F, Zhu G, Li P, Guo H, Yang P. Effects of CaF_2 on the Sintering and Crystallisation of CaO-MgO-Al_2O_3-SiO_2 Glass-Ceramics. Cermics international. 2020;46:17825-35.

22. Wang S, Chen M, Guo Y, Jiang T, Zhao B. Comparison of Phase Equilibria Between FactSage Predictions and Experimental Results in Titanium Oxide-Containing System. Calphad. 2018;63:77-81.

23. Rocha VC, Alves PC, Pereira JM, Leal LP, Bielefeldt WV, Vilela ACF. Experimental and Thermodynamic Analysis of MgO Satration in the CaO-SiO_2-Al_2O_3-MgO Slag System Melted in a Laboratory Resistive Furnace. J mater Res technol. 2019;8(1):861-70.

24. Wang Z, Sohn I. Effect of the Al_2O_3/SiO_2 Mass Ratio on the Crystallization Behavior of $CaO-SiO_2-MgO-Al_2O_3$ Slags using Confocal Laser Scanning Microscopy. Ceram Int. 2018;44:19268-77.

25. S. K. Lee, Stebbins JF. Extent of Intermixing Among Framework Units in Silicate Glasses and Melts. Geochimi Cosmochim Acta. 2002;66(2):303-9.

VI EVALUATION OF THE EFFECTS OF MOLYBDENUM ON THE HARDNESS OF RO-Al_2O_3-SiO_2 GLASSES

VI.1 Abstract

It has been proposed that indentation hardness is promoted by increasing the complexity of the glass structure and cation field strength. To test this hypothesis Mo^{6+}, with CFS of ~11.26 $Å^{-2}$, was added to high hardness CaO-Al_2O_3-SiO_2 glasses. The glass compositions were centered around the composition $CaO{\cdot}Al_2O_3{\cdot}1.5SiO_2$ which was shown to produce a glass with high hardness and a minimal level of non-bridging oxygen atoms. Three levels of Mo^{6+} were added to three parent glasses (containing 0.8, 1.0, and 1.2 Al_2O_3 and 1.5 SiO_2) prepared by quenching and by slow cooling. The results indicate that Mo serves as a heterogeneous nucleation site for crystallization resulting in anorthite precipitation with slow cooling. At 1.2 Al_2O_3 corundum precipitated as a secondary crystallization product proposed to be due to a shift in the residual glass composition with anorthite crystallization. Even lower alumina levels (0.8) exhibited anorthite crystallization even though this composition resides well within the glass formation region.

Keywords: Glass hardness, Cation field strength, Mo-doped glass, Calcium aluminosilicate glasses

VI.2 Introduction

The indentation hardness of glass is linked to compressibility of the glass network and can be increased by increasing the atomic density of the system.[1-4] It is proposed that it should be possible to locally increase the atomic density through the use of highly charged cations with high field strengths such as Cr^{6+}, Mo^{6+}, or W^{6+}. It was anticipated that the local network distortion due to high cation field strengths would resist plastic deformation and local densification of the glass structure and thus increase the indentation hardness.

Three routes were proposed to increase glass hardness: (1) the elimination of NBO by the incorporation of Al^{3+};[5, 6] (2) the substitution of other divalent cations, i.e., Mg^{2+} for

$Ca^{2+}$to increase the cation field strength for the overall glass network;[6] and (3) introduce small amounts of Mo^{6+} as dopants to maintain glass formation but alter the structure.

In alkaline earth aluminosilicate glasses, the incorporation of one mole of alumina per mole of RO (alkaline earth oxides, CaO, MgO, etc.) compensates for charge imbalance and generates the minimum level of NBOs. The addition of Mo^{6+} cations would tie up any remaining NBOs to further enhance hardness. The high bonding energy of Mo reduces the Mo-O bond length, and the small size distorts the local structure, resulting in localized compaction of the glass structure. The desirable scenario would be to start with a high hardness initial glass (i.e., a parent glass) composition and add to that glass small amounts of Mo^{6+}.

All glass compositions are represented on a molar ratio basis normalized to flux level (defined at 1.0 moles). The molar composition of 1.0:1.0:1.5 ($CaO:Al_2O_3:SiO_2$), containing one mole of flux (CaO in this case), one mole of alumina and 1.5 moles of silica, was chosen as the parent glass. Three alumina levels were evaluated: 0.8, 1.0, and 1.2. The compositions were melted and initially cooled in the furnace (not quenched) and a second set was quenched to address crystallization tendencies. Mo^{6+} additions ranged from 100 to 1000 ppm. These samples were evaluated for chemistry, microstructure, glass transformation temperature, and hardness.

High valency cations, i.e., Mo^{6+}

The high valency cation concept proposes that the high bond strength reduces the cation-oxygen (Mo-O) distance to create local regions of high density. It is reported that the saturation limit of Mo in glass is relatively low, <5 mole%,[7] so low levels of Mo^{6+} are necessary to keep the Mo-Mo distances sufficiently large within the melt to prevent MoO_3 nucleation and crystallization. Due to high charge and high CFS, Mo^{6+} can bond to six non-bridging oxygens to maintain charge balance.

Mo^{6+} was the best candidate for several reasons. In general, molybdenum oxide (MoO_3), is categorized as a glass former while Cr^{6+} is categorized as an intermediate.[8] Molybdenum has two oxidation states, 3+ and 6+, with the 6+ state the more stable form.[9]

Mo (VI) in glasses can be coordinated by 4 to 6 oxygens, however, it is mostly four-fold coordinated. Typical Mo-O distance in glass ranged from 0.176-0.178 nm[10] with a cation field strength (CFS = $Z/Å^2$) of ~11.26 $Å^{-2}$. Table I lists pertinent CFS values. It was reported that Mo tetrahedrons are often not connected to the glass tetrahedral framework meaning that Mo oxide has a strong tendency to crystallize. Typical Mo-O bond valence is high, therefore the connection with bridging oxide is restricted.

It was anticipated that the use of Mo for hardness improvement requires avoiding crystallization. It is proposed that the role of Mo^{6+} on hardness would be independent of the silicate and aluminosilicate matrix glass structure, and the formation of $[MoO_4]^{2-}$ tetrahedra would increase the hardness compared to the parent glass composition.

Table VI-i. Examples of ionic radii and their cation field strengths.[11]

	Si^{4+}		Al^{3+}		Mg^{2+}	Ca^{2+}	Mo^{6+}
CN	4	6	4	6	6	6	6
Valency	4	4	3	3	2	2	6
Ionic Radii, r (Å)	0.26	0.39	0.39	0.53	0.72	1	0.73
Z/r^2 ($Å^{-2}$) (CFS)	59.17	26.30	19.72	10.68	3.86	2.00	11.26

VI.3 Experimental procedure

Glass preparation was similar to that described in previous work.[6, 11] The parent glass compositions and designations are presented in Table II. The maximum hardness was obtained with the composition $CaO·Al_2O_3·1.5SiO_2$.[5] Thus, two additional alumina levels at 0.8 and 1.2 with a constant silica level of 1.5 were also prepared to which Mo^{6+} was added at levels of 100, 300, and 1000 ppm, equivalent to 1.0 x 10^{-5}, 3.0 x 10^{-4}, and 1.0 x 10^{-4} mole % Mo, respectively.

Two sets of batches were melted for 3 hours at 1600°C in zircon crucibles. In this study, one set was naturally cooled in the furnace for experimental consistency with previous work[6, 12] and the other set was quenched. Chemistry of each glass of the first set was confirmed using energy dispersive spectroscopy (EDS, EDAX Inc., Mahwah, NJ) in a SEM (Quanta 200F, FEI, Hillsboro, OR) and is presented in Table II.

Table VI-ii. Sample designations according to the target compositions. Chemistry was measured using EDS.

	Target (Constant @1.5 SiO_2:CaO)		Measured using EDS				
Sample ID	Al_2O_3/CaO	Mo^{6+} addition (ppm)	CaO	Al_2O_3	SiO_2	Al_2O_3/CaO	SiO_2/CaO
0.8-100	**0.80**	100	28.85	23.26	47.71	**0.81**	1.65
0.8-300	**0.80**	300	29.10	23.28	47.62	**0.80**	1.64
0.8-1000	**0.80**	1000	29.14	23.34	47.52	**0.80**	1.63
1.0-100	**1.00**	100	28.08	26.24	45.68	**0.93**	1.63
1.0-300	**1.00**	300	27.47	26.92	45.61	**0.98**	1.66
1.0-1000	**1.00**	1000	27.61	27.55	44.84	**1.00**	1.62
1.2-100	**1.20**	100	25.47	29.79	44.68	**1.17**	1.75
1.2-300	**1.20**	300	26.47	28.49	45.04	**1.08**	1.70
1.2-1000	**1.20**	1000	26.46	29.39	44.15	**1.11**	1.67

Addition of Mo^{6+} to the Glass Batch

To avoid the addition of crystalline MoO_3, Mo^{6+} was added as molybdenum ions introduced via a water soluble salt, $(NH_4)_6Mo_7O_{24}$.[13] It was proposed that, similar to the adsorption of Ce^{3+} ions on kaolinite surfaces,[14] Mo^{6+} would have a similar affinity for kaolinite allowing ionic Mo^{6+} to be added to the batch as an immobilized species adsorbed on the surface of kaolinite particles. It is well documented that cation adsorption on kaolinite is a stable process and difficult to reverse.[15] Mo^{6+} adsorption was conducted as an aqueous-based pre-batching process step. A commercial kaolinitic clay (EPK, Edgar Minerals, Florida) was selected as the carrier and it is proposed that specific adsorption occurs on the silica-like surface of the kaolin particles.[16]

To determine the amount of clay necessary for the target levels of Mo, a depletion method was employed where the amount of Mo added is compared to the amount of Mo left in the bulk solution after the introduction of kaolinite particles.[15] The difference is the amount of Mo adsorbed on the clay particle surface. In this study, clay was dispersed in water and the pH was adjusted to 7.0 with one normal NH_4OH, the Mo salt was then added, and the slurry mixed for 30 minutes with a magnetic stir bar. After mixing the suspensions were centrifuged and the supernatant analyzed via ICP (Water Chemistry, Bureau Veritas Minerals Laboratories, Vancouver, Canada.) Figure 1 shows the Mo adsorption levels as a function of the Mo/kaolin ratios (molar basis). Relatively high adsorption was observed even from the highest Mo addition levels (the lowest carrier

amount, ~20 mole%). Saturation adsorption was achieved at ~0.02 mole % (200ppm) of Mo/kaolin. Only small amount of clay was necessary to introduce the target level of Mo^{6+} ions. To reach the maximum desired Mo^{6+} level only one percent kaolin was necessary to be added to the batch.

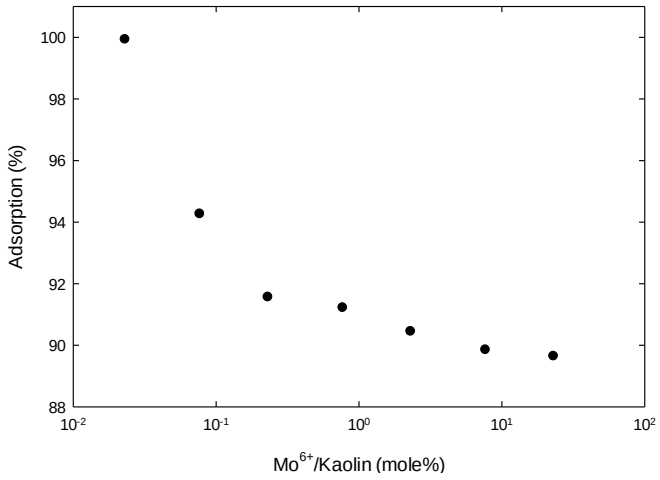

Figure VI.1. Mo^{6+} adsorption on kaolin surface as a function of the addition ratio, Mo^{6+}/Kaolin.

Characterization

The resulting glasses were characterized for chemistry and elemental distribution, mineralogy, bulk properties, and Vickers indentation hardness. The distribution of molybdenum was evaluated by mapping via wavelength dispersive spectroscopy (WDS, JXA-8200F, Jeol, Ltd, Tokyo, Japan). Mineralogy was obtained using powder X-ray diffraction (XRD, D2 Phaser, Bruker, Madison, WI) and density via a pycnometer method (He-pycnometer, AccuPyc II 1340, Micromeritics, Norcross, GA). The chemistry and density results were combined to calculate the molar volume. Micro Vickers hardness was measured (V-100-A2, Leco, Japan) at a load of 1.0 kilogram applied for 15 seconds. Dimension of the indents were measured using an optical microscope (Polyvar, Leica, Buffalo, NY). The Vickers hardness measurements were verified against an NIST traceable standard (Standard 2831, NIST, Gaithersburg, MD).

VI.4 Results and Discussion

VI.4.1 Naturally cooled Glasses

The Mo^{6+} spacing was calculated assuming a cubic array with Mo^{6+} ions linearly positioned between 10, 15, and 20 silica tetrahedra. For the calculation, a published Si-Si distance of 3.12 Å was used.[17] It was further assumed that Si-Si and Si-Al distances were similar, so tetrahedrally coordinated Al was assumed to be identical to tetrahedrally coordinated Si. For these calculations, the glass composition was assumed to be $CaO{\cdot}Al_2O_3{\cdot}1.5SiO_2$. The results of the calculations are summarized in Table III. The Mo ion separation is therefore directly related to the number of silica tetrahedra. For example, there is one Mo^{6+} ion per 10,000 tetrahedra at an addition level of 100 ppm. The number of tetrahedrons (T) in one dimension of a 3-D cubic network can be estimated by the cube root of the number of tetrahedra involved: $10{,}000^{1/3}$ = ~21.5 tetrahedra linearly. In a similar manner, 1,000 tetrahedra equate to $\sim 10^3$ tetrahedra, a cubic edge dimension of 67.2 Å, and correlates to 1,000 ppm Mo^{6+} ions.

Table VI-iii. Calculated distance and number of Si or Al tetrahedra between two Mo^{6+} ions based on their addition levels, assuming a center-center tetrahedra distance of 3.12 Å.[17]

Composition (mole)							
CaO	Al_2O_3	SiO_2	# Al+Si	Mo addition (ppm)	# T* per Mo^{6+}	# T* between Mo^{6+}	Distance between two Mo^{6+} ions in 3D network (Å)
1.0	1.2	1.5	3.9	100	10000	22.0	67.2
				300	3300	15.3	46.6
				1000	1000	10.2	31.2

* Al + Si tetrahedrons

It is known that there are two "anomalies" in the glass structure: NBOs (to a minor extent) and Al^{3+} ions coordinated either 4-fold or 5-fold with oxygen. [5, 6] These are assumed to not significantly affect these calculations. These calculations indicate that the average distance between Mo^{6+} ions ranged from 31 – 67 Å which reasonably matches 20, 15, and 10 tetrahedrons for Mo^{6+} ion concentrations of 100, 300, and 1,000 ppm,

respectively. The micro-indentation depression in these glasses was generally approximately 50 μm from corner to corner, and thus would be testing a volume containing at least 10^4 Mo^{6+} ions assuming a uniform Mo distribution.

All the glasses crystallized when slow cooled. With crystallization, the hardness of the 1.0:0.8:1.5 decreased slightly compared to the glass without Mo additions.[6] In 1.0:1.0:1.5 and 1.0:1.2:1.5 both the crystallization of anorthite and precipitated molybdenum oxide were observed. Hardness measurements were attempted for all samples, but it was only possible to collect hardness values for 1.0:0.8:1.5 containing 100, 300, and 1000 ppm Mo due to severe damage in vicinity of the indentation. The measured average hardness of the parent glasses was 7.7 (±0.4) GPa, but the addition of Mo reduced the hardness to a range of 6.3 (± 0.5) to 6.8 (± 0.5) GPa.

Figure 2 presents the XRD results showing the crystallization of anorthite and corundum for the 300 and 1000 ppm Mo additions. The maximum Mo^{6+} addition was 1000 ppm, or ~0.02% on a mass basis, confirmed by independent chemical analysis (ICP), so it was unexpected to detect MoO_3 as a precipitated crystalline phase. In addition, the lack of peak shift in XRD indicated that there was limited Mo substitution in the anorthite lattice, but the dramatic increase in anorthite crystallization indicates that Mo is likely acting as a heterogeneous nucleation site.

Semi-quantitative analysis of the anorthite patterns was conducted based on peak area of the major peaks under consistent measurement conditions. In general, the results indicated a small increase in anorthite concentration with an increase in Mo level from 100 to 300 ppm but remaining constant above 300 ppm.

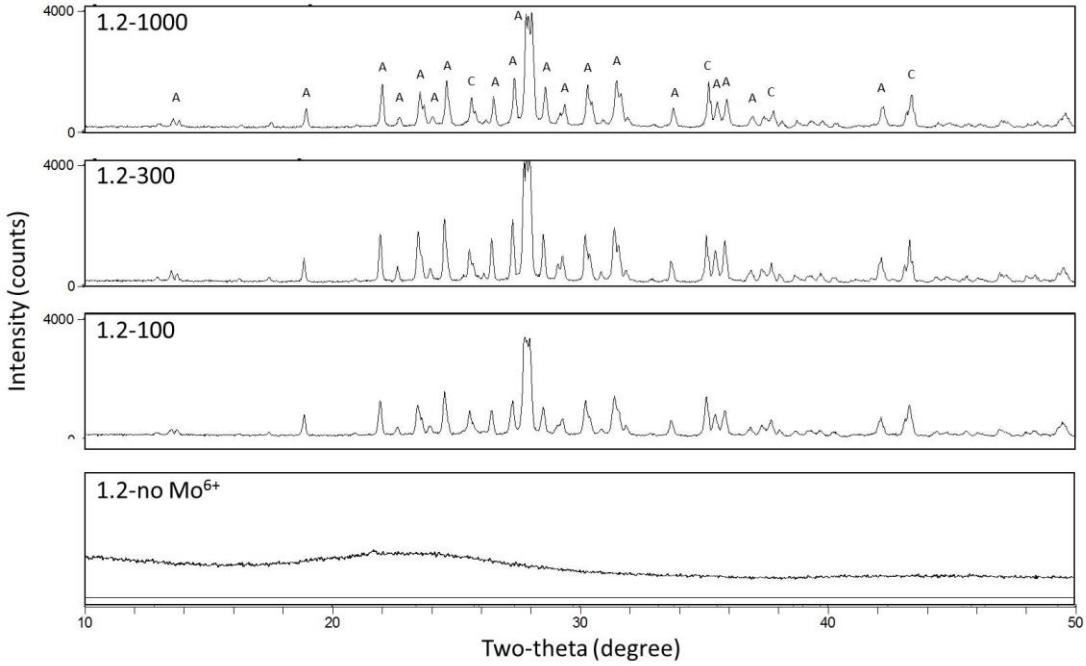

Figure VI.2. XRD patterns of 1.2-100 (bottom), 300 (middle), and 1000 (top) samples. Anorthite ($CaAl_2Si_2O_8$, A) and corundum (Al_2O_3, C) were major phases in all samples. Crystallization was not observed in similar compositions prepared without Mo^{6+}.

Crystallization of corundum was observed, as presented in Figure 3, for 100 ppm Mo additions. All the samples contained anorthite as the major precipitated phase, but corundum was also observed in the 1.0 and 1.2 alumina samples. Ordered and disordered anorthite was observed in the 1.0 and 1.2 alumina samples but only ordered anorthite was found in the 0.8-300 sample (Figure 4). In addition, peak broadening was observed in the 0.8-300 specimen compared to 1.2-300 indicating a significantly finer crystallite size in 0.8-300 specimens.

For both compositions possessing disordered anorthite, the SiO_2:Al_2O_3 ratios were 1.5 and 1.25 which is sufficient to satisfy the Al-avoidance rule.[18] However, it is proposed that high melting temperature and Mo^{6+} incorporation promote Al-O-Al bond formation. When the heat treatment temperature approaches the melting point, the Al-Si bonding is less ordered compared to room temperature due to the temperature dependence of system

entropy.[19] In addition, the melt structure denoted by tetrahedra bonding angles or Al-O-Al and Si-O-Al population, can be altered by the valency of the modifier cations.[20] Further, it is more likely that higher valency cations promote Al-O-Al bonding as a charge compensation mechanism. The disordered anorthite in 1.0 and 1.2 Al_2O_3 samples is proposed to be a consequence of Mo additions and conversion to Al-O-Al bonding.

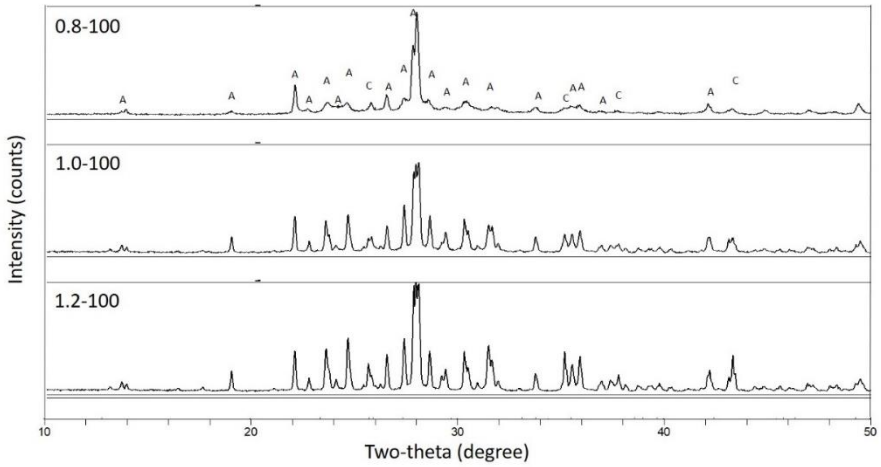

Figure VI.3. XRD patterns of 0.8- (top), 1.0-(middle), and 1.2- 100 (bottom) samples. Anorthite (A) and corundum (C) were major phases.

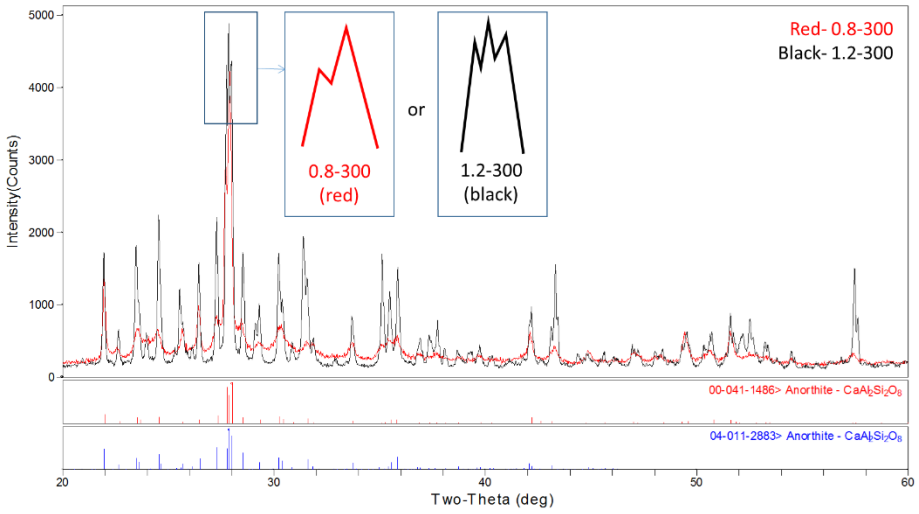

Figure VI.4. XRD patterns of ordered anorthite (0.8-300 in red) and disordered anorthite (1.2-300 in black).

Microstructure development was intensely affected by the Mo^{6+} additions. SEM images of the 0.8-Al_2O_3 samples are presented in Figure 5. Very fine oriented and uniformly distributed anorthite needles precipitated in the 0.8 mole alumina samples with the addition of Mo. The microstructures confirm the XRD results that indicate only one precipitated phase (see Figures 3 and 4) and independent of Mo addition level.

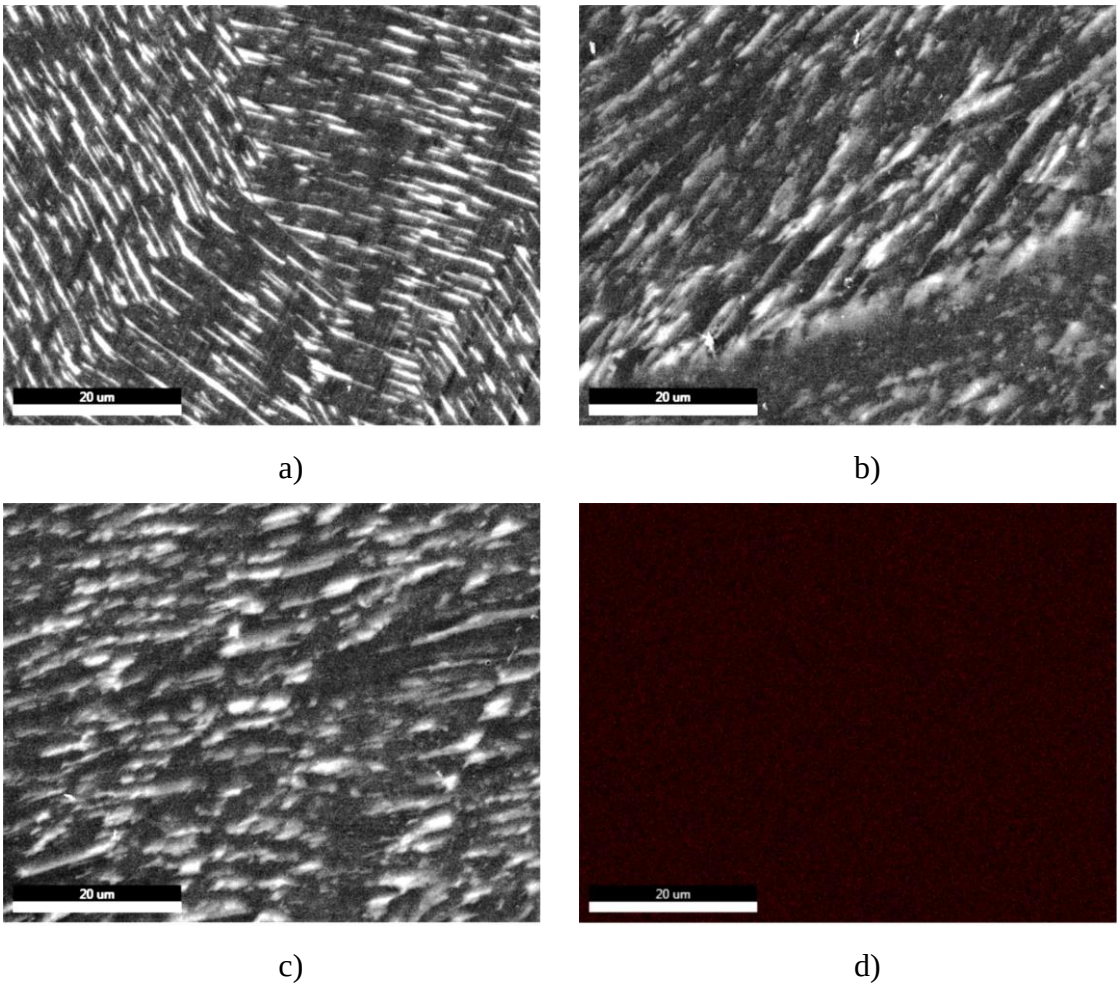

a) b)

c) d)

Figure VI.5. BSE images of the sample a) 0.8-100, b) 0.8-300, and c) 0.8-1000 compared to d) WDS map of molybdenum showing no Mo precipitation was observed. The white streaks in BSE images are anorthite crystallites.

Anorthite crystalline size was significantly enhanced in both 1.0 and 1.2 mole alumina samples compared to the 0.8 mole alumina sample. (Figure 6) Large anorthite crystallites are observed at higher alumina contents. In addition to anorthite, needle-shaped

corundum precipitates were observed in the microstructures of 1.0 alumina level and blocky corundum precipitates at an alumina level of 1.2.

Molybdenum precipitation was occasionally observed within the anorthite crystals in the 1.2-1000 as illustrated in Figure 7, but it was not uniformly detectable via chemical mapping. EDS spectrum and BSE images indicated MoO_3 precipitation in 1.2-1000. There does not appear to be any Mo incorporation in corundum crystallites.

At low Mo levels (<300 ppm) the Mo is uniformly dispersed and evidently below the level necessary to allow MoO_3 precipitation. At higher levels (>300 ppm) Mo both facilitates anorthite crystallization and allows MoO_3 precipitation. The precipitation of corundum does not appear to correlate with Mo additions, but instead is related to the alumina level in the glass. The precipitation of anorthite extracts chemistry from the glass and pushes the residual glass chemistry into the corundum phase field, resulting in corundum crystallization as a secondary crystallization step.

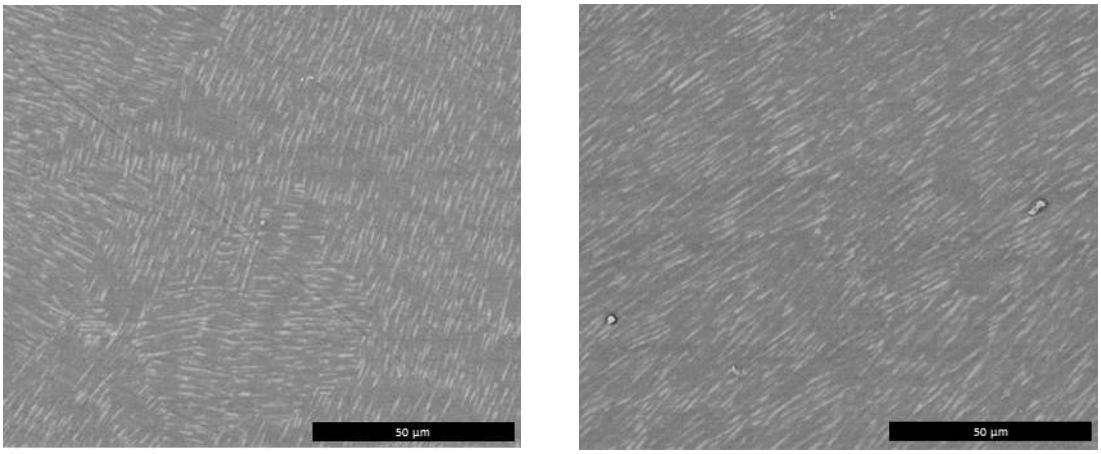

a) BSE images of the sample 0.8-100 (left) and 0.8-1000 (right)

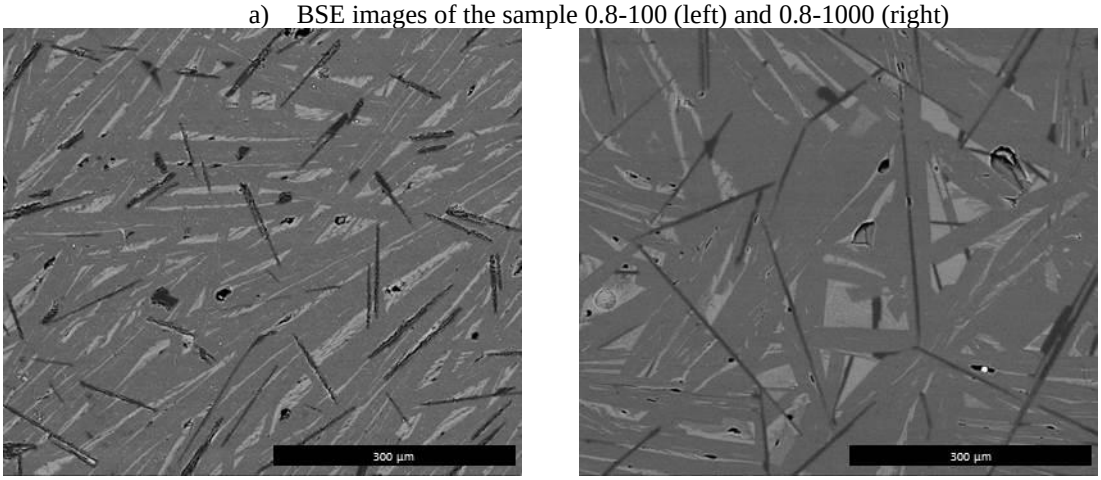

b) BSE images of the sample 1.0-100 (left) and 1.0-1000 (right)

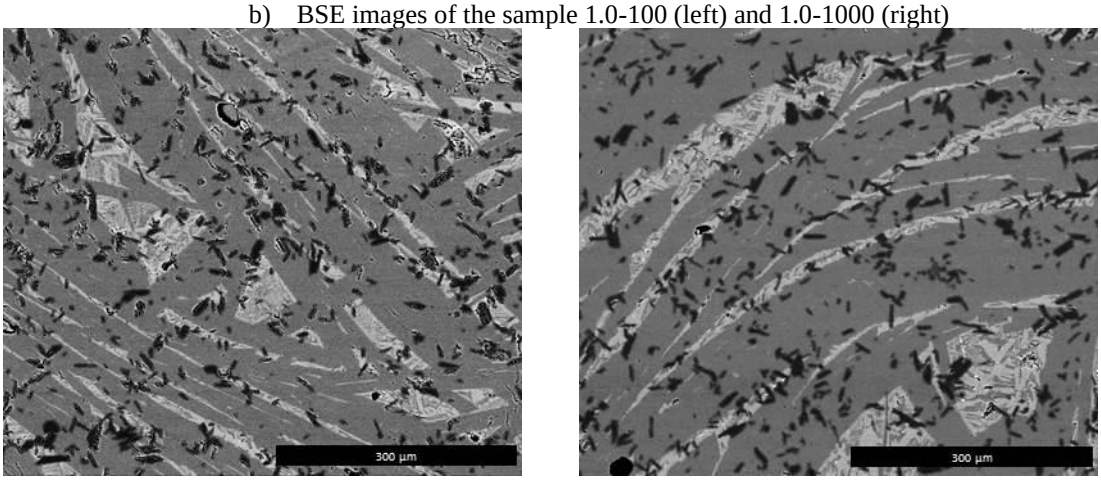

c) BSE images of the sample 1.2-100 (left) and 1.2-1000 (right).

Figure VI.6. SEM backscatter images of polished cross sections of six melted samples. Black spots in b) are alumina particles based on EDS analysis. (Light grey crystallites: anorthite; black crystallites: corundum)

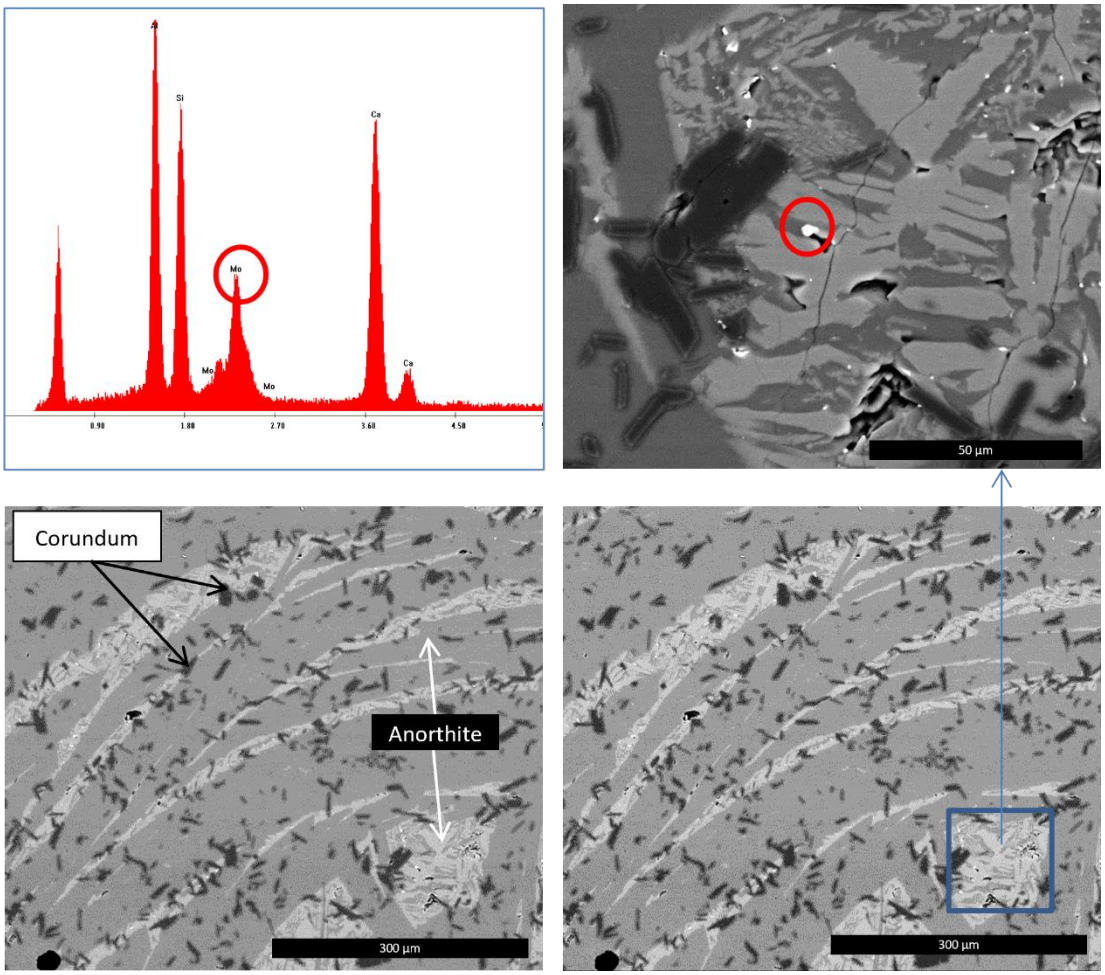

Figure VI.7. EDS spectrum and BSE images of precipitated molybdenum oxide (bright spots) in anorthite crystals (1.2-1000), confirmed by EDS (bottom left). Corundum crystals present as prismatic particles and anorthite crystals show as light gray needles.

The 0.8 mole alumina samples precipitated fine-grained anorthite, but precipitated MoO_3 was not observed. Heterogeneous nucleation is proposed to facilitate anorthite formation. Mo ions, coordinated by oxygen, compress the glass network, creating strain. Local disorder, with residual strain, can act as heterogeneous nucleation sites, thus supporting anorthite crystallization.[21]

The precipitation of anorthite causes a shift in the chemistry of the remaining glass, as illustrated in Figure 8. The 1.2 Al_2O_3 glass resides on the glass formation boundary.[12] Even small amount of anorthite formation alters the remaining glass composition

sufficiently to move out of the glass formation region into the corundum phase field, resulting in corundum precipitation. Anorthite crystallization is ultimately limited by CaO level. In the case of the 0.8 alumina samples, even after anorthite crystallization, the glass chemistry balance remains in the glass formation region and does not enter the corundum phase field, thus avoiding corundum precipitation.

The reduction in hardness of 0.8 Al_2O_3 is a result of anorthite precipitation that shifts the composition to lower alumina levels on a trajectory away from anorthite and potentially moves the composition into the invert glass region. This shift in chemistry also drops the viscosity of the glass phase and is consistent with a reduction in the liquidus temperature based on the phase diagram. A correlation between liquidus temperature and hardness was discussed in previous studies.[5, 6]

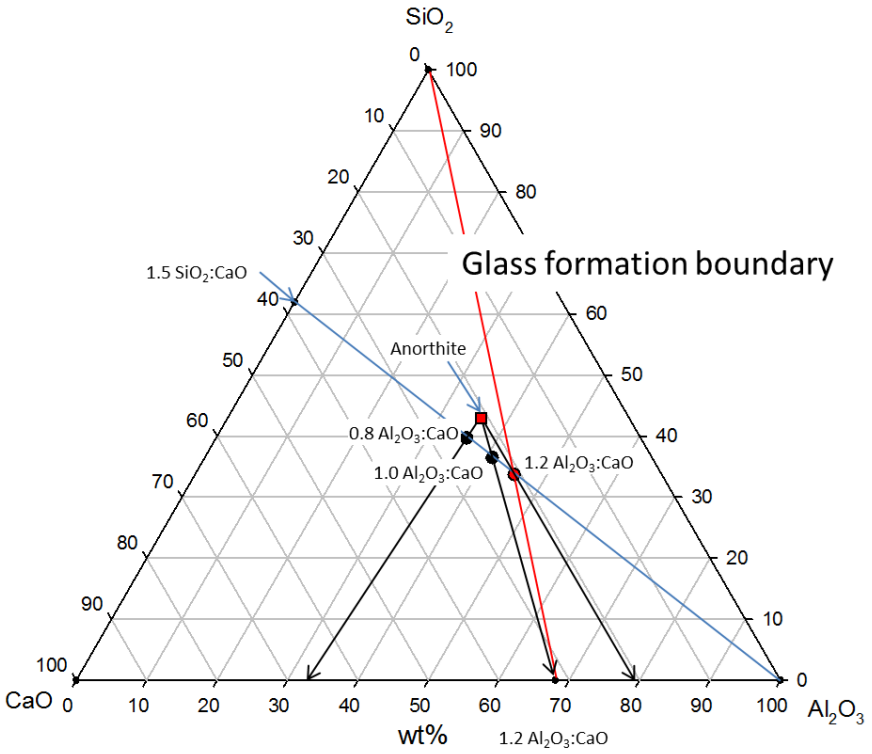

Figure VI.8. Glass compositional paths when anorthite (identified as a square) crystallizes from the glass. Three original batching compositions are presented as two black points one red (1.2 Al_2O_3:CaO glass). The compositional change directions of each composition are indicated with arrows.

VI.4.2 Normal melting glasses

To better evaluate the role of Mo on hardness in CAS glasses, additional samples were prepared by quenching to avoid crystallization. The glasses were melted in zircon crucibles, and it was verified that these crucibles were inert with respect to the glass melt, i.e., no corrosion was observed and no Zr was present in the resulting glasses, as shown in Figure 9, and no Mo precipitation was observed in association with zircon. All samples were heat treated for 3 hours at 1600°C and were immediately moved to an annealing furnace at 800°C.

Three parent glass compositions were prepared with 300 ppm Mo^{6+} additions and two additional Mo levels of 600 ppm and 1000 ppm were added to the $1.0Al_2O_3$ glass.

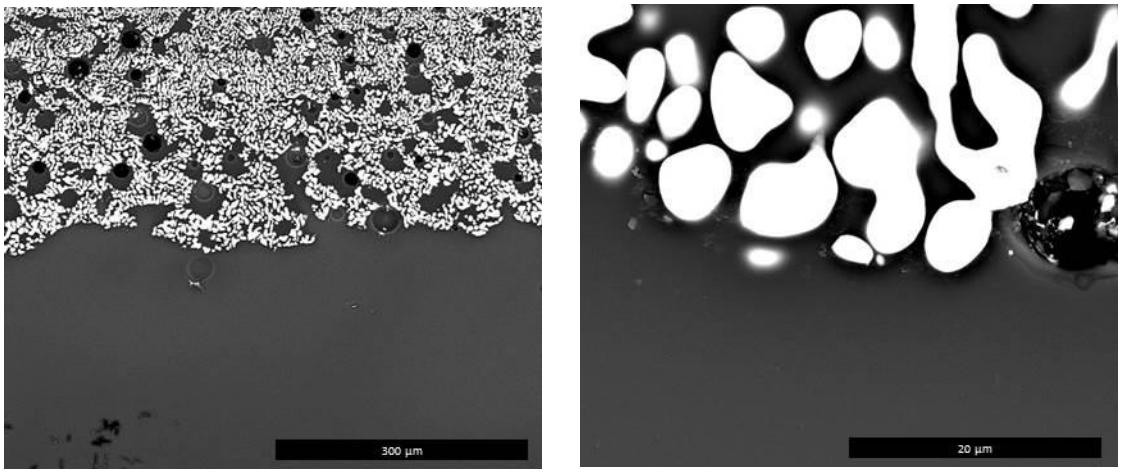

Figure VI.9. SEM (back scattered electron) images of the interface between glass and zircon crucible (Sample 1.2-300). No molybdenum precipitation was observed on the zircon crucible materials.

Figure 10 summarizes hardness of the quenched glasses with values approximately 7.2 GPa (±0.3) indicating no increase in hardness. The high standard deviation is attributed to cracking at the indentation corners, as shown in Figure 11. Cracking at the indentation corners was not observed in glasses doped with Mo – a phenomena that may be related to a change in elasticity.

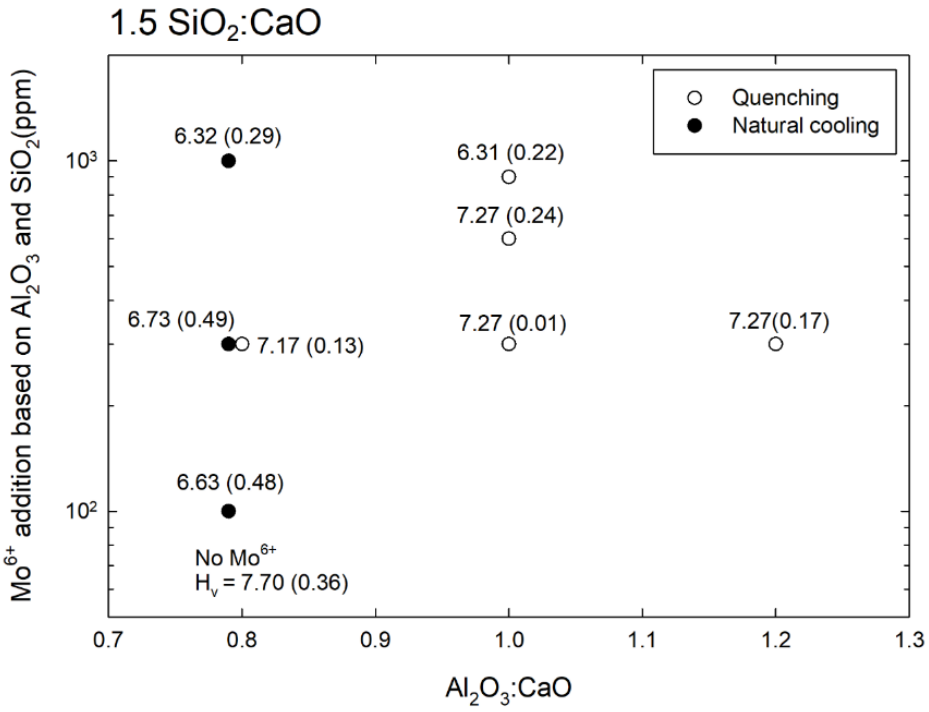

Figure VI.10. Vickers Hardness of glasses quenched (○) and natural cooled (●). Average hardness values are presented in GPa and standard deviation of five specimens are reported in parentheses.

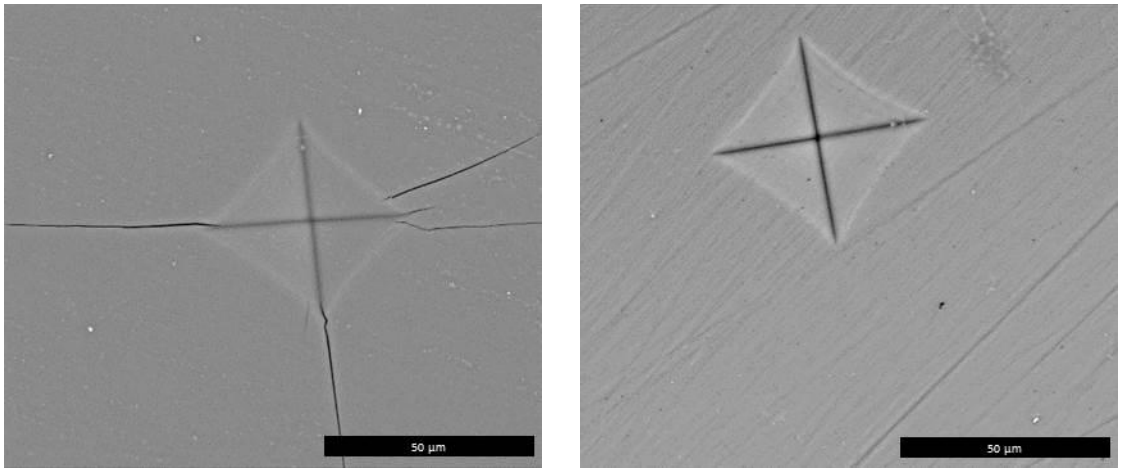

Figure VI.11. Indents on the 1.0:0.8:1.5 ($CaO:Al_2O_3:SiO_2$) samples by Vickers indentation: left, parent glass and right, with 300ppm Mo^{6+} addition. No cracks were observed in the molybdenum ions added sample. Mineralogy and microstructure data supported that the added Mo is uniformly distributed in the structure without precipitation when the system is properly prepared.

Anorthite was not observed in the normal glasses, and this was confirmed by XRD (Figure 12), however all samples, except for 1.2-300, contained precipitated corundum.

The microstructures support the mineralogy data of the quenched samples (Figure 13). Only the $CaO:1.2Al_2O_3:1.5SiO_2$ sample exhibited crystallization with corundum appearing as dark precipitates in the BSE image.

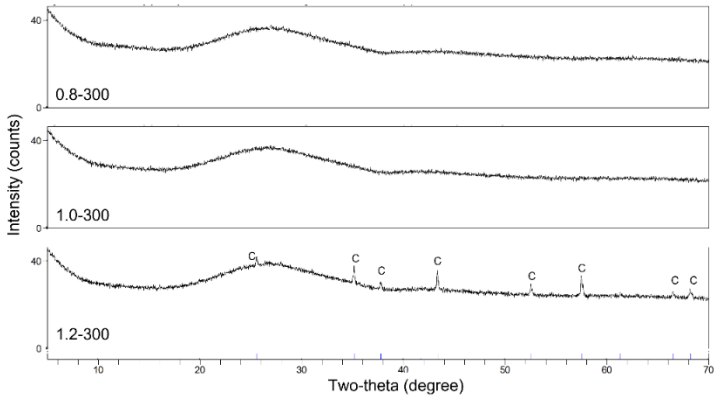

Figure VI.12. XRD patterns of the quenched 0.8-, 1.0-, and 1.2-300 samples. No anorthite crystallization was observed with intermediate level of Mo^{6+} addition. Further, even at higher Mo^{6+} levels, 600ppm and 900ppm do not promote anorthite crystallization. A marginal amount of corundum (C) was observed in the 1.2-300 samples.

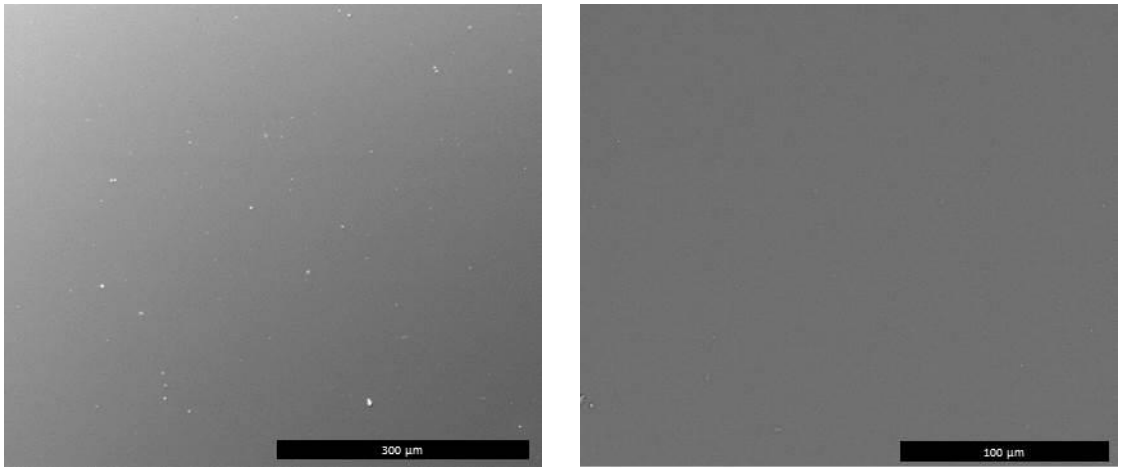

(a)

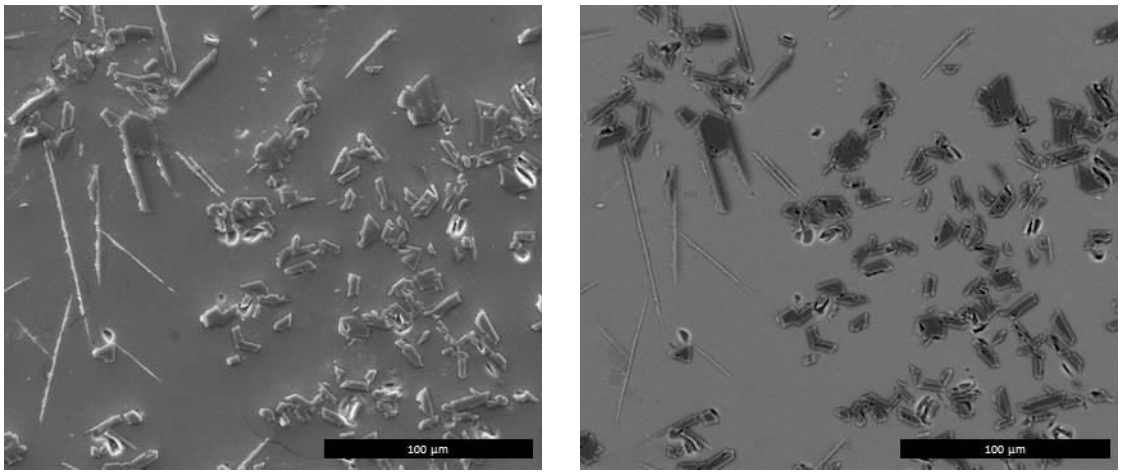

(b)

Figure VI.13. SEM images of quenched (a) 1.0:1.0:1.5 ($CaO:Al_2O_3:SiO_2$) sample and quenched (b) 1.0:1.2:1.5 ($CaO:Al_2O_3:SiO_2$) sample. Both samples contain 300ppm Mo^{6+}. (left -- SE images and right -- BSE images) (Light grey needles - anorthite and black- corundum)

VI.5 Conclusion

Three calcium aluminosilicate glasses were prepared at 0.8, 1.0, and 1.2 Al_2O_3, with constant SiO_2 level of 1.5, to which 100, 300, 600, and 1000 ppm was added in an ionic form. Even small Mo additions facilitated crystallization in slow-cooled specimens. Higher Mo levels generated disordered anorthite suggesting Mo incorporation into the anorthite lattice. Quenching the melts avoided anorthite crystallization producing homogeneous glasses, but without a measurable increase in hardness. Glasses with 1.0 and 1.2 alumina levels also resulted in secondary crystallization of corundum.

VI.6 References

1. Weigel C, Losq CL, Vialla R, Dupas C, Clément S, Neuville DR, et al. Elastic Moduli of $XAlSiO_4$ Aluminosilicate Glasses: Effects of Charge-Balancing Cations. J Non-Cryst Solids. 2016;447:267-72.

2. Metwalli E, Brow RK. Modifier Effects on the Properties and Structures of Aluminosilicate Glasses. J Non-Cryst Solids. 2001;289:113-22.

3. Wu J, Stebbins JF. Effects of Cation feld Strength on the Structure of Aluminoborosilicate Glasses: High-Resolution ^{11}B, ^{27}Al and ^{23}Na MAS NMR. J Non-Cryst Solids. 2009;355:556-62.

4. Macedo G, Sawamura S, Wondraczek L. Lateral Hardness and the Scratch Resistance of Glasses in the Na_2O-CaO-SiO_2 System. J Non-Cryst Solids. 2018;492:94-101.

5. Lee H, Carty WM. Potential Correlation of the Hardness of CaO-Al_2O_3-SiO_2 Glasses with Melting Behavior. In process. 2021.

6. Lee H, Carty WM. Correlation of Vickers Hardness of RO-Al_2O_3-SiO_2 Glssses with Predicted Liquidus Temperatures. In process. 2021.

7. Tan S, Ojovan MI, Hyatt NC, Hand RJ. MoO_3 Incorporation in Magnesium Aluminosilicate Glasses. J Nucl Mater. 2015;458:335-42.

8. Sun K. Fundamental Condition of Glass Formation. J Am Ceram Soc. 1947(30):277.

9. Short RJ, Hand RJ, Hyatt NC. An Investigation into the Oxidation State of Molybdenum in Simplified High Level Nuclear Waste Glass Compositions. MRS Proceedings. 2004;807.

10. Farges F, Siewert R, Jr GEB, Guesdon A, Morin G. Structural Environments Around Molybdenum in Silicate Glasses and Melts. I. Influence of Composition and Oxygen Fugacity on the Local Structure of Molybdenum. Can Mineral. 2006;44:731-53.

11. Kingery W, Bowen H, Ullmann D. Introduction to Ceramics. New York: John Wiley & Sons; 1976.

12. Lee H, Carty WM. The Glass Formaiton Boundary in Aluminosilicate Systems. In process. 2021.

13. Lide D. CRC Handbook of Chemistry and Physics: CRC Press; 2005.

14. Wahlberg JS, Fishman ML. Adsoption of Cesium on Clay Minerals. Washington, DC: United state government printing office; 1962.

15. Brumbach MT. Surface Charge, Rheology, and Variability of Kaolinic Clays [M.S. Thesis]. Alfred, NY: Alfred University; 2002.

16. Carty WM. The Colloidal Nature of Kaolinite. Carty W, Sinton W, editors. Westerville, OH: American Ceramic Society; 2001.

17. Doremus RH. Glsas Scinece. New York: A Wiley-Interscience Publication; 1973.

18. Loewenstein W. The Distribution of Aluminum in the Tetrahedra of Silicates and Aluminates. Am Mineral. 1954;39(1-2):92-6.

19. Bruno E, Chiari G, Facchinelli A. Anorthite Quenched from 1530°C. I. Structure Refinement. Acta Cryst. 1976;B32:3270-80.

20. Kjeldsen J, Smedskjaer MM, Mauro JC, Youngman RE, Huang L, Yue Y. Mixed Alkaline Earth Effect in Sodium Aluminosilicate Glasses. J Non-Cryst Solids. 2013:61-8.

21. Maeda K, Yasumori A. Effect of Molybdenum and Tungsten Oxides on Nucleation and Crystallization Behaviors of $MgO–Al_2O_3–SiO_2$ Glasses. J Non-Cryst Solids. 2015;427:152-9.

VII CONCLUSION

The hardness of aluminosilicate glasses was evaluated in this study. To accomplish this, four experimental matrices were executed: (1) identifying glass formation region in alkaline earth aluminosilicate system; (2) map hardness for a model system, CAS, to identify the correlation of hardness with composition and liquidus temperature; (3) evaluate how mixed RO correlates with glass hardness; and finally (4) evaluate how the incorporation of Mo^{6+} affects the hardness of a high hardness CAS glass.

For the understanding of glass formation compositions, the glass phase formation boundary in aluminosilicate systems, including individual and combined alkali or alkaline earth fluxes, were investigated. Glass formation in aluminosilicate system was found to uniformly be limited to 1.2 moles of alumina per mole of flux for alkali, alkaline earth, and mixed alkali plus alkaline earth flux systems. This fixed alumina limit extended over a range of silica levels that were dictated by the fluxes in the system. Similar to the results observed for CaO-fluxed melts, mixed alkali and alkaline earth fluxes exhibited a broad silica range along the alumina saturation limit of 1.2, but the silica range was significantly narrower when MgO was substituted for CaO. These results extend the range of alumina saturation level by 20% from the 1:1 molar ratio alumina to flux level commonly reported for alumina-containing glasses. The effects of MgO substitution for CaO appeared to create melts that differ both structurally and thermodynamically. It was also noted that the glass formation region for MAS glasses is significantly smaller than that observed for CAS glasses, which consequently limits the possible range of RO blending. In general, the glass formation boundary deviated linearly with the blending of CaO and MgO, indicating that the mixed RO effect does not affect glass formation.

Hardness of CAS glasses significantly improves with higher alumina content. Glasses can be readily formed with excess alumina, above 1.0:1.0 Al_2O_3:CaO due to the formation of 4-fold, 5-fold, and 6-fold Al-O polyhedral creating structures that promote high hardness. Specifically, the prediction of AlO_5 structures, the formation of Al-Si triclusters, and the elimination of NBO, were all consistent with the correlation of hardness and melting behavior. The formation of varied AlO_x sites also appear to align

with melting behavior as predicted by the phase diagram, thus showing a correlation of hardness with melting point in the CaO-Al_2O_3-SiO_2 system, exhibiting a maximum in the vicinity of the composition of the stable ternary compound, anorthite. As the composition moves away from the composition of anorthite, the hardness decreases. The determined composition for the superior hardness is CaO:(1.0 – 1.2) Al_2O_3:(1.5 – 2.3) SiO_2.

To evaluate the contribution of the second modifier on hardness and melting behavior, CAS-MAS, CAS-SAS, and CAS-BAS systems were evaluated. The correlation of Vickers hardness with melting temperature was observed in the $RO{\cdot}Al_2O_3{\cdot}SiO_2$ systems. The replacement of Ca with the larger cations of Sr^{2+} and Ba^{2+} indicated that above a critical substitution level, the lower CFS afforded by the larger substitution cation, resulted in a substantial reduction in glass hardness. Alumina additions at optimized level dominates glass hardness compared to other compositional variations. The hardness was marginally improved linearly when CaO was replaced by MgO. Above the critical second RO addition level, Vickers hardness strongly depends on the blended (composite) CFS due to the addition of a second RO. However, for the improvement of the hardness of alkaline earth aluminosilicate glasses, it is recommended to saturate the alumina level at $1.2Al_2O_3$. The capability to improve hardness by adding MgO has limited potential due to the compositional restriction for glass formation.

Three calcium aluminosilicate glasses were prepared at 0.8, 1.0, and 1.2 Al_2O_3, with constant SiO_2 level of 1.5, to which 100, 300, 600, and 1000 ppm $Mo^{6+}$was added in an ionic form. No increase in hardness was observed, but even small Mo additions facilitated crystallization. Normal glass melting procedure avoided anorthite crystallization producing homogeneous glasses. In slow-cooled samples, higher Mo levels generated disordered anorthite suggesting Mo incorporation into the anorthite lattice. Glasses with 1.0 and 1.2 alumina levels also resulted in secondary crystallization of corundum. While crystallization could be avoided by normal glass melting, there was still no improvement in measured hardness.